VNIVERSITAT DE VALÈNCIA

Departament de Medicina
Facultat de Medicina i Odontologia
Universitat de València
Programa de Doctorat 3139 Medicina

HIGH-TECH IMAGING AND MOLECULAR BIOMARKERS OF FIBROSIS IN HYPERTENSION-INDUCED LEFT VENTRICULAR HYPERTROPHY

Doctoral Thesis

Author: Gernot Helmut Pichler

Directors: Prof. Josep Redon Mas
Dr. Fernando Martínez García
Dr. Alicia Maceira González

Valencia, October 2017

University of Valencia

Josep Redon Mas, Professor of Medicine at the University of Valencia,
Fernando Martínez García, Associate Professor of Medicine at the University of Valencia,
Alicia Maciera González, Doctor in Medicine

CERTIFY

That the work embodied in the accompanying thesis entitled "**High-tech imaging and molecular biomarkers of fibrosis in hypertension-induced left ventricular hypertrophy**" has been carried out by Gernot Helmut Pichler under our direct supervision, fulfils the requirements of the regulations laid down for the Doctor of Philosophy in Medical Science with International Mention degree examination of the University of Valencia and is suitable for examination.

Valencia, October 2017

Josep Redon Mas Fernando Martínez García Alicia Maciera González

It is only with the heart that one can see rightly,

what is essential is invisible to the eye.

Antoine de Saint-Exupéry

Acknowledgements

I would like to express my sincere appreciation to my principal supervisor, Prof. Josep Redon: You will always be a role model for me, not only for your enthusiasm and dedication in medicine, but especially for the way you treat life and the human beings that surround you. I owe you so much!

To Fernando Martínez, my close friend and first teacher in clinical investigation: Thank you for your patience and the countless hours we spent together enjoying both science and leisure time! Si buscas, encuentras…
I am also deeply grateful to Alicia Maceira: Without you, this project would not have been feasible at all. I hope this is the beginning of a long-lasting collaboration.

A very special gratitude goes out to Oscar Calaforra and Elena Solaz: Your professional support and positive energy were essential for this dissertation. I also want to address a special mention to Javier Díez and Begoña López from the University of Navarra, Lorena Peiró and the girls from the biobank INCLIVA, and Juana Mari Vaquer from the central laboratory of the Clinical University Hospital of Valencia: Thanks for your support with biomarkers, your guidance and your time!

To the entire team of Internal Medicine at the Clinical University Hospital of Valencia, who supported me during long hours in the tiny and air condition-free office called "estar malalts": You are my Spanish family, and I will always carry you in my heart. El chico del norte os quiere a todos!
Also, a big hug goes to my friends and staff of INCLIVA: I will miss our delightful coffee breaks and almuerzos.

I am deeply grateful to my parents Helmut and Gerti, my brother Markus and my sister Ute for their emotional and moral support, even though there are 2000km between us. Long distance relationships are challenging, nobody knows that better than my future wife Verena: Your love, passion and optimism kept me going when I was down. I would like to dedicate this thesis to you - weil du die Liebe meines Lebens bist!

Abbreviations

ABPM	Ambulatory blood pressure monitoring
ACE	Angiotensin-converting enzyme
AV	Atrioventricular
β	Beta coefficient
BMI	Body mass index
BNP	Brain natriuretic peptide
BP	Blood pressure
bpm	Beats per minute
BSA	Body surface area
C	Carboxy
Ca	Calcium
CCL	Collagen cross-linking
CITP	Collagen type I carboxy-terminal telopeptide
CMR	Cardiac magnetic resonance
CMR-FT	Cardiac magnetic resonance feature tracking
CVD	Cardiovascular disease
CVF	Collagen volume fraction
DT	Deceleration time
E/A	Peak early / Late diastolic ventricular filling velocity
ECG	Electrocardiography
ECM	Extracellular matrix
ECV	Extracellular volume fraction
EDV	End-diastolic volume
EF	Ejection fraction
eGRF	Estimated glomerular filtration rate

ELISA	Enzyme linked immunosorbent assay
ESC	European Society of Cardiology
ESH	European Society of Hypertension
ESV	End-systolic volume
ET-1	Endothelin-1
HHD	Hypertensive heart disease
HR	Heart rate
hs-Troponin T	High sensitive troponin T
HTN	Hypertension
IR-FISP	Inversion recovery fast imaging with steady state precession
IV	Interventricular
LA	Left atrial
LGE	Late gadolinium enhancement
LV	Left ventricular
LVED	Left ventricular end-diastolic
LVES	Left ventricular end-systolic
LVH	Left ventricular hypertrophy
MAP	Mean arterial pressure
MMP	Matrix metalloproteinase
MOLLI	Modified Look-Locker Inversion-recovery
N	Amino
n	Number
NPR	Natriuretic peptide receptor
NT-proBNP	N-terminal pro-brain natriuretic peptide
p	P-value
PP	Pulse pressure

PICP	C-terminal propeptide of procollagen type I
PIIICP	C-terminal propeptide of procollagen type III
PINP	N-terminal propeptide of procollagen type I
PIIINP	N-terminal propeptide of procollagen type III
PWV	Carotid-femoral pulse wave velocity
r	Pearson´s product-moment correlation coefficient
R^2	Coefficient of determination
RAAS	Renin-angiotensin-aldosterone system
ROS	Reactive oxygen species
SAPPHIRE	Saturation Pulse Prepared Heart rate independent Inversion recovery
SASHA	Saturation recovery Single-Shot Acquisition
SCMR	Society for Cardiovascular Magnetic Resonance
SD	Standard deviation
shMOLLI	Shortened Modified Look-Locker Inversion recovery
SSFP	Steady state fee precession
STE	Speckle tracking echocardiography
STIR	Short-tau inversion recovery
TDI	Tissue Doppler imaging
TGF	Transforming growth factor beta
TIMP	Tissue inhibitor of metalloproteinase
TTE	Transthoracic echocardiography
VIF	Variance inflation factor

Index

Index of tables

4. Results

Index of figures

1. Introduction

3. Methods

4. Results

1. Introduction

1.1. From hypertension to hypertensive heart disease

Hypertension (HTN) is the leading risk factor for global death and disability, according to the World Health Organization (WHO) (1). Cardiovascular disease (CVD) is the number one mortality cause worldwide, accounting for 17 million deaths a year. It is estimated that HTN-related complications account for 9.4 million fatal cardiovascular events per year (2). Approximately half of global deaths due to heart disease, stroke and heart failure can be attributed to HTN.

The cardiovascular system is sensitive to physiological and pathological stimulants (3). Elevation of blood pressure (BP) and subsequent mechanical stress lead to changes in the heart and blood vessels (4). HTN is the most important cause for pressure overload in the cardiovascular system. The main compensatory mechanism to pressure overload in the heart is remodeling of myocardial tissue. Cardiac remodeling is accompanied by an increase in left ventricular (LV) mass and concentric hypertrophy of myocardial chambers, with consecutive alterations in cardiac size, shape, structure and functioning (5).

The disproportionate growth of the left ventricle involves all cardiac cell types and is mediated by a complex series of mechanical, neurohumoral, inflammatory, and oxidative stimuli (6). However, biomechanical stress related to HTN-mediated hemodynamic load seems to be the key player of myocardial remodeling (6). LV adaption to HTN results ultimately in left ventricular hypertrophy (LVH), the anatomical hallmark of hypertensive heart disease (HHD) (figure 1.1). The prevalence of HHD is high, up to 60% of individuals with uncomplicated HTN have evidence of increased LV mass on echocardiography (7).

A change in ventricular form or mass inevitably induces an alteration in cardiac contractile and relaxation properties. Therefore, LVH is directly related to cardiac function (8). LVH is also a strong independent predictor of survival in both patients with previous cardiac disease and in the general population (9). In fact, LVH increases the risk for both fatal and non-fatal cardiovascular events, including heart failure, coronary heart

disease, stroke, arrhythmia and sudden death (10). The magnitude of baseline values of LVH further determinates the magnitude of a given individual´s cardiovascular risk (11). Moreover, adequate treatment in patients with LVH slows the natural progression to heart failure and reduces subsequent mortality (12,13). Consequently, LVH is a well-established surrogate for heart failure and other adverse cardiac outcomes. Importantly, patients with heart failure typically progress from an asymptomatic phase (when LVH might already be present) to symptomatic phases (14). It is clinically relevant, therefore, to understand the pathways leading from HTN to LVH, and early identification of these individuals is mandatory in order to initiate or intensify medical treatment and consequently reduce morbidity and mortality.

Figure 1.1. Increase in LV wall thickness and mass in HHD. Adapted from Berk *et al*, 2007 (15).

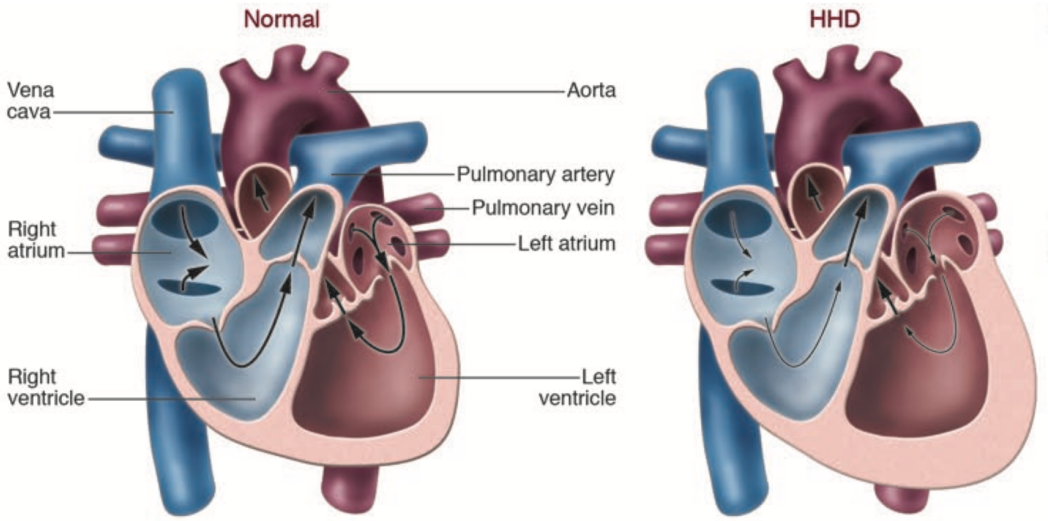

1.1.1. Cardiomyocyte

Cardiac muscle cells respond to HTN-induced pressure overload with either hypertrophic growth or anomalously enhanced apoptosis.

Hypertrophy of cardiomyocytes together with functional systemic mechanisms including the activation of the sympathetic system and the renin-angiotensin-

aldosterone system (RAAS) are critical compensatory mechanisms in order to reduce LV wall stress and preserve cardiac mechanical function (16). The hypertrophic growth of cardiomyocytes is mainly mediated by the activation of gene expression via intracellular signalling cascades. Subsequently, upregulation of protein synthesis and stability result in an increase in protein content and size of sarcomeres, the main determinants of cardiac contraction force (17). This increase in size and organization of sarcomeres entails an increment in cardiomyocyte size, which ultimately leads to an increase in LV mass.

HTN-induced apoptosis of cardiomyocytes is mainly promoted by mechanical stress and angiotensin II (18). A reduction in cardiac muscle cells implies that the remaining cells are exposed to an increased workload, ending up in depression of ventricular function (19). In addition to cardiomyocyte cell loss, mechanisms activated during the apoptotic process including caspase-3 and mitochondrial release of cytochrome-3 deteriorate function and performance of cardiac cells (20). Furthermore, ongoing apoptosis of cardiac muscle cells has a negative impact on ventricular wall geometry, leading to progressive thinning and dilatation of cardiac chambers and subsequently to alterations of cardiac function (21).

1.1.2. Extracellular matrix

The extracellular matrix (ECM) consists of interstitial fluid and several proteins produced by fibroblasts, mainly collagen and proteoglycans. Collagen provides cardiac tensile strength, actively transduces force during systole and is the main determinant of cardiac relaxation during diastole. The myocardial collagen network consists of 3 components: the epimysium, collagen fibers surrounding the epicardium and endocardium; the perimysium, collagen fibers grouping muscle fibers into muscle bundles; and the endomysium, collagen fibers that connect each individual myocyte.

Excessive accumulation of collagen types I and III fibers within the myocardial ECM leads to progressive myocardial fibrosis and subsequently to an alteration in cardiac shape, mass and stiffness (22). The quantity and quality of collagen types I and III in the ECM

are main determinants of the active relaxation process during diastole. Progressive accumulation of collagen fibers with altered spatial orientation impairs cardiac filling during diastole. Impaired diastolic filling further impairs myocardial contraction and therefore systolic performance.

Several mechanisms contribute to an exaggerated accumulation of collagen types I and III fibers in the myocardial interstitium (15) (figure 1.2).

Figure 1.2. Mechanisms of excessive accumulation of collagens in the ECM. Adapted from Berk *et al*, 2007 (15).

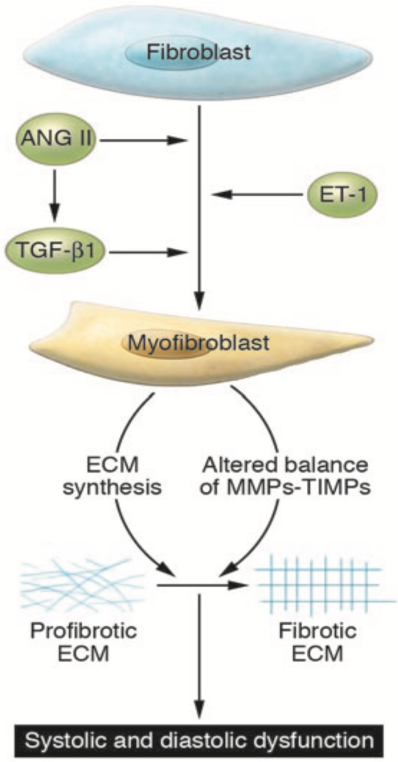

First, an increased synthesis of collagens has been observed in fibrotic hearts. Procollagen is synthesized by fibroblasts in healthy individuals and additionally by transformed fibroblast-like cells (myofibroblasts) in subjects with cardiac disease (23). The transition of fibroblasts to myofibroblasts is mainly regulated by hormones of the RAAS system, endothelin (ET-1) and transforming growth factor beta (TGF-β1). After secretion into the pericellular space, procollagen forms collagen fibrils that assemble into fibers.

Second, the quality of collagens in the ECM is altered in the fibrotic state. Elevated extracellular conversion of procollagen into microfibril-forming collagen, spontaneous microfibril assembly to form fibrils, and increased cross-linking of fibrils to form fibers contribute to the disruption of coordination of myocardial excitation-contraction coupling in systole and diastole (24).

Third, fiber degradation is decreased or unchanged in the hypertensive heart. The degradation of the ECM is mainly mediated by matrix metalloproteinases (MMPs) and their inhibitors, the tissue inhibitor of metalloproteinases (TIMPs). An imbalance between the activity of MMPs and TIMPs leads to alterations in collagen breakdown and ultimately adverse changes in cardiac geometry.

In addition, a change in collagen structure in the ECM induces alterations in myocyte signalling. Myofibroblasts express a gene program favouring the excessive production of collagen and the progression of the fibrotic state (25).

1.1.3. Cardiac vasculature

Intramyocardial blood vessels and the coronary vasculature endure structural and functional alterations in the hypertensive heart (26). Vascular smooth cells undergo hypertrophy or hyperplasia, leading to changes in the cellular alignment and an increase in the medial thickness/lumen ratio. Capillary rarefaction and disturbed vascular growth due to increasing myocardial mass lead to a decrease in vascular density. Coronary microvascular endothelial inflammation reduces nitric oxide bioavailability and protein kinase G activity, favouring the development of hypertrophy. Ultimately, perivascular fibrosis is a main determinant of the altered coronary flow reserve observed in HHD (27).

In summary, HTN-induced myocardial fibrosis is mainly characterized by alterations in cardiomyocytes, ECM and cardiac vasculature (figure 1.3). The resulting increase in LV stiffness and impairment of LV contraction favour the development of adverse clinical outcomes including altered electrical conduction, arrhythmias, heart failure, coronary heart disease and sudden cardiac death.

Figure 1.3. Schematic representation of changes in cardiomyocytes, ECM and cardiac vasculature in HHD. Adapted from Berk *et al*, 2007 (15).

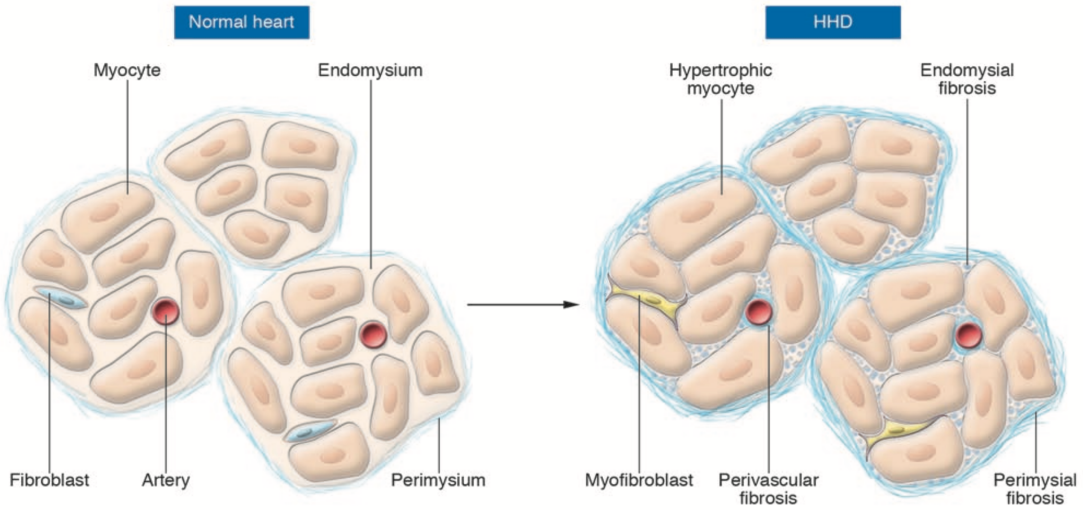

1.1.4. Patterns of myocardial fibrosis

Morphologically distinct patterns of fibrosis have been observed in cardiac disease. The onset, progression and histopathological type of fibrosis are mainly determined by the underlying cardiomyopathic process.

1.1.4.1. Reactive interstitial fibrosis

Reactive interstitial fibrosis is characterized by an expansion of the myocardial interstitium without cardiomyocyte loss. Diffuse deposition of mature collagen in the ECM and accumulation of fibrillary collagens in the cardiac vasculature are the histological hallmarks of reactive interstitial fibrosis (28).

HTN and diabetes are the main conditions related to diffuse myocardial fibrosis. Activation of the sympathetic system and RAAS, overproduction of reactive oxygen species (ROS) and metabolic disorders induced by hyperglycemia all result in a progressive increase in collagen synthesis and collagen turnover in the heart (29).

Diffuse reactive fibrosis has further been observed in conditions such as the aging heart, idiopathic dilated cardiomyopathy and aortic valve disease (30–32). In addition, reactive interstitial fibrosis has been found in the remote non-infarcted myocardium after

myocardial infarction (33). The exact pathophysiological mechanisms leading to reactive fibrosis remain unclear. However, the presence and extension of diffuse reactive fibrosis is a surrogate for disease severity in HTN, potentially reversible under specific therapy (34,35). Importantly, diffuse reactive fibrosis can precede irreversible replacement fibrosis (36). It is therefore important from a clinical point of view to detect and quantify diffuse fibrosis at an early disease stage in order to initiate, modify or intensify treatment and subsequently reduce the progression of the fibrotic state.

1.1.4.2. Replacement fibrosis

Replacement fibrosis, also known as scarring fibrosis, is characterized by the replacement of cardiomyocytes by collagen fibers after cell damage. Cardiac cell replacement corresponds to the accumulation of mainly collagen type I in the heart and can be observed as soon as the cardiomyocyte integrity is altered (37).
Scarring fibrosis can be locally distributed or diffuse. Myocardial ischemia, hypertrophic cardiomyopathy, myocarditis and sarcoidosis are typically followed by focal replacement fibrosis. In contrast, systemic diseases including chronic kidney disease, systemic inflammatory disease and toxic cardiomyopathy are related to diffuse scarring fibrosis (38,39). Focal replacement fibrosis after myocardial infarction is considered an essential repair process, nevertheless, diffuse scarring fibrosis in non-infarct areas contributes to alteration in cardiac elasticity and diastolic dysfunction. The mechanisms of cardiomyocyte replacement depend on the underlying disease (40).

1.1.4.3. Infiltrative interstitial fibrosis

Infiltrative fibrosis of the cardiac interstitium has been observed in metabolic diseases characterized by the deposition of insoluble proteins or glycosphingolipids (41). In cardiac amyloidosis, penetration of the ECM by nodular deposits and branching filaments interlacing cardiomyocytes has been found. Besides mechanical alterations, amyloid deposits can induce ROS production, interfere in the balance of MMPs involved in collagen turnover, and induce microvascular disease (42). Thus, myocardial infiltration

by insoluble molecules contributes directly and via activation of systemic mechanisms to progressive myocardial fibrosis and dysfunction.

1.2. Molecular biomarkers in hypertensive heart disease

The development of HHD is mediated by numerous hemodynamic and non-hemodynamic factors. The presence of overt LVH can reliably be confirmed by electrocardiography (ECG), echocardiography and cardiac magnetic resonance (CMR). However, the detection of subtle cardiac dysfunction preceding the appearance of overt cardiac wall and mass increase is challenging. A growing number of molecular biomarkers derived from the complex pathophysiological mechanisms resulting in HHD has been proposed over the past years. The potential benefits of molecular biomarkers include early detection of individuals prone to develop LVH, diagnosis of preclinical alterations in cardiac geometry and function, refinement of cardiovascular risk prediction, early implementation of treatment and monitoring response to treatment (43).

1.2.1. Fibrosis

Collagen type I and type III fibers are the predominant components of myocardial ECM, accounting for approximately 85% and 11% of the cardiac collagen, respectively (44,45). During synthesis and degradation of mature collagen fibers, propeptides and telopeptides are cleaved by endopeptidases and released into the bloodstream (46) (figure 1.4). The propeptides, telopeptides and endopeptidases involved in collagen turnover in the ECM have been studied for non-invasive assessment of diffuse myocardial fibrosis.

Figure 1.4. Formation, structure and degradation of mature collagen. Cleavage of propeptides during formation and cleavage of telopeptides during degradation of mature collagen. Adapted from Fan *et al*, 2012 (47).

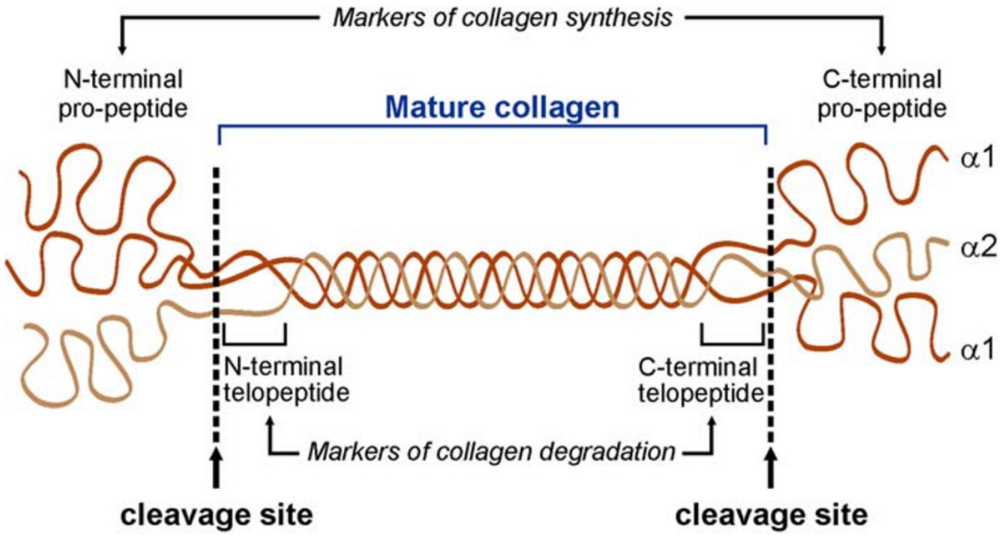

1.2.1.1. Collagen synthesis

In the heart, collagen type I and III are synthesised by fibroblasts as preprocollagens: 3 pro-α-collagen chains form a triple helix structure in the endoplasmatic reticulum, known as procollagen (48). Procollagens contain 2 propeptides, the carboxy (C)-propeptide and the amino (N)-propeptide. Cleavage of the propeptides by proteinases results in mature collagen molecules with short telopeptides at either end. The mature collagen can assemble into highly ordered, string-like aggregates known as fibrils.

Cleavage of the C-terminal propeptide of procollagen type I (PICP) and type III (PIIICP) is accomplished by procollagen C-proteinases (figure 1.5) (49). The N-terminal propeptide of procollagen type I (PINP) and type III (PIIINP) is cleaved by members of the ADAMTS family, a group of extracellular protease enzymes with desintegrin and metallopreoteinase activity (figure 1.6). After cleavage, PICP, PIIICP, PINP and PIIINP are released into the bloodstream and degraded in the liver.

Figure 1.5. Release of PICP into the bloodstream. Adapted from Lopez *et al*, 2015 (50).

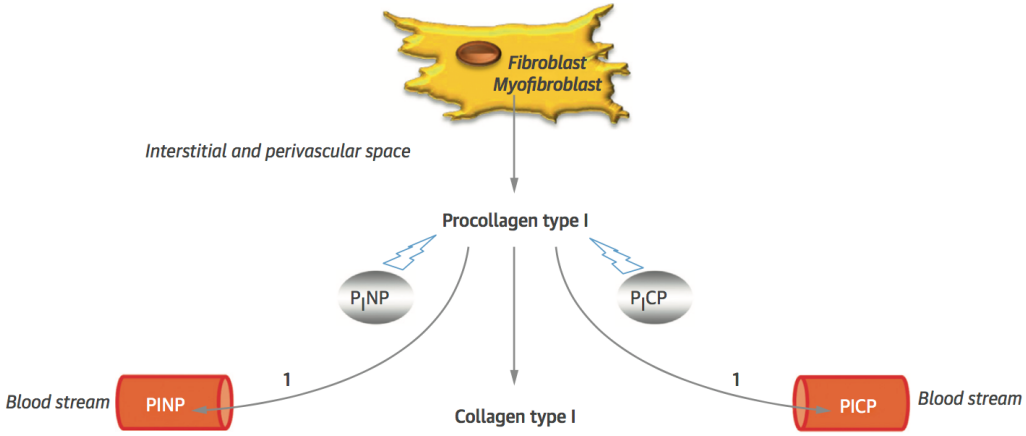

Figure 1.6. Release of PIIINP into the bloodstream. Adapted from Lopez *et al*, 2015 (50).

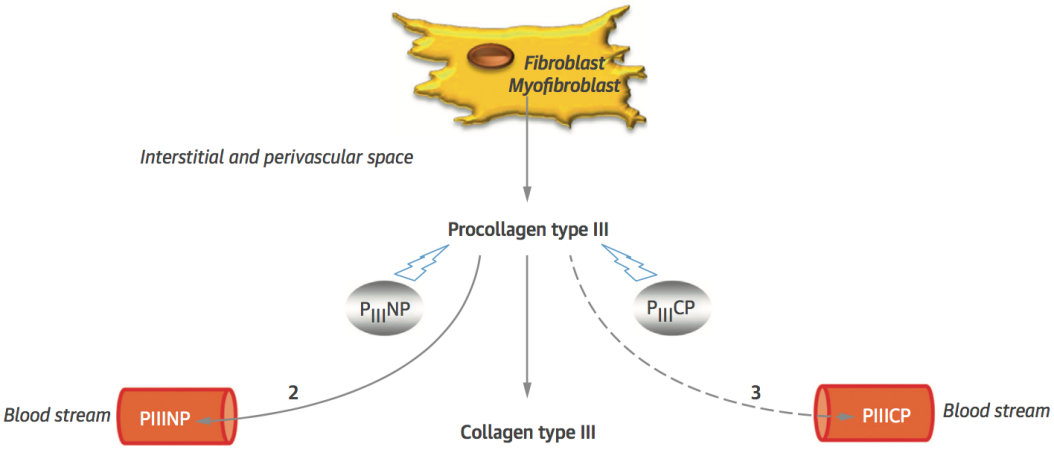

PICP is formed in a 1:1 stoichiometric ratio to the formation of collagen type I molecules. As a consequence, PICP concentration in blood is a direct indicator of collagen type I synthesis (51). In contrast, cleavage of the N-terminal domain of procollagen type III proceeds at a slower rate, and partially processed procollagens can be found on the surface of collagen type III fibers. Serum PIIINP concentration is therefore not a direct indicator of collagen type III synthesis, however, PIIINP levels have shown to be directly related to fibrosis of the ECM (52).

1.2.1.2. Collagen degradation

Breakdown of mature collagen fibers is accomplished with MMPs. The MMP family contains more than 25 zinc- and calcium-dependent enzymes, mainly synthesised by fibroblasts and leucocytes (53). Several MMPs are expressed in the heart. MMP-1 is a protease highly specific for collagen type I and III, and a key player in collagen fragmentation. MMP-1-mediated endopeptidase cleavage of mature collagen type I leads to a release of collagen type I carboxy-terminal telopeptide (CITP) into the bloodstream. Under physiological conditions, the amount of CITP molecules in blood and the amount of fibrillary collagen degraded is proportional (54). Consequently, CITP is considered a molecular biomarker of collagen breakdown.

The denatured collagen fragments are metabolized by MMPs known as gelatinases, namely MMP-2 and MMP-9. Several members of the MMP family can further induce activity of profibrotic proteins such as TGF-β and therefore interfere in the complex mechanisms of collagen turnover in the ECM. MMP activity is regulated at a transcriptional and activity level. Growth factors, mechanical stress and endogenous proteinases, the TIMPs, are key players in the regulation of MMP activity.

1.2.1.3. Collagen cross-linking

Despite excessive accumulation and degradation of collagen fibers, an increased cross-linking of collagen fibrils within the fibers has been observed in the hypertensive heart (55). During collagen cross-linking (CCL), collagen fibrils are covalently connected by the enzyme lysyl oxidase, resulting in insoluble fibers with increased stiffness (56). Although the structures of collagen type I and III are similar, they have different characteristics regarding CCL and elastic properties. Collagen type I forms thick fibers with a high rate of CCL, responsible primarily for the tensile strength of the heart. Collagen type III, in contrast, forms relatively thin fibers that provide elasticity and create a network providing the structural integrity of the myocardial connective tissue (57).

The role of CCL is not limited to the properties regarding structure and quality of the accumulated collagen. CCL determines the sensitivity of collagen fibers to degradation by MMP-1, and subsequently the amount of CITP in blood: the higher the CCL, the lower the ratio of circulating CITP to MMP-1 (58). Individuals with a low CITP/MMP-1 ratio, thus, are characterized by a high myocardial collagen type I cross-linking (figure 1.7).

Figure 1.7. CCL determines the sensibility of collagen type I fibers to degradation by MMP-1. In HHD, high cross-linking results in reduced cleavage of CITP by MMP-1 and consequently lower serum CITP/MMP-1 ratio. Adapted from Lopez *et al*, 2016 (59).

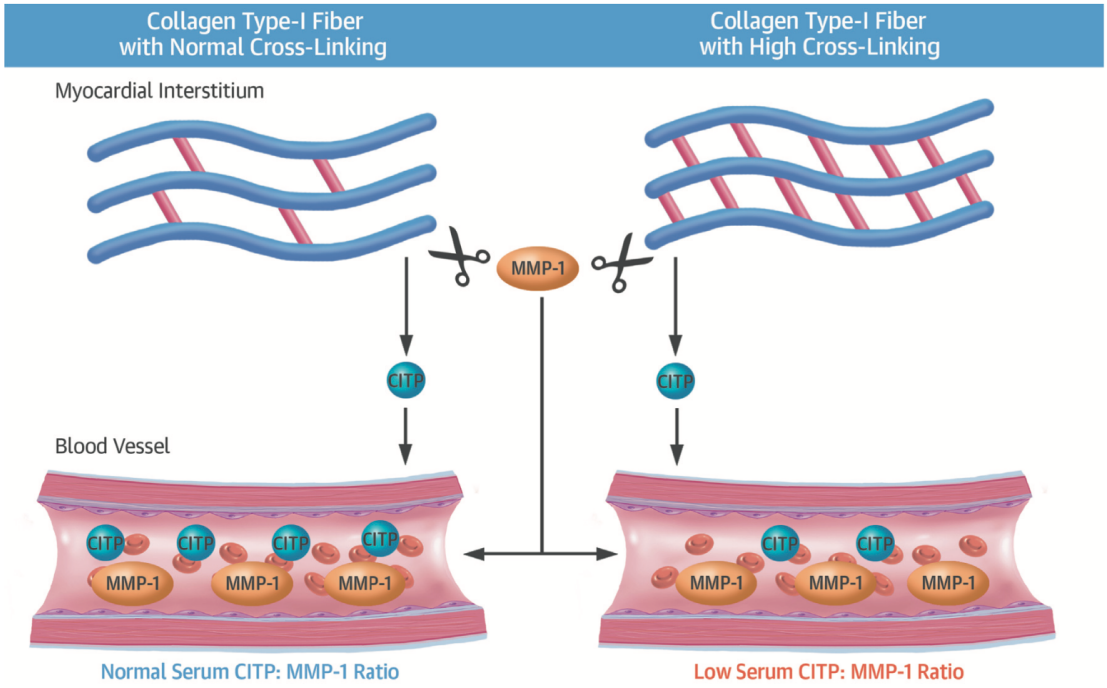

1.2.2. Myocardial stretch

Myocardial wall stress is the main stimulus for the synthesis and secretion of brain natriuretic peptide (BNP), a 32-amino acid cardiac natriuretic peptide originally discovered in porcine brain tissue (60). Ventricular myocytes and, to a lesser degree, fibroblasts have been shown to be the major source of BNP-related peptides. BNP is synthesized as proBNP, a 108-amino acid prohormone. Upon release into the bloodstream, proBNP is cleaved into C-terminal fragment, the biologically active BNP,

and into the biologically inactive 76-amino acid N-terminal fragment (NT-proBNP) (61). Both BNP and NT-proBNP can be detected in systemic circulation and are considered established biomarkers of myocardial stretch.

Ventricular production of BNP and NT-proBNP is upregulated globally in heart failure and locally in the area adjacent to myocardial ischemia (62). In addition, endocrine and paracrine activity by cytokines and neurohormones have been shown to modulate the synthesis and secretion of natriuretic-related peptides. The half-life of BNP and NT-proBNP is 20 minutes and 120 minutes, respectively. As a consequence, NT-proBNP levels in serum are approximately 6 times higher than BNP levels.

The physiological effects of BNP result from interaction with natriuretic peptide receptor type A (NPR-A). NPR-A mediated production of cyclic GMP leads to natriuresis, peripheral vasodilatation, as well as inhibition of the RAAS and the sympathetic nervous system (figure 1.8). Clearance of BNP is accomplished by binding to natriuretic peptide receptor type C (NPR-C) and proteolysis by neural endopeptidases. On the other hand, clearance of NT-proBNP is mainly driven by renal excretion.

Figure 1.8. BNP and NT-proBNP synthesis, release and receptor interaction. Adapted from Weber *et at*, 2006 (62).

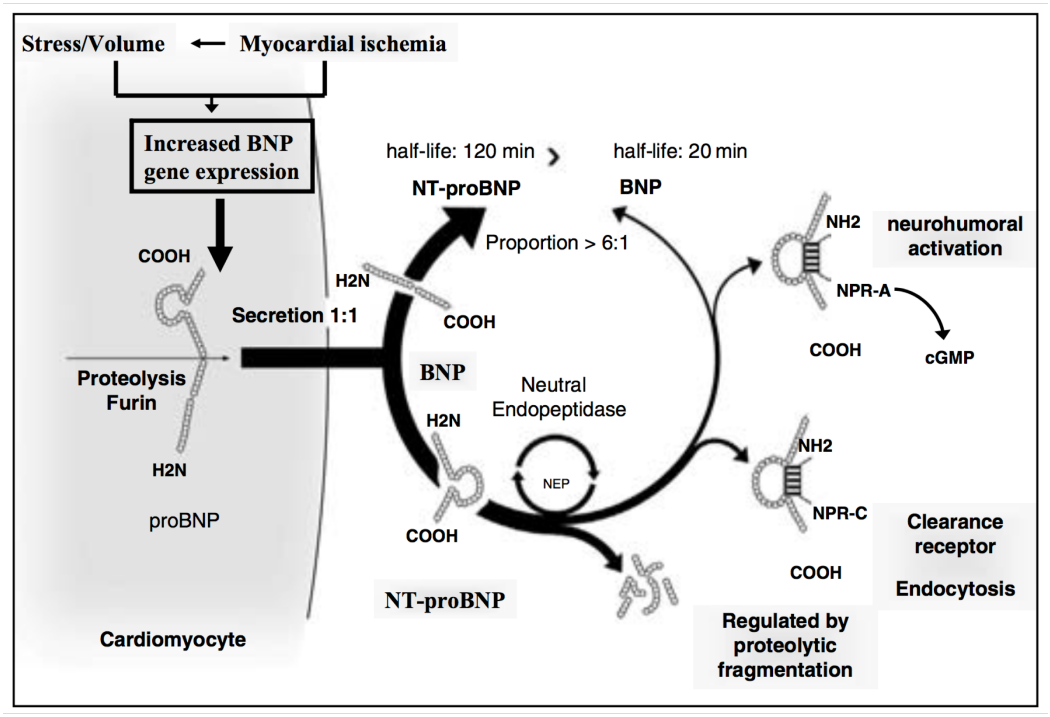

1.2.3. Myocardial injury

Cardiac troponins are established biomarkers of cardiac injury routinely used in clinical practice. Troponins are regulatory proteins of the interaction between actin and myosin and form part of the contractile apparatus of cardiac and skeletal muscle. The troponin complex is located on the actin filament and consists of 3 subunits: troponin T, troponin C and troponin I (63).

Prolonged ischemia in the heart leads to an irreversible damage of myocytes and to the release of cytosolic complexes. In HTN, pressure-induced cardiac wall stress may result in myocardial injury (64). As a consequence, troponin T and other troponins are released into systemic circulation. Clearance of troponin T is accomplished with renal and extrarenal mechanisms. Renal excretion and scavenger receptor-mediated endocytosis of troponin T in the mononuclear phagocyte system have been proposed as the main mechanisms of troponin T clearance (65).
Despite myocardial ischemia and pressure overload, other conditions have shown to lead to an increase in circulating troponin T including increased membrane permeability (e.g. in sepsis), end-stage renal disease, excessive training routines in athletes, and non-cardiac cardiovascular events (66–68). In addition, baseline levels of troponin T are detectable in healthy individuals probably due to ongoing physiological loss of cardiomyocytes via apoptosis (69).

High-sensitivity assays accurately measure low concentrations of troponin T, known as high sensitive troponin T (hs-Troponin T), with a small coefficient of variation (70). In hypertensive patients, hs-Troponin T levels are frequently above normal values despite the absence of cardiovascular or overt cardiac disease (64). The use of highly sensitive assays has further shown that even very low levels of troponin T are independent predictors of adverse clinical outcomes (71). Besides myocardial ischemia, serum troponin T concentrations at low levels have shown prognostic value in HTN and heart failure.

1.3. Cardiac imaging in hypertensive heart disease

During decades, ECG and echocardiography were the only available techniques for the evaluation of LVH in hypertensives. 3 main patterns of LVH and remodelling in HHD have been described: concentric hypertrophy, characterized by an increase in LV mass due to wall thickening; eccentric hypertrophy, characterized by an increase in LV mass due to chamber dilatation; concentric remodelling, characterized by an increase in relative wall thickness with normal LV mass (72).

It is unknown why individuals develop a specific morphologic pattern in response to HTN. Several factors including pressure- and volume overload, gender, ethnicity, body constitution, and activation of the sympathetic system and RAAS are determinants of cardiac adoption mechanisms to HTN (22). The clinical implications and prognostic value of the different patterns of HHD are still unclear. However, ECG-derived criteria of LVH lack sensitivity and specificity for the assessment of morphologic patterns in HHD, especially in young male subjects (73). Although ECG-derived assessment of LVH predicts cardiovascular events in hypertensives, preclinical alteration of cardiac function cannot be reliably evaluated with ECG (74). In addition, discrepancies regarding the diagnostic and prognostic performance of LVH assessed by ECG compared to LVH assessed by CMR have been found, suggesting that each technique reflects a different phenotype of LVH (75).

1.3.1. Transthoracic echocardiography

The use of transthoracic echocardiography (TTE) in numerous clinical trials has provided widespread knowledge about the development and progression of HHD (76). Various techniques for the assessment of LV mass have been developed over the last decades. M-mode echocardiography is a quick and simple procedure that provides highly accurate endocardial definition. Nevertheless, LV mass assessment using M-mode is performed in one dimension and assumes an ellipsoid shape with uniform wall thickness throughout the LV, resulting in low accuracy (77). 2-dimensional TTE techniques permit a more accurate and reproducible assessment of LV volumes, and LV mass can be

estimated using the Devereux equation (78). However, the formula is applicable only to individuals without major alterations of the LV geometry. 3-dimensional echocardiography has been developed in the past years. LV mass assessment using 3-dimensional echocardiography does not rely on geometric assumptions and provides better reproducibility as compared to other echocardiographic techniques. In contrast, the diagnostic and prognostic value of 3-dimensional echocardiography relies on an adequate acoustic window and experienced practitioner, and is not commonly available in clinical routine (79).

TTE-based assessment of LV mass is useful in patients with overt LVH. The high interobserver and interstudy variablitiy of TTE-assessed LV mass, in contrast, raise the question whether TTE can reliably assess subtle preclinical changes in LV geometry at early stages.

Besides LVH, patients with HHD are at increased risk for the development of diastolic dysfunction and heart failure with preserved ejection fraction, a clinical syndrome characterized by normal systolic function but clinical signs and symptoms of heart failure. Several TTE-derived methods are available for the estimation of diastolic dysfunction, detectable in up to 50% of hypertensive patients (14). LV mechanics is a determinant of left atrial (LA) dimension and performance, for example, LA dilatation reflects elevated LV filling pressure and subsequently diastolic dysfunction. Isovolumetric ventricular relaxation time is measured as the time period between aortic valve closure and mitral valve opening and a valuable screening tool for approximating the LA pressure. Early diastolic dysfunction is characterized by stiffening and impaired relaxation of the myocardium, affecting transmitral inflow velocities. Consequently, a reduction in the ratio between peak early filling (E-wave) and late diastolic filling (A-wave) velocity, expressed as E/A ratio, can be observed in patients with mild diastolic dysfunction. Tissue Doppler imaging (TDI) enables direct quantification of mitral annular flow velocities, and TDI-derived values can be corrected for changes in preload or heart rate.

Speckle tracking is an emerging technique with a promising potential to detect very early, preclinical alterations in cardiac function. TDI-, 2-dimensional, and 3-dimensional

derived LV strain patterns have been found to be altered in hypertensives and may be useful as early markers of impaired LV mechanics (80).

1.3.2. Cardiac magnetic resonance

CMR has become the gold standard for the non-invasive early diagnosis and treatment assessment of HHD due to its excellent reproducibility, unrestricted field of view, and non-radiating tissue characterization. Cardiac geometry, function and fibrosis can all be reliably assessed with the use of different CMR techniques, including steady state fee precession (SSFP) cines for cardiac geometry and function evaluation; phase contrast sequences for velocity measurement; T2-weighted short-tau inversion recovery (STIR) for oedema assessment; T1- and T2-weighted fast spin-echo; T1-weighted perfusion; myocardial late gadolinium enhancement (LGE) sequence and T1 mapping for tissue characterisation (81).

1.3.2.1. Strain imaging

Myocardial strain is defined as the degree of deformation of a myocardial segment from its initial length to its maximum length and expressed as a percentage. In systole, the LV deforms along different directions according to the complex LV myocardial architecture: the subendocardial layer is formed by fibers oriented longitudinally from base to apex; the mid-wall layer is formed by circumferentially oriented fibers; and the subepicardial layer is formed by fibers oriented longitudinally from apex to base. Consequently, LV deformation during systole determines longitudinal and circumferential shortening, as well as radial thickening and torsion, allowing the calculation of longitudinal, circumferential and radial strain (figure 1.9).

Longitudinal strain represents longitudinal shortening from the base to the apex, and is expressed in negative values. Circumferential strain represents fibre shortening along the circular perimeter on a short-axis view, and is expressed in negative values. Radial strain results from the radially directed myocardial deformation towards the centre of

the LV cavity, therefore, radial strain represents LV thickening and thinning motion, and is expressed in positive values.

Figure 1.9. Myocardial deformation directions. L, longitudinal shortening; C, circumferential shortening; R, radial thickening. Adapted from Scatteia *et al*, 2017 (82).

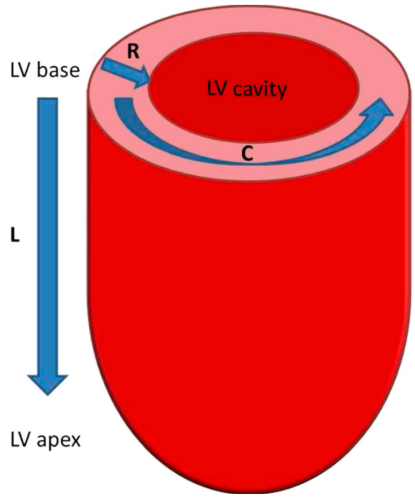

Several CMR techniques have been developed for the assessment of myocardial strain. Direct strain acquisition techniques include CMR tagging, phase velocity mapping, strain-encoded imaging and displacement encoding with stimulated echoes. These techniques require dedicated acquisition time in the scanner and cannot be applied to routine CMR scans. In contrast, feature tracking technology is a post-processing technique based on the identification and tracking of features along the successive phase of routinely acquired cine CMR sequences (83).

Feature tracking is based on optical flow technology: A pattern of interest (feature) is identified in one image and tracked in the successive images of a CMR cine sequence. In a first step, endocardial and epicardial borders are manually drawn at end-diastole in all short and long axis cines. Next, a dedicated feature tracking software is used to automatically track this pattern through all the phases of the cine sequence. Then, the displacement of the feature between 2 images can be identified with the help of a search window (figure 1.10).

Figure 1.10. Principle of feature tracking. Small square windows are centered about the points of interest (red) on the first image of the sequence (left) and searching the as-much-as-possible-similar grayscale pattern on the following image (right) in the vicinity of the original window. Once the red point is found, the window is centered again about it, to provide an estimate of the local displacement. This procedure is repeated through all phases of the cine sequence. Adapted from Pedrizzetti *et al*, 2016 (84).

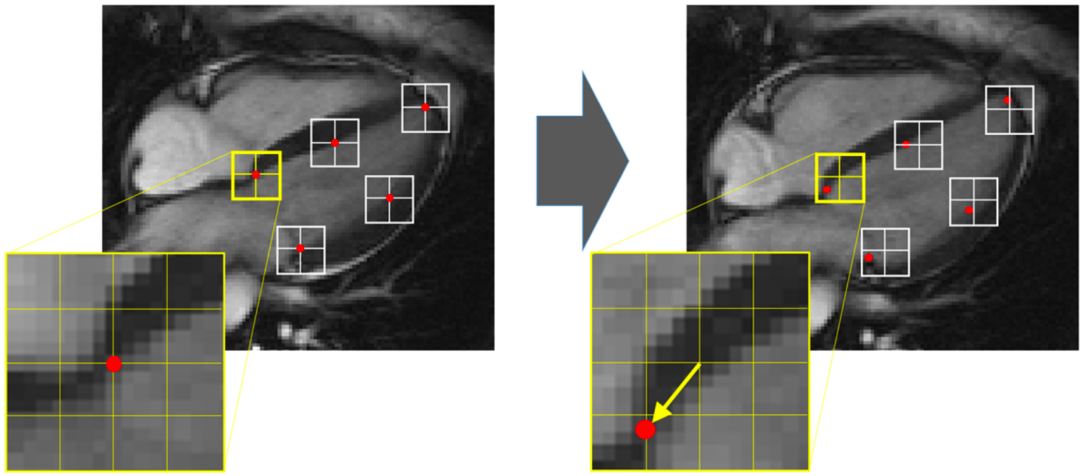

The size of the search windows depends on the displacement of the identified pattern between frames and determines the accuracy of feature tracking. Pattern similarities are averaged in large windows, resulting in a reduction of tracking accuracy. In contrast, small windows might be unable to recognize extensive pattern displacements. Besides window size, the accuracy of strain analysis is determined by the temporal resolution of the cine sequences used for feature tracking. A low temporal resolution requires larger search areas for the comparison of patterns, as a consequence, local patterns might become less comparable (known as image de-correlation) (85). CMR feature tracking (CMR-FT) has been validated in numerous clinical studies and is considered a valid method for the assessment of myocardial strain (86).

1.3.2.2. T1 mapping

The non-invasive quantification of myocardial fibrosis has numerous potential benefits, including the detection and identification of individuals with preclinical alterations in

myocardial collagen-turnover which can lead to disturbed cardiac functioning, monitoring of treatment response, and refinement of individual cardiovascular risk.
T1-mapping sequences allow direct in-vivo quantification of T1 values for each voxel in the heart (87). T1 values reflect the spin-lattice relaxation time, which is the time it takes for the longitudinal magnetization to recover 63% of its initial value after a 90° pulse. Importantly, the spin-lattice relaxation times are specific for any given tissue, therefore, the deviation of reference values can be used to detect and quantify myocardial alterations including diffuse fibrosis. The measured T1 values before and after administration of a contrast agent are represented in a parametric map and can be used for the calculation of the partition coefficient and the extracellular volume fraction (ECV), parameters that reflect the amount of interstitial fibrosis (88).

Initially, T1 mapping was performed using the Look-Locker sequence, which required acquisition times of around 35-40 seconds per image and tedious image post-processing. Subsequently, the Modified Look-Locker Inversion-recovery (MOLLI) sequence was developed for the assessment of myocardial fibrosis (89). In this technique, images from 3 consecutive inversion-recovery experiments are merged into 1 data set, and the procedure can be performed during a single breath-hold. Nowadays, fast, accurate and reliable T1 mapping techniques are available, including shortened Modified Look-Locker Inversion recovery (shMOLLI) (90), which can be performed during 9 heartbeats of a single breath-hold, Saturation recovery Single-Shot Acquisition (SASHA) and Saturation Pulse Prepared Heart rate independent Inversion recovery (SAPPHIRE) (91). With the use of the shMOLLI technique, the partition coefficient and ECV can be calculated by means of the obtained values of native T1 and post-contrast T1 values.

Native T1 is the spin-lattice relaxation time before administration of a contrast agent. An increase in native T1 has been observed in cardiac diseases involving an expansion of the extracellular space, including fibrosis, edema and amyloid deposits (92–94). In contrast, a decrease in native T1 has been found in intramyocardial haemorrhage, fat infiltration and excessive iron deposition (95). Some alterations in the composition of

the extracellular space can be detected determining native T1. Thus, native T1 could be considered a promising surrogate for early stages of cardiac disease.

Post-contrast T1 is the spin-lattice relaxation time measured 15 minutes after the administration of a contrast agent. Myocardial post-contrast T1 mapping directly correlates with LV stiffness and is a marker of myocardial interstitial space expansion as happens in diffuse fibrosis, among other conditions (96). However, the isolated use of post-contrast T1 for the quantification of myocardial fibrosis is not appropriate, because post-contrast T1 values are determined by renal function, type and dosage of the contrast agent used, body composition, acquisition time and the cellular fraction of blood, resulting in a relatively low reproducibility.

For the quantification of myocardial fibrosis, the partition coefficient can be derived from native and post-contrast T1 mapping. The myocardium consists of the intracellular compartment (cardiomyocytes and other cell types), the ECM, and the intravascular compartment. Partition coefficient and ECV comprise the ECM and the intravascular compartment, and it is generally accepted that alterations in these compartments are mainly mediated by changes in the ECM rather than the intravascular compartment. Consequently, the extension of the ECM can be assessed when changes in T1 in the myocardium are related to changes in T1 in blood (figure 1.11). In fact, the partition coefficient is derived from changes in T1 relaxation rate (1/T1) in myocardium and blood before and after the administration of the contrast agent:

$$Partition\ coefficient = \frac{\frac{1}{post\ T1\ myo} - \frac{1}{native\ T1\ myo}}{\frac{1}{post\ T1\ blood} - \frac{1}{native\ T1\ blood}}$$

Figure 1.11. T1 mapping. Relation of changes in 1/T1 of myocardium and blood can be used to determine the partition coefficient (slope of lines 1-3). Adapted from Taylor *et al*, 2016 (88).

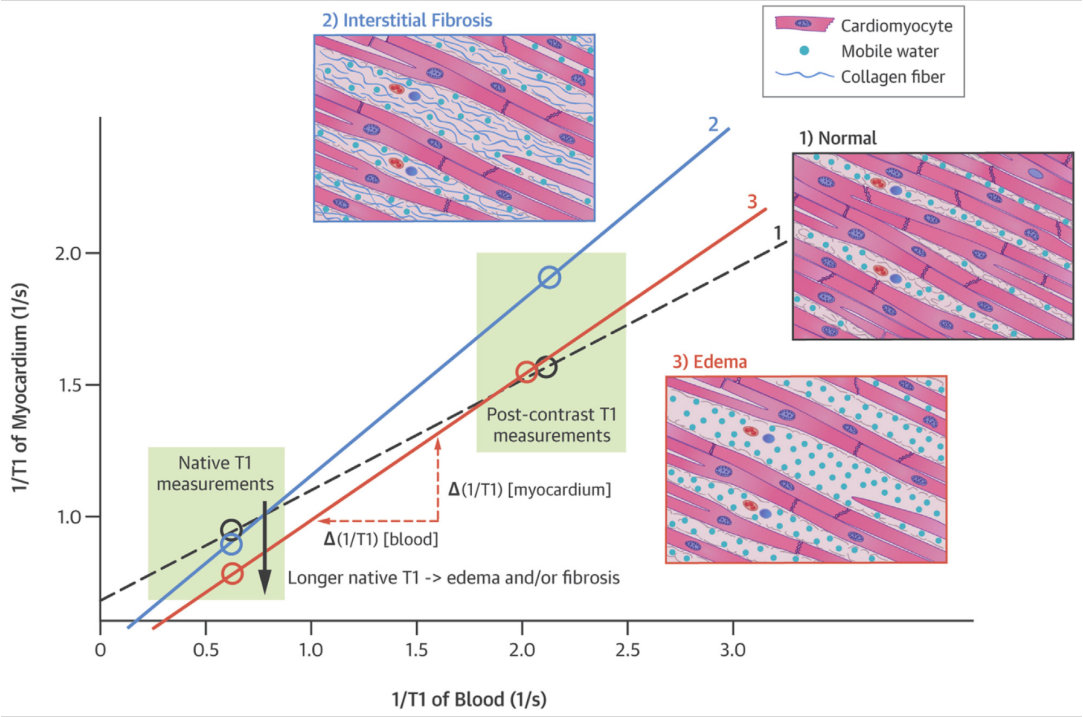

For the assessment of ECV, the partition coefficient is multiplied by the hematocrit factor (1-hematocrit) in order to adjust for the contrast agent plasma volume (88). Consequently, ECV is independent of potentially confounding factors that might have an impact on the measured values of post-contrast T1, like the rate of contrast agent clearance from blood and tissue.

It is important to point out that both ECV and the partition coefficient reflect the expansion of the interstitial space, they are not a direct measure of the amount of fibrotic tissue in the cardiac wall. Expansion of the ECM is frequently, but not exclusively, due to diffuse fibrosis. However, in absence of infiltrative or ischemic cardiac disease, ECV and the partition coefficient can be considered as imaging markers of diffuse fibrosis: The higher ECV or the partition coefficient, the higher the degree of cardiac fibrosis.

1.4. Central hemodynamics in hypertensive heart disease

In clinical practice, the diagnosis, treatment decisions and follow-up of HTN are based on the measurement of brachial BP. Peripheral BP is an established predictor of cardiovascular risk, and BP-lowering treatment is followed by a reduction in cardiovascular and all-cause morbidity and mortality (97). However, over the past years, interest in central BP and carotid-femoral pulse wave velocity (PWV) has grown owing to their potential value in the assessment of cardiovascular phenotypes and cardiovascular risk.

Central BP is closely related to the pressure directly exerted on the heart, the brain and the kidneys. Available evidence has shown that central BP is an independent marker of cardiovascular risk and changes under antihypertensive treatment result in a reduction of cardiovascular mortality (97).

PWV is considered the gold standard for the assessment of arterial stiffness and has been found to be an independent marker of cardiovascular disease both in the high-risk and in the general populations. Increasing evidence has revealed that measurement of PWV improves cardiovascular risk stratification and has a promising potential as a surrogate endpoint of cardiovascular disease. The current European Society of Hypertension (ESH) and European Society of Cardiology (ESC) guidelines recommend determining PWV for risk assessment in hypertension, and a cut-off value for 'high' PWV of more than 10 m/s has been established as a conservative estimate of significant alterations in aortic function in middle-aged hypertensive individuals (98).

Both central BP and PWV can be measured with automatic, non-invasive devices. The SphygmoCor device (SphygmoCor; AtCor Medical) is based on arterial applanation tonometry for recording pressure waveforms (figure 1.12). Central aortic BP waveforms can be reconstructed from radial artery pressure waveforms applying a mathematical transfer function. For the assessment of PWV, the propagation time from the foot of the carotid waveform to that of the femoral waveform can be measured (99). The arterial

tree length is estimated by measuring the distance between the carotid and the femoral notch.

Figure 1.12. Assessment of PWV (left) and central BP (right) using arterial applanation tonometry. P1, first systolic peak; P2, second systolic peak; PP, pulse pressure; AIx, augmentation index. Adapted from Coutinho *et al*, 2014 (100).

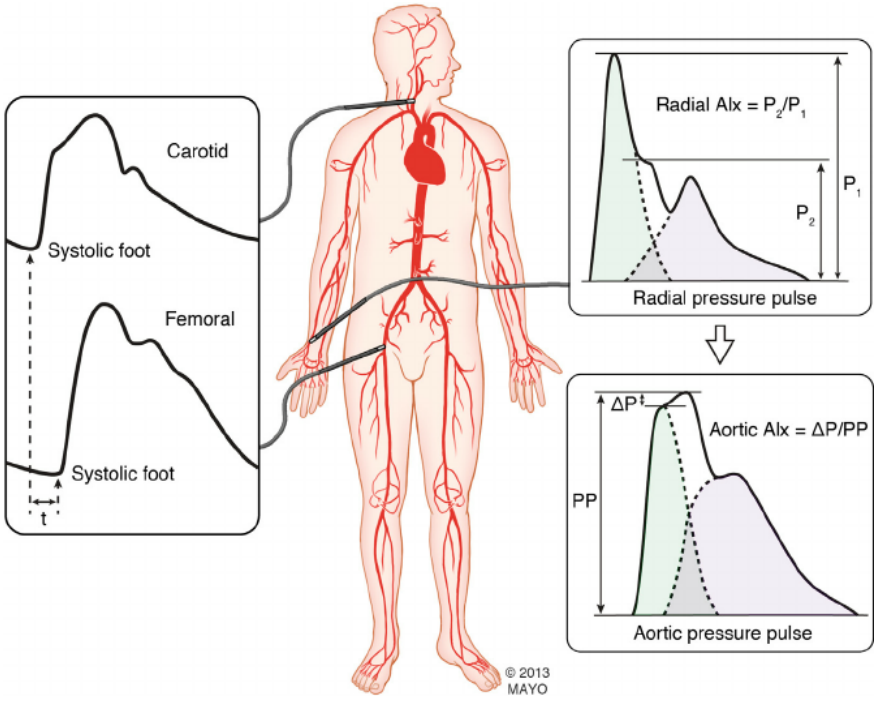

In summary, the development and progression of LVH in hypertensives is characterized by complex mechanical and non-mechanical mechanisms. HHD is an important predictor of cardiovascular morbidity and mortality, even at subclinical stages of disease. It is therefore crucial to understand the pathophysiology of HHD and to dispose of techniques for the early detection of LVH and cardiac dysfunction in order to initiate or intensify treatment and ultimately improve patient outcome.

2. Hypothesis and objectives

2.1. Hypothesis

Hypertensive heart disease is characterized by a disproportionate growth of the left ventricle that involves all cardiac cell types. Cardiac magnetic resonance imaging has become the gold standard for non-invasive measurement of cardiac geometry and function. In addition, novel cardiac magnetic resonance imaging techniques have shown potential in estimating preclinical dysfunction of the left ventricle, with strain analysis, and quantification of diffuse cardiac fibrosis, withT1 mapping. Molecular biomarkers of myocardial fibrosis and their breakdown products are promising tools for diagnosis and estimation of prognosis in heart failure patients.

The hypothesis of the present study is that cardiac magnetic resonance-derived measures of myocardial geometry, strain and fibrosis are related to vascular hemodynamics and molecular biomarkers of fibrosis in hypertensive patients with left ventricular hypertrophy.

2.2. Primary objective

- Investigate the relationship between CMR-assessed myocardial strain, cardiac fibrosis and molecular biomarkers of fibrosis in hypertensive subjects with positive ECG-derived criteria for LVH

2.3. Secondary objectives

- Investigate the association between peripheral hemodynamics with CMR-derived parameters of cardiac geometry, strain, fibrosis, and molecular biomarkers of fibrosis
- Investigate the association between central hemodynamics and arterial stiffness with CMR-derived parameters of cardiac geometry, strain, fibrosis, and molecular biomarkers of fibrosis
- Explore the independent factors associated with myocardial strain
- Explore the independent factors associated with cardiac fibrosis
- Investigate the association between molecular biomarkers of myocardial stretch and injury with vascular hemodynamics, CMR-derived cardiac geometry, strain, and fibrosis

3. Methods

3.1. Study design and study population

The present doctoral thesis integrated data obtained from 2 different baseline studies conducted in the Hypertension Unit of the Department of Internal Medicine, Clinical University Hospital of Valencia, Spain. The baseline studies were:

1. "Validación de la técnica de mapeo T1 con cardioresonancia magnética para la cuantificación de la fibrosis miocárdica difusa", conducted under the direction of Prof. Josep Redón and approved by the Ethics Committee of the Clinical University Hospital of Valencia on January 30th 2014.
2. "Relación entre los biomarcadores de Fibrosis Cardíaca y la función de los grandes vasos en una población hipertensa con miocardiopatía hipertensiva", conducted under the direction of Dr. Fernando Martínez and approved by the Ethics Committee of the Clinical University Hospital of Valencia on March 27th 2014.

The Hypertension Unit of the Department of Internal Medicine, Clinical University Hospital of Valencia, is staffed by specialists in clinical HTN and receives patients referred by primary care physicians in the event of difficult-to-manage HTN.

3.1.1. Inclusion criteria

1. Caucasian race
2. Age from 40 to 60 years
3. Essential hypertension according to the ESH (101)
4. ECG criteria for LVH according to the Sokolow-Lyon voltage criteria or the Cornell voltage criteria
5. Signed informed consent

3.1.2. Exclusion criteria

1. Secondary hypertension
2. Known cardiac arrhythmia or anti-arrhythmic drug treatment
3. Known structural cardiac disease other than LVH

4. Known heart failure
5. Obesity class III (body mass index > 40kg/m^2)
6. Chronic kidney disease stage 3A or higher (estimated glomerular filtration rate < 60ml/min/1.73m^2)
7. Active treatment with non-steroidal anti-inflammatory drugs
8. Current alcohol consumption higher than 30g/day in men and 20g/day in women
9. Known hypersensitivity to gadolinium-based contrast
10. Known claustrophobia
11. Pregnancy or lactation
12. Inability to fully comprehend and/or perform study procedures

The present study was approved by the Ethics Committee of the Clinical University Hospital of Valencia on October 27th 2016.

3.2. Clinical parameters and peripheral hemodynamics

Body composition and peripheral BP values were obtained as previously published (99). Weight and height were assessed with precise scales while the individuals were without shoes and with light clothing. Body mass index (BMI) was calculated using the following formula 'weight (kg) divided by height (m^2)'. Measurement of waist circumference was performed in the horizontal plane of the superior border of the iliac crest.

Office BP was measured using a semiautomatic device (OMRON M-6) with the use of an appropriate cuff according to the circumference of the non-dominant arm. Measurements followed the recommendations of the ESH (101). Briefly, BP was measured in a quiet room in a seated position. The patient did not smoke or take any stimulant substance during the 2 hours prior to BP assessment. 3 measurements were taken with a minimum of 3-minutes intervals. The average of the last 2 measurements was considered the real BP value of the patient. When large differences existed among them, additional measurements were performed. Patients were classified as hypertensive or normotensive according to ESH guidelines. Pulse pressure was

calculated by subtracting diastolic BP from systolic BP. Mean arterial pressure was calculated by doubling diastolic BP, adding the sum to systolic BP and then dividing by 3.

3.3. Central hemodynamics

Central BP and PWV were assessed using the SphygmoCor device (AtCor Medical, Australia) as previously reported (98). Measurement was performed in a quiet room and patients were instructed to avoid large meals, smoking, caffeine and vasoactive medication the 3 hours prior to assessment of central hemodynamic parameters. After 10 minutes of rest in supine position, peripheral BP was recorded using the OMRON M6 device with a minimum interval of 3 minutes to examine hemodynamic steadiness.
For the assessment of central BP, radial artery pressure waveforms were obtained with the participants in the supine position from a 10 s epoch. A central aortic BP waveform was reconstructed from the radial artery pressure waveforms using a generalized validated transfer function (102) (figure 3.1).

Figure 3.1. Sample of radial artery pressure waveform and derived central (aortic) pressure waveform.

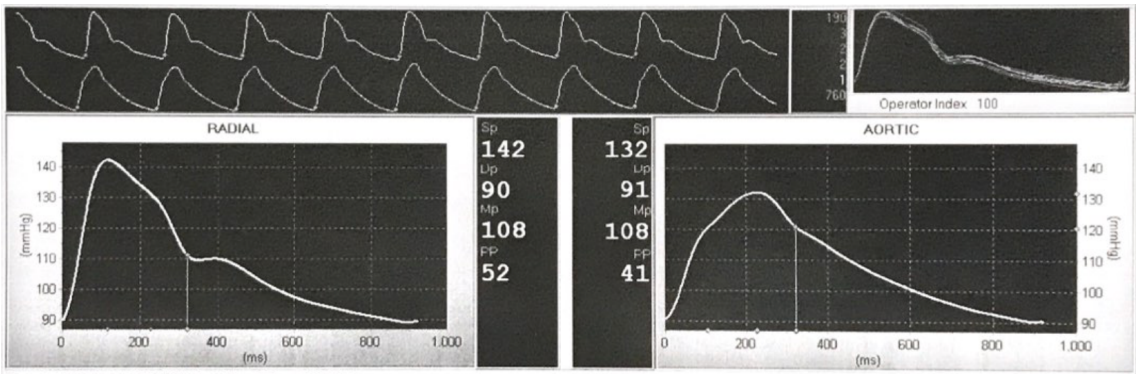

PWV was determined by sequentially recording ECG-gated carotid and femoral artery pressure waveforms. A total of 10 s of high-quality waveforms was captured for each reading. The intersecting tangents algorithm was applied to determine the foot-to-foot

transit time using the integrated software and the R wave as a reference frame. The length of the arterial segment was estimated by subtracting the distance from the carotid location to the suprasternal notch from the distance between the suprasternal notch and the femoral site of measurement. PWV was calculated as the ratio of distance (D) to transit time (T) (figure 3.2).

Figure 3.2. Sample of carotid-femoral pulse wave velocity assessment.

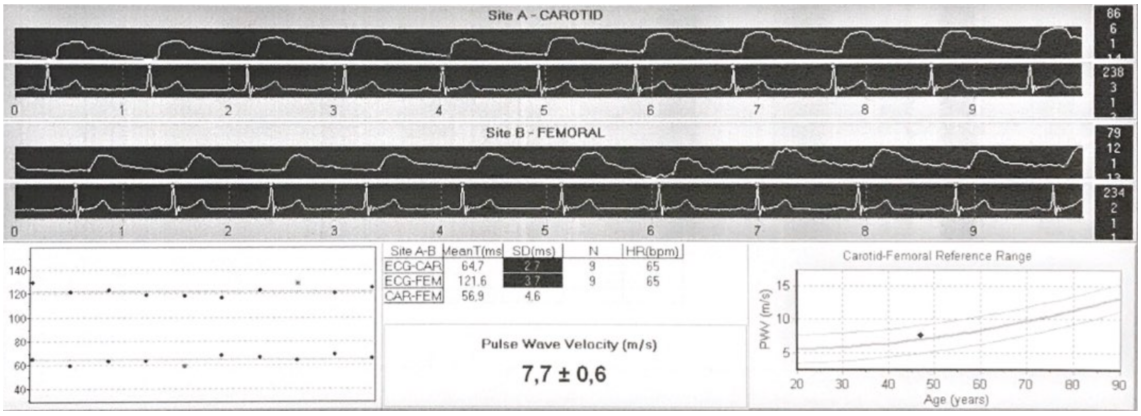

3.4. 24-hour ambulatory blood pressure monitoring

24-hour ambulatory blood pressure monitoring (ABPM) was performed using a Spacelabs 90207 oscillometric monitor (Spacelabs Healthcare, USA) on a regular working day during the usual intake of BP-lowering treatment. Recording began between 8:30 and 9 AM, readings were taken every 20 minutes from 6 AM until midnight and every 30 minutes from midnight to 6 AM. Reliability of BP values measured with the monitor were checked against simultaneous measurement with a semiautomatic device (OMRON M-6) before beginning of recording, differences between devices < 5 mmHg were allowed. Mean 24-hour systolic and diastolic BP values were calculated as the average of systolic and diastolic BP values obtained during a total of 24 hours (figure 3.3).

Figure 3.3. Sample of 24-hour ambulatory blood pressure monitoring.

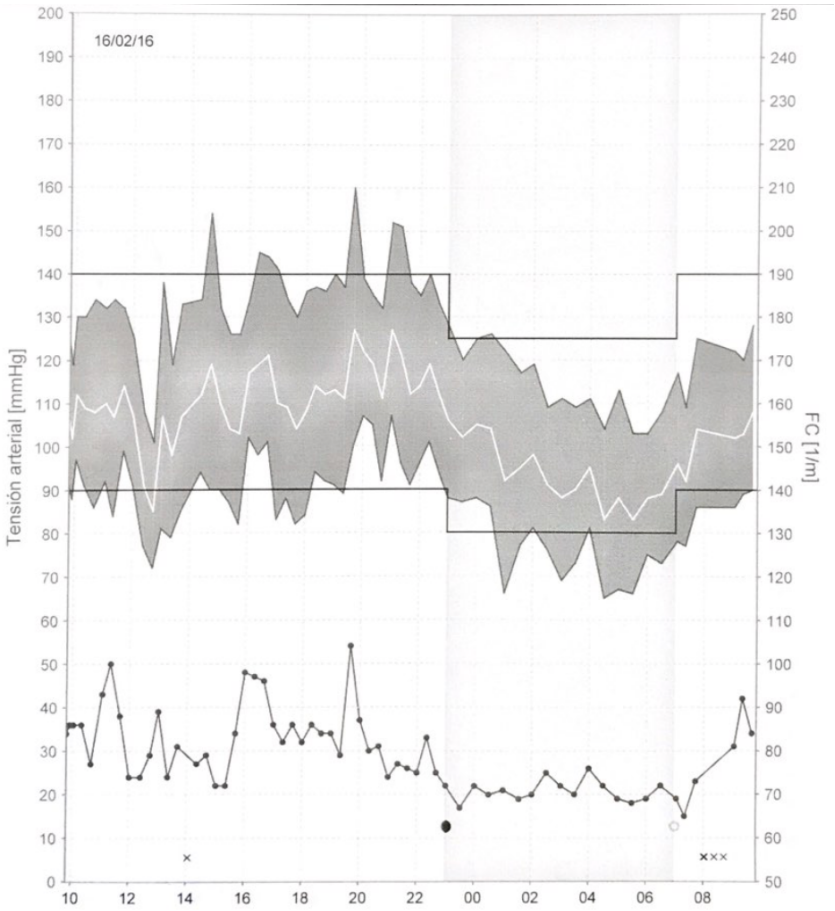

3.5. Electrocardiography

Standard 12-lead electrocardiograms were recorded by skilled ECG technicians at 25 mm/s and 1 mV/cm according to standard American Heart Association recommendations and their results were interpreted by 2 physicians (103). Sokolow-Lyon index was calculated as the sum of the amplitude of the S wave in V1 and the greatest R wave in either V5 or V6 (104). Cornell voltage was calculated as the sum of the R wave in aVL plus the S wave in V3 (105). LVH was defined as Sokolow-Lyon index greater than 3.5 mV, or Cornell voltage greater than 2.8 mV in men and 2.0 mV in women (figure 3.4).

Figure 3.4. ECG sample. LVH with strain pattern, positive Sokolow-Lyon criteria and positive Cornell voltage criteria.

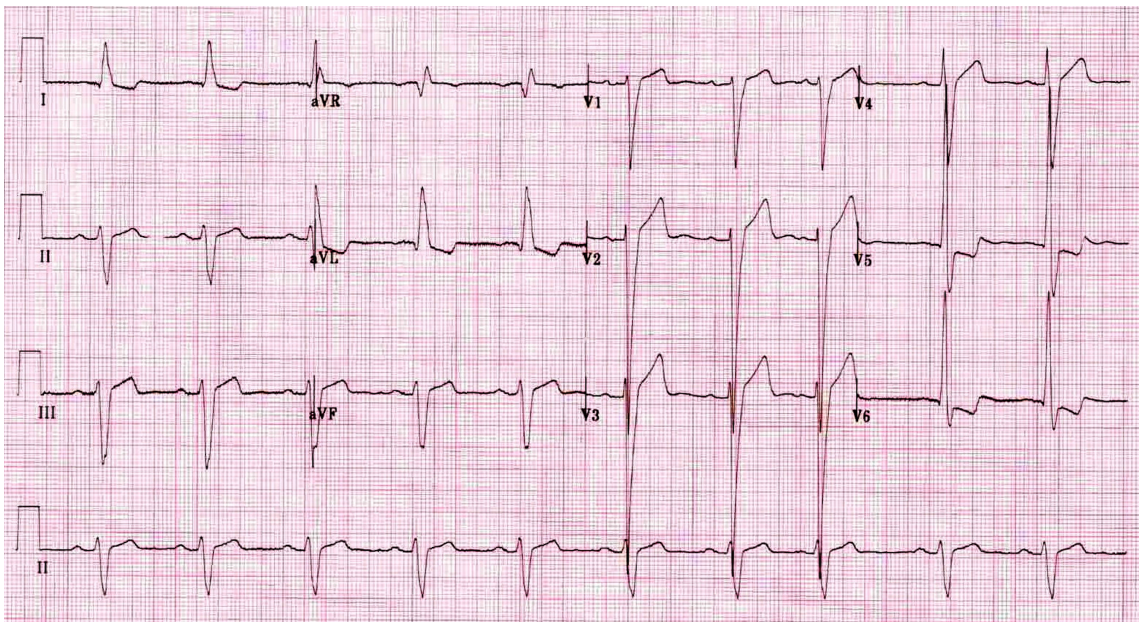

3.6. Transthoracic echocardiography

TTE was performed using a commercially available ultrasound system (Aloka Pro-Sound alpha 10, Hitachi Healthcare, Japan) in the left lateral decubitus position and reviewed offline by 2 readers. Standard parasternal and apical views were used to assess cardiac geometry, systolic function and diastolic function (figure 3.5). M-Mode echocardiography was used to measure cardiac dimensions and wall thickness. Interventricular and posterior LV wall thickness were measured by American Society of Echocardiography recommendations (106). LV mass was obtained by an anatomically validated formula and normalized for body surface area (BSA) for the assessment of LV mass index (78). LV volumes were estimated from linear dimensions by the z-derived method and used to derive stroke volume (107). Ejection fraction (EF) was calculated dividing stroke by end-diastolic volume. Preserved systolic function was defined as EF > 50 %. LV diastolic function was evaluated by Doppler interrogation. Transmitral early (E) and late (A) LV filling velocities were measured at the mitral valve leaflet tips and used to compute the early peak rapid filling velocity to peak atrial filling velocity ratio (E/A ratio). Similarly, deceleration time (DT) of early diastolic LV filling was calculated. Tissue

Doppler echocardiography was used to assess peak early diastolic velocity (e´) at the septal ring of the mitral valve. Diastolic dysfunction was defined as alteration of either E/A ratio, deceleration time or E/e´ compared to reference values established by the American Society of Echocardiography and the European Association of Cardiovascular Imaging (108).

Figure 3.5. Sample of LV mass assessment in parasternal long axis view.

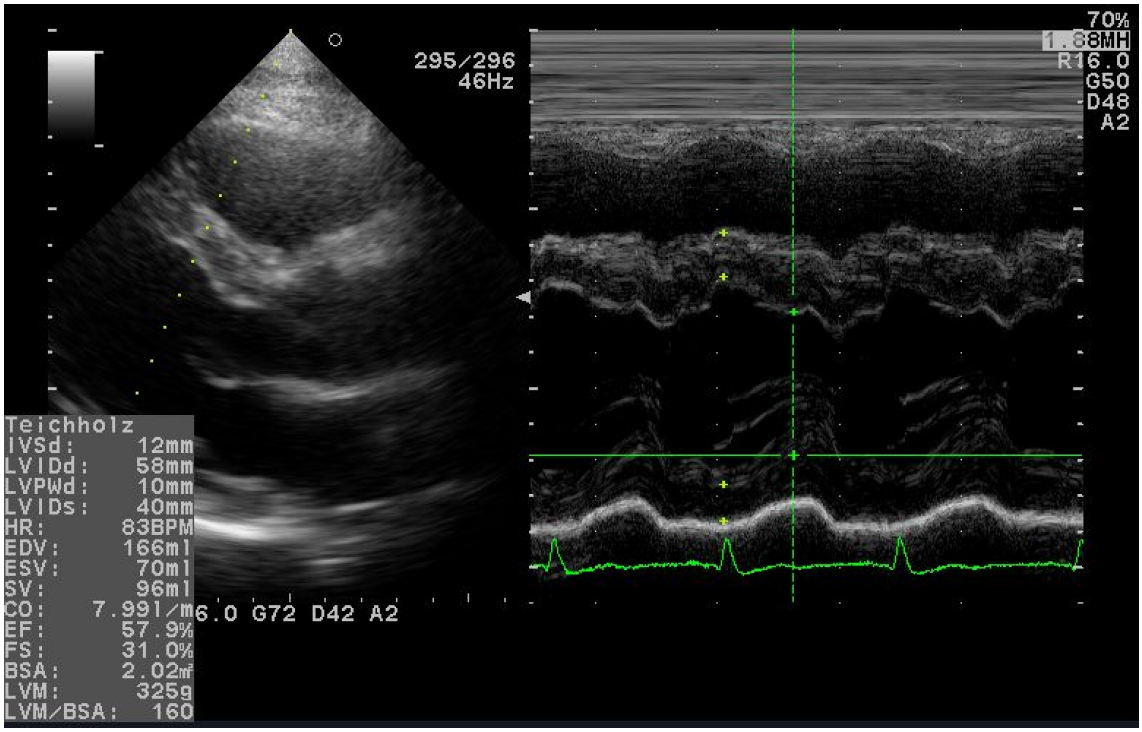

3.7. Cardiac magnetic resonance

CMR was performed on a 3T scanner (Tx, Philips, The Netherlands) using front and back surface coils and retrospective ECG triggering for capture of the entire cardiac cycle including diastole. Balanced-SSFP end-expiratory breath-hold cines were acquired in the vertical and horizontal long axis planes, with subsequent contiguous short-axis cines from the atrioventricular (AV) ring to the apex and acquisition of 2-chamber, 4-chamber and 3-chamber view cines (figure 3.6). Slice thickness was 7 mm. Typically 40 phases were acquired in each cine sequence and the average temporal resolution was 21±1.5 ms. Sequence parameters included TR/TE 3.2/1.6 ms, matrix 256x90, voxel size

1.6x1.5x7 mm, flip angle 50◦, acquisition time 12 s. Cine sequences with the same parameters were also used to acquire an atrial short axis stack, from the AV ring to the base of the atria.

For T2 mapping analysis, balanced-SSFP T2 prep sequences were acquired in 3 short axis slices (basal, middle, apical levels). For T1 mapping analysis, shMOLLI sequences were also acquired in 3 short axis slices (basal, middle, apical levels) before contrast administration. This acquisition was repeated in the same orientations 15 minutes after contrast administration.

Rest first pass myocardial perfusion images were acquired by using a saturation prepared gradient-echo sequence (TR/TE/matrix/spatial resolution of 2.8ms/1.2ms/190x128/2.8x2.0x7mm), in 3 ventricular short-axis sections during administration of a gadolinium bolus (0.1mM/kg).

Segmented inversion-recovery sequences (IR-FISP) were acquired for detection of LGE, starting at least 5 minutes after contrast administration in the same views as the cines (TR/TE/matrix/segments = 6.2ms/3.1ms/240x210/25). The TI was adjusted to the value required to null the signal from the healthy myocardium. In case LGE was detected, the same sequence with swapped phase encoding direction and different TI would be repeated to rule out artefacts.

Figure 3.6. Main CMR views and corresponding appearance on SSFP sequences. Adapted from Ginat *et al*, 2011 (109).

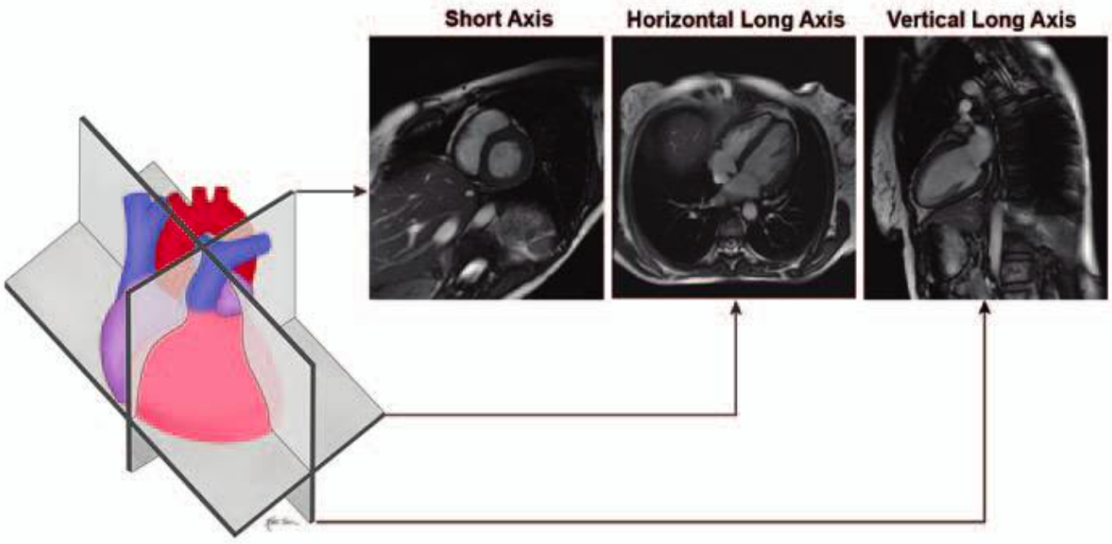

3.7.1. Cardiac geometry

All images were analysed with a dedicated software (Medis, Leiden, The Netherlands) by an observer with more than 10-year experience in CMR (figure 3.7). The following variables were quantified: LV end-diastolic (EDV) and end-systolic (ESV) volumes, LV mass, segmental LV wall thickness, LA dimension and volumes. Regional wall motion abnormalities and myocardial oedema were investigated. Myocardial perfusion was visually assessed. Localization, pattern of transmural extent and quantification of LGE were evaluated.

Figure 3.7. Sample of LV geometry assessment using Medis software.

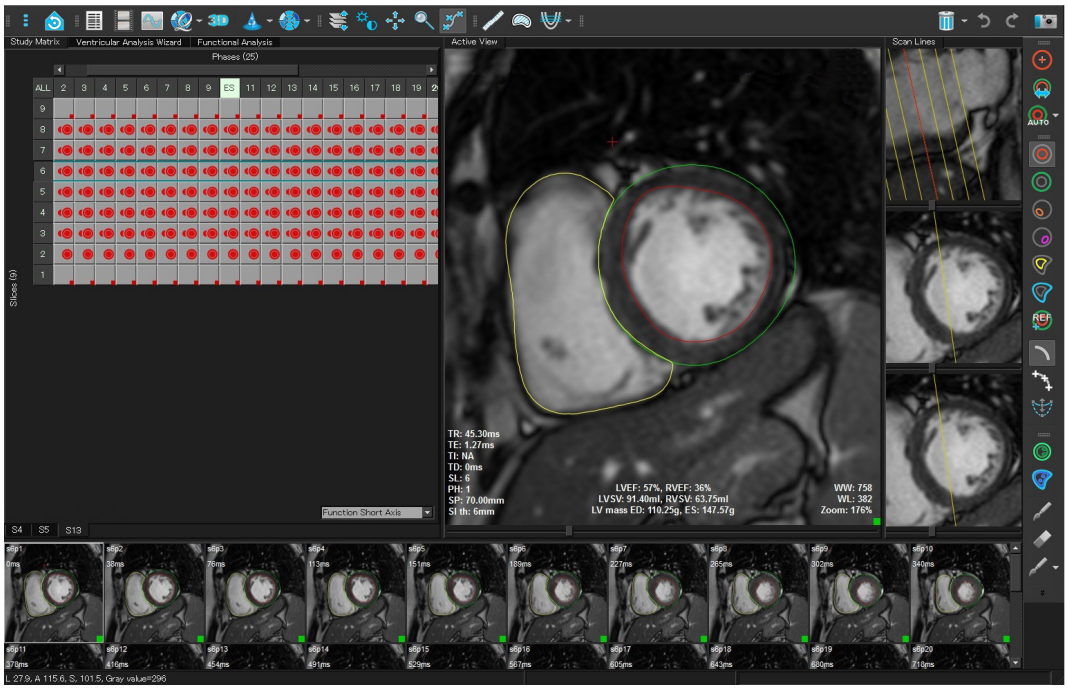

3.7.2. Myocardial strain and left atrial function

For the assessment of myocardial strain, a surrogate for LV function, images were analysed with a dedicated CMR-FT analysis software package (CVI42, Circle Cardiovascular Imaging Inc., Canada) that allows for the measurement of 2-dimensional strain derived parameters based on user definition of myocardial borders on standard cine SSFP images (figure 3.8).

Figure 3.8. Strain assessment. From long-axis 4-chamber cine image (A), longitudinal strain was obtained (B). Short-axis cine image (C) was used for calculation of circumferential (D) and radial (E) strain. Adapted from Scatteia *et al* (82).

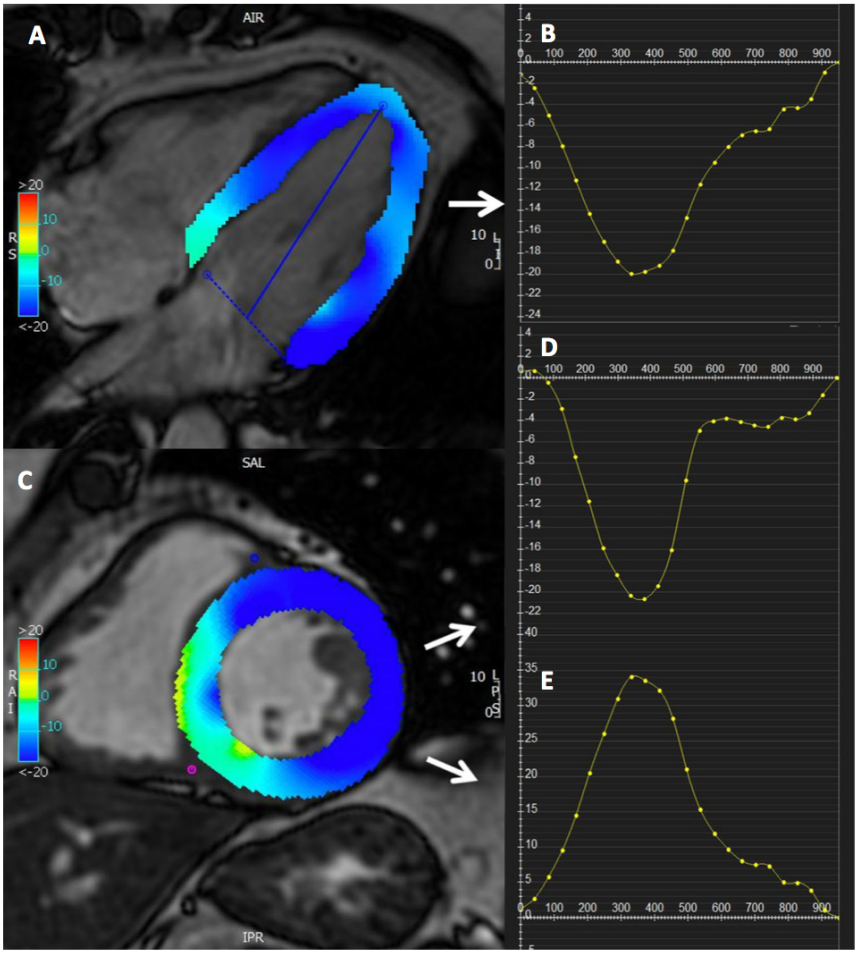

For the short axis stack analysis, all the short axis slices showing the endocardial cavity entirely surrounded by myocardium through all the phases along the cardiac cycle were included, thus avoiding the distortion due to the LV outflow tract in very basal slices. For long axis analysis, 2-chamber, 4-chamber and 3-chamber cines were used.

Endocardial and epicardial borders were manually drawn at end-diastole in all short and long axis cines, excluding papillary muscles from the endocardial contour. An automated tracking algorithm was applied in all the cine sequences throughout the cardiac cycle. Tracking performance was visually reviewed in all the slices to ensure accurate tracking. Tracing of the myocardial borders was manually adjusted in case of inadequate automated border tracking.

Long-axis cines were tracked to derive longitudinal strain parameters; short-axis cines were used to derive circumferential and radial strain parameters.
Segmental and global peak systolic radial, circumferential and longitudinal strains were quantified. Global peak systolic radial, circumferential and longitudinal strain rates were also registered.

LA reservoir function was assessed using the volumetric method (110). LA total emptying volume was calculated by subtracting the minimal LA volume at the closure of the mitral valve from the maximal LA volume just before the opening of the mitral valve. LA total emptying fraction was calculated by dividing the LA total emptying volume by the maximal LA volume just before the opening of the mitral valve.

3.7.3. Cardiac fibrosis

Partition coefficient and extracellular volume fraction were assessed according to the Society for Cardiovascular Magnetic Resonance (SCMR) and CMR Working Group of the ESC consensus statement (111). T1 and T2 were quantified in the short axis slices using the 16-segment model. Both segmental, average slice value and average global value for the whole LV myocardium were obtained for T2, native T1 and post-contrast T1 (figure 3.9). Gadolinium-based contrast agents are distributed throughout the extracellular space and shorten T1 relaxation times of the myocardium proportional to the local concentration of gadolinium, therefore, areas of fibrosis will exhibit shorter T1 relaxation times. The assessment of the partition coefficient requires the measurement of myocardial and blood T1 before (native T1 myo and native T1 blood, respectively) and after (post T1 myo and post T1 blood, respectively) administration of the contrast agent. Partition coefficient was calculated using the following formula:

$$Partition\ coefficient = \frac{\frac{1}{post\ T1\ myo} - \frac{1}{native\ T1\ myo}}{\frac{1}{post\ T1\ blood} - \frac{1}{native\ T1\ blood}}$$

In-house reference values for T1 in myocardium in a set of 50 healthy subjects were 952 ± 9 ms and 536 ± 6 ms for native T1 and post-contrast T1, respectively.

For the assessment of ECV, the cellular fraction of blood is required, which is represented by the hematocrit. ECV was calculated using the formula:

$$ECV = (1 - hematocrit) * partition\ coefficient$$

Figure 3.9. Sample of native T1 and post-contrast T1 assessment in myocardium and blood for calculation of partition coefficient and ECV.

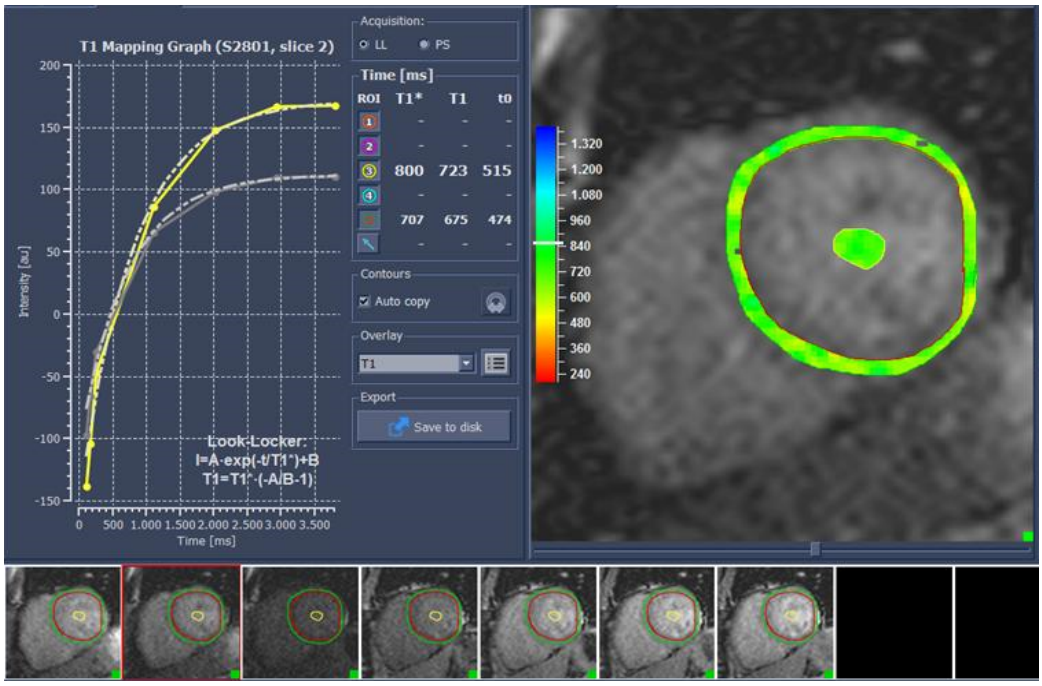

ECV and the partition coefficient reflect the expansion of the ECM. In the present study, individuals with structural cardiac disease other than LVH (e. g. infiltrative disease, ischemic cardiomyopathy) were excluded. As a consequence, ECV and the partition coefficient were considered as imaging markers of cardiac fibrosis.

3.8. Laboratory procedures and molecular biomarkers

Laboratory analyses were performed on blood samples obtained under fasting conditions after 30 minutes of supine rest. Plasma glucose and serum sodium, potassium, creatinine and lipoproteins were measured using standard enzymatic automated methods.
For the determination of molecular biomarkers, blood samples were immediately centrifuged at +4°C, and serum and plasma were frozen at -80°C until further analysis.

3.8.1. Molecular biomarkers of myocardial fibrosis

Serum PICP was assessed using a sandwich enzyme linked immunosorbent assay (ELISA) (METRA EIA kit; Quidel Corporation, USA). The lower limit of detection was 0.2 μg/L. The inter-assay and intra-assay coefficients of variation were 6.3% and 6.4%, respectively. The minimum analytical detection limit was 1 μg/L.

PIIINP was measured using radioimmunoassay (Orion Diagnostica, Finland). The inter-assay and intra-assay coefficients of variation were 7.2% and 4.1%, respectively. The lower detection limit was 0.30 μg/L.

CITP was assessed using a quantitative enzyme immunoassay (Orion Diagnostica, Finland). The inter-and intra-assay variations were 7.5% and 9.8%, respectively. The lower detection limit was 0.30 μg/L.

MMP-1 was assessed using a 2-site ELISA method with a monoclonal antibody to human MMP-1 (Human Biotrack ELISA System; Amersham Biosciences Corp, USA). The inter- and intra-assay variations were 12% and 6.8%, respectively. The minimum analytical detection limit was 1.7ng/ml.

The CITP/MMP-1 ratio, of collagen type I crosslinking, was calculated dividing CITP by MMP-1 levels adjusted by osmolarity.

3.8.2. Molecular biomarkers of myocardial stretch and injury

Hs-Troponin T and NT-proBNP were assessed with the use of the Elecsys® 2010/cobas e™ 601 analyzer (Roche Diagnostics). Both biomarkers were measured using immunoassays based on a one-step sandwich principle with electrochemoiluminescent relevation.

NT-proBNP was assessed using the Elecsys® proBNP II STAT assay, following the instructions of the manufacturer. The assay contains 2 monoclonal antibodies which recognize epitopes located in the N-terminal part (1-76) of proBNP (1-108) and has an analytical range from 5 to 35,000 pg/ml.

Hs-Troponin T was assessed with the Elecsys® Troponin T hs STAT assay, following the instructions of the manufacturer. The assay employs 2 monoclonal antibodies specifically directed against human cardiac troponin T which recognize 2 epitopes (amino acid positions 125-131 and 136-147) located in the central part of the cardiac troponin T protein. It has an analytical range from 3 to 10,000 ng/L, a 99^{th} percentile cut-off point of 14 ng/L, and a coefficient of variation of < 10% at 13 ng/L.

3.9. Statistical analysis

Statistical analysis was performed using Stata/MP 14.1 for Mac (StataCorp LLC, USA). Clinical, BP-related and CMR-derived variables were presented as mean ± standard deviation (SD), and biomarker concentrations were presented as median (interquartile range). Differences between the total study population and individuals with complete dataset were checked for using *t* tests on the equality of means for continuous variables and Pearson's chi-squared for categorical variables. Shapiro-Wilk test for normality was performed for all continuous variables. Asymmetrically distributed variables were log-transformed for statistical analysis of association.

In univariate analysis, the Pearson product-moment correlation coefficients (*r*) between all variables of peripheral and central hemodynamics, CMR-derived data and molecular biomarkers were determined in order to assess the relationship between available variables and identify potential predictors of outcomes of interest.

For multivariate analysis, multiple linear regression analysis with CMR-derived cardiac geometry, strain, fibrosis and molecular biomarkers as the dependent variables were performed using 2 different models: Model 1 was constructed using gender, age and variables with $p < 0.1$ for the observed relationships in univariate analysis as the independent variables. Model 2 further contained height, weight, heart rate and mean 24-hour systolic BP among the independent variables in order to control for parameters that are known determinants of vascular hemodynamics and cardiac function. Regression models with statistically significant associations in model 2 are presented in tables. Models are not shown for variables with marginal or significant association in univariate analysis but $p > 0.5$ for the same comparison in fully adjusted models. Regression lines and scatter plots of independently associated variables were plotted in order to graphically visualize the relationship among variables of interest. Multicollinearity was checked for calculating the variance inflation factor (VIF) for each regression model. The VIF is an index which measures how much variance of an estimated regression coefficient is increased because of multicollinearity. VIF values greater than 5 indicate that the associated regression coefficients are poorly estimated because of multicollinearity (112).

A two-sided p-value of less than 0.05 was considered statistically significant throughout the manuscript.

4. Results

4.1. Characteristics of the study population and the variables of interest

4.1.1. Study population

4.1.1.1. Clinical and biochemical characteristics

A total of 49 participants was initially included into the present study. 9 individuals refused to undergo CMR for personal reasons after informed consent was obtained, consequently, CMR was performed in 40 individuals. One patient was excluded for statistical analysis due to technical problems and resulting bad quality of the obtained images, one patient due to presence of myocardial infarction in CMR-obtained images, one patient due to detection of apical hypertrophic cardiomyopathy and one patient due to onset of nephropathy (eGRF < 60ml/min/m^2), leaving a total study population of 46 individuals and a total of 36 individuals with available CMR-derived data of cardiac geometry for statistical analysis.

Feature tracking analysis for assessment of myocardial strain measures was performed in 33 patients, and T1 mapping for assessment of cardiac fibrosis was performed in 29 patients. These techniques require additional exploration time and could not be performed in all patients due to technical issues or lacking of patient compliance.

The clinical characteristics of the study population are shown in table 4.1. The total study population consisted mainly of male participants (85%). Overweight and obesity were predominant among participating individuals (mean BMI 30.3 kg/m^2): 5 individuals (11%) had normal weight, 19 individuals (41%) had overweight and 22 individuals (48%) had obesity. Nearly 75% of participating individuals were active or former smoker. In terms of cardiovascular risk factors, HTN was present in all subjects, diabetes mellitus in 28.3% and dyslipidaemia in 78.3% of the participants. All participants were free of overt cardiovascular events at study enrollment.

Table 4.1. Clinical characteristics of the study population.

	Total study population (n=46)	Participants with CMR (n=36)	Participants with T1 mapping (n=29)
Age, ys	50.5 ± 5.5	50.6 ± 4.3	50.1 ± 4.3
Gender, male	39 (85)	30 (83)	23 (79)
Weight, kg	88.9 ± 15.2	89.4 ± 15.8	89.4 ± 15.6
Height, cm	171 ± 9.6	172.3 ± 10	172.4 ± 10.8
BMI, kg/m^2	30.3 ± 3.8	30 ± 3.9	30 ± 3.6
Waist circumference, cm	103 ± 11	101.5 ± 10.6	101.4 ± 9.2
Smoking status			
Current	21 (45.6)	16 (44.4)	15 (51.7)
Former	13 (28.3)	11 (30.6)	8 (27.6)
Never	12 (26.1)	9 (25)	6 (20.7)
Diabetes mellitus	13 (28.3)	10 (27.8)	8 (27.6)
Dyslipidaemia	36 (78.3)	29 (80.6)	23 (79.3)

Data are mean ± SD or Number (%).

Differences regarding clinical and biochemical characteristics between the total study population, the population with available CMR-derived data on cardiac geometry and the population with available T1-mapping were checked for using *t* test on the equality of means for continuous variables and chi-square test of independence for categorical variables. No significant differences were observed.

The biochemical characteristics of the total study population are shown in table 4.2.

Table 4.2. Biochemical characteristics of the study population (n=46).

	Mean ± SD	Reference values
Glucose, mg/dL	112.6 ± 20.6	64-106
Sodium, mmol/L	140.4 ± 2.6	135-145
Potassium, mmol/L	4.3 ± 0.4	3.5-5.1
Creatinine, mg/dL	0.92 ± 0.2	0.65-1.35
Total cholesterol, mg/dL	200.7 ± 48.2	140-200
Triglycerides, mg/dL	160.8 ± 99.5	40-160
HDL-cholesterol, mg/dL	50.6 ± 11.9	>35
LDL-cholesterol, mg/dL	128.8 ± 38.1	<130

4.1.1.2. Anti-hypertensive treatment

At study enrollment, all participants were under anti-hypertensive treatment (table 4.3). Regarding drug classes, all individuals were treated with an inhibitor of the renin-angiotensin system. More than half of the study population further received treatment with calcium channel blockers or diuretics. Approximately 85% of the study participants was treated with 2 or more BP-lowering drugs.

Table 4.3. Characteristics of BP treatment (n=46).

	Number (%)
Drug class	
ACE inhibitor	6 (13)
AR blocker	41 (89.1)
Ca channel blocker	27 (58.7)
Diuretic	25 (54.4)
Beta-blocker	10 (21.7)
Alpha-blocker	10 (21.7)
Number of drugs	
1	7 (15.2)
2	14 (30.4)
3	16 (34.8)
4	4 (8.7)
5	4 (8.7)
6	1 (2.2)

4.1.2. Peripheral and central hemodynamics

Office BP, 24-hour, central BP and PWV were assessed in all participants (table 4.4). BP control was poor in the study population: 29 individuals (63%) had office SBP values greater than 140mmHg or office DBP values greater than 90mmHg, 31 individuals (67%) had mean 24-hour SBP values greater than 130mmHg or mean 24-h DBP values greater than 80mmHg, and 27 individuals (59%) had central SBP values greater than 135mmHg or central DBP values greater than 85mmHg. Regarding arterial stiffness, 9 individuals (20%) had PWV values greater than 10 m/s, a cutoff established as a conservative

estimate of significant alterations in aortic function in middle-aged hypertensive individuals (101).

Table 4.4. Peripheral and central hemodynamics of the study population (n=46).

	Mean ± SD
Office systolic BP, mmHg	140 ± 19.6
Office diastolic BP, mmHg	92.5 ± 12.8
HR, bpm	73.2 ± 13.1
PP, mmHg	47.6 ± 12.1
MAP, mmHg	108.3 ± 14.3
Mean 24-h systolic BP, mmHg	131.1 ± 16.6
Daytime 24-h systolic BP, mmHg	134.1 ± 16.3
Nighttime 24-h systolic BP, mmHg	123.4 ± 18.5
Mean 24-h diastolic BP, mmHg	83.5 ± 8.8
Daytime 24-h diastolic BP, mmHg	86.8 ± 9
Nighttime 24-h diastolic BP, mmHg	76 ± 10
Mean 24-h HR, bpm	74.5 ± 12.1
Daytime 24-h HR, bpm	77.9 ± 12.8
Nighttime 24-h HR, bpm	66.1 ± 11
Central systolic BP, mmHg	129.8 ± 19.2
Central diastolic BP, mmHg	93.7 ± 12.5
Central PP, mmHg	36.2 ± 11.4
Central MAP, mmHg	105.7 ± 14.1
Pulse wave velocity, m/s	8.6 ± 1.7

4.1.3. Transthoracic echocardiography

Table 4.5 shows the echocardiographic characteristics of cardiac geometry and function in the study population. Compared to reference values, all participants showed either increased LV wall thickness, increased LV mass or both, independent of gender. LVH defined as LV mass/BSA > 115 g/m^2 in men and > 95 g/m^2 in women, respectively, was present in 95% of male participants and in all women. All participants who underwent CMR (n=36) fulfilled TTE-derived criteria of LVH.

Systolic function defined as ejection fraction > 50% was preserved in all individuals. Echocardiographic signs of diastolic dysfunction were present in approximately 75% of the study participants: 12 patients (26%) had an E/A ratio lower than 0.8 or higher than 1.5, deceleration time was out of normal range in 30 participants (65%) and septal E´ velocity was altered in 36 individuals (78%).

Table 4.5. Echocardiography-derived parameters of cardiac geometry and function (n=46).

	Mean ± SD
Cardiac geometry	
Interventricular septum thickness, mm	12.8 ± 1.9
Posterior wall thickness, mm	11.9 ± 1.9
Relative wall thickness	0.47 ± 0.10
LV mass, g	307.7 ± 81.1
LV mass/BSA, g/m^2	153.3 ± 28
LV end-diastolic volume, ml	129.5 ± 34.5
LV end-systolic volume, ml	47.5 ± 20.2
LA diameter, mm	38.6 ± 7
Cardiac function	
Stroke volume, ml	81.8 ± 20.5
Ejection fraction, %	64.7 ± 8.3
Mitral E-velocity, cm/s	61.8 ± 12.6
Mitral A-velocity, cm/s	60.6 ± 11.7
E/A ratio	1.06 ± 0.3
Deceleration time, ms	235.2 ± 106.5
E´ velocity tissue doppler, cm/s	6.9 ± 1.5
E/E´ ratio	9.3 ± 2.8

4.1.4. Cardiac magnetic resonance

Table 4.6 shows the mean values and SD of CMR-derived data. Mean cardiac wall thickness parameters were in the upper limit of reference values. Likewise, mean LV mass was high in both men and women (mean LV mass was 183.6 g (SD 53.2 g) in men and 123.3 g (SD 16.2 g) in women; for the present CMR technique, reference values for LV mass were 108-184 g in men and 72-144 g in women, respectively).

Reference values for strain parameters have been published but depend heavily on the imaging technique used for the assessment of myocardial strain. However, longitudinal and circumferential strain have shown consistent results in healthy individuals (113). It is generally accepted that mean longitudinal strain lower than -17 % (i. e., higher absolute values than -17 %) and mean circumferential strain lower than -20 % (i. e., higher absolute values than -20 %) are considered as abnormal, whereas the establishment of reference values for radial strain is challenging due to higher inter- and intra- observer variability (114). In the present study, both mean longitudinal and mean circumferential strain were reduced compared to previously reported normal values in healthy populations (113).

Normal reference ranges for ECV and partition coefficient are not definitively established. In a multicentre setting using 3T scanners, normal values for ECV and the partition coefficient were defined as 0.26% ± 0.04 and 0.44 ± 0.07, respectively (115). In the present study, mean ECV was higher compared to available reference values in healthy individuals.

Table 4.6. CMR-derived parameters of cardiac geometry, function and fibrosis.

	Mean ± SD
Cardiac geometry (n=36)	
Interventricular septum thickness, mm	11.1 ± 2.5
Posterior wall thickness, mm	9.8 ± 2
LV mass, g	173.6 ± 53.8
LV end-diastolic volume, ml	161.6 ± 37.3
LV end-systolic volume, ml	53 ± 22
LA diameter, mm	36.2 ± 5.8
Cardiac function (n=33)	
Radial strain, %	32.3 ± 9.7
Circumferential strain, %	-17.5 ± 4.3
Longitudinal strain, %	-14.9 ± 4.2
LA total emptying volume, ml	53.2 ± 13.6
LA total emptying fraction, %	0.54 ± 0.09
Cardiac fibrosis (n=29)	
Extracellular volume fraction, %	0.31 ± 0.09
Partition coefficient	0.45 ± 0.05

4.1.5. Molecular biomarkers of cardiac fibrosis, stretch and injury

Molecular biomarkers of fibrosis were determined in 48 participants. 3 participants were excluded due to onset of nephropathy (n=1) or detection of structural cardiac disease other than LVH (n=2), leaving a total of 45 individuals for statistical analysis. A total of 8 study participants showed MMP-1 levels below the analytical detection limit. For statistical analysis, the minimum analytical detection limit of MMP-1 levels were used, a valid approach for MMP-1 levels with non-detects (116).

Assessment of circulating biomarkers of cardiac stretch and injury was performed in all 49 participating individuals, leaving a total of 46 individuals for statistical analysis after applying criteria of exclusion.

Table 4.7 and figure 4.1 show the concentration and distribution of circulating biomarkers in the study population, respectively. None of the included biomarkers was normally distributed.

Table 4.7. Biomarker concentration in the study population (n=45).

	Median (interquartile range)
Fibrosis (n=45)	
PICP, µg/L	69.4 (63.4, 91.8)
PIIINP, µg/L	3 (2.2, 3.4)
CITP, µg/L	6.2 (5.1, 7)
MMP-1, µg/L	8.6 (5.3, 18.7)
CITP/MMP-1	2.6 (1.2, 3.4)
Myocardial stretch (n=46)	
NT-proBNP, pg/ml	48.5 (21, 85.5)
Myocardial injury (n=46)	
Hs-Troponin T, pg/ml	8.1 (6.5, 10.4)

Figure 4.1. Biomarker distribution and normal density in the study population (n=45).

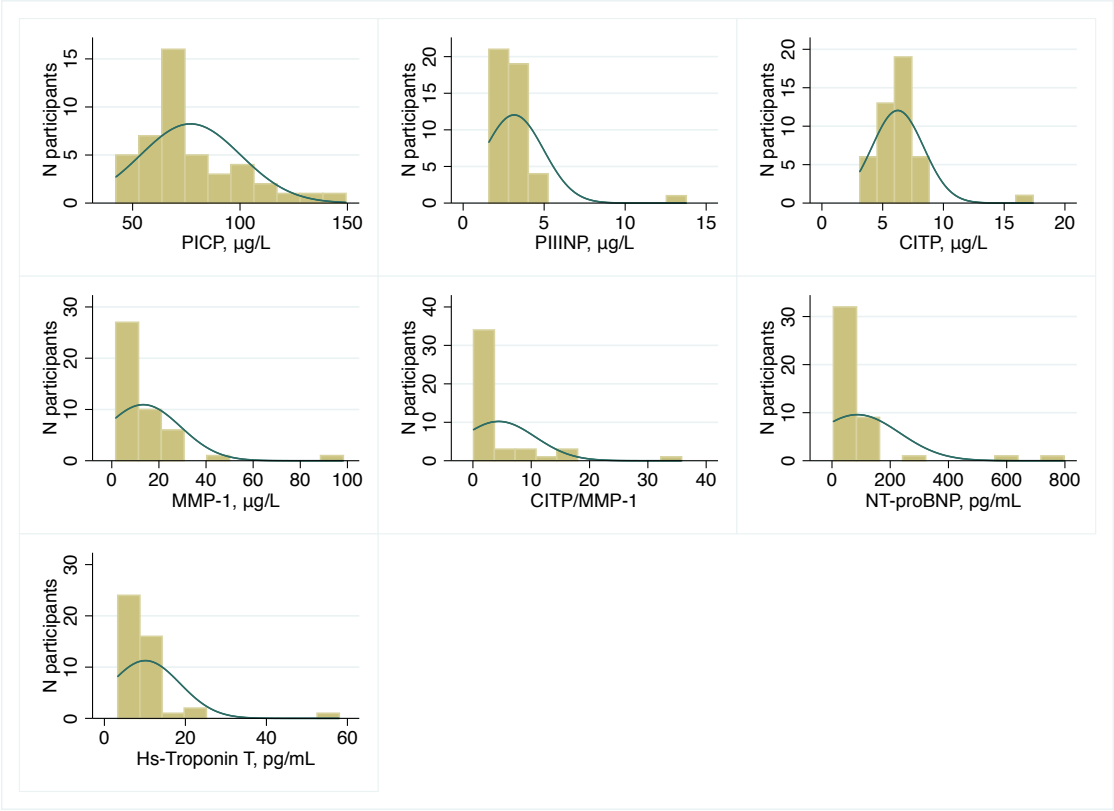

4.2. Association among analyzed parameters

The relationship between parameters from vascular hemodynamics, CMR-derived measures and molecular biomarkers were explored using Pearson´s correlation coefficients.

4.2.1. Peripheral hemodynamics, CMR-derived measures and circulating biomarkers

24-hour systolic BP was related to LV geometry (table 4.8). Higher 24-hour systolic BP values were significantly associated with greater LV mass, in addition, there was a trend towards greater LV posterior wall thickness.

Myocardial strain and 24-hour systolic BP were marginally related, a trend to higher 24-hour BP levels when radial strain increased was observed. Both office and 24-hour systolic BP were inversely related to LA emptying fraction: the higher the central and peripheral systolic BP, the lower the LA reservoir function.

Office BP values were not related to CMR-assessed measures of cardiac fibrosis. In contrast, 24-hour systolic BP was significantly associated with circulating biomarkers of fibrosis (ratio CITP/MMP-1).

Table 4.8. Pearson's correlation coefficients among peripheral hemodynamics, CMR-derived measures and biomarkers.

	Office SBP, mmHg	24h-SBP, mmHg
Cardiac geometry (n=36)		
Interventricular septum, mm	-0.01	0.21
Posterior wall, mm	0.01	**0.33°**
LV mass, g	0.10	**0.36***
LV end-diastolic volume, ml	0.15	0.07
LV end-systolic volume, ml	-0.04	-0.18
LA diameter, mm	0.18	0.22
Cardiac function (n=33)		
Radial strain, %	0.22	**0.30°**
Circumferential strain, %	-0.19	-0.27
Longitudinal strain, %	-0.02	-0.08
LA total emptying volume, mL	-0.06	-0.15
LA total emptying fraction, %	**-0.38***	**-0.51****
Cardiac fibrosis (n=29)		
Extracellular volume fraction, %	-0.01	-0.10
Partition coefficient	-0.11	0.18
Biomarkers (n=45)		
PICP, µg/L	0.18	0.05
PIIINP, µg/L	-0.01	0.06
MMP-1, µg/L	0.02	-0.1
CITP, µg/L	0.15	0.13
CITP/MMP-1	0.02	0.13
NT-proBNP, pg/ml	0.09	0.25
Hs-Troponin T, pg/ml	0.08	0.19

** p<0.01; * p<0.05; ° p<0.1

4.2.2. Central hemodynamics, CMR-derived measures and circulating biomarkers

No significant relationship between central systolic BP and cardiac geometry, function, fibrosis or biomarkers was found (table 4.9). However, a trend to higher radial strain when central systolic BP values increased was observed.

Table 4.9. Pearson's correlation coefficients among peripheral hemodynamics, CMR-derived measures and biomarkers.

	Central SBP, mmHg	PWV, m/s
Cardiac geometry (n=36)		
Interventricular septum, mm	-0.14	0.18
Posterior wall, mm	-0.10	**0.34°**
LV mass, g	-0.09	0.10
LV end-diastolic volume, ml	0.03	-0.12
LV end-systolic volume, ml	-0.07	**-0.35***
LA diameter, mm	0.06	0.14
Cardiac function (n=33)		
Radial strain, %	**0.30°**	**0.34°**
Circumferential strain, %	-0.25	**-0.32°**
Longitudinal strain, %	-0.18	-0.29
LA total emptying volume, ml	-0.09	-0.14
LA total emptying fraction, %	-0.28	-0.08
Cardiac fibrosis (n=29)		
Extracellular volume fraction, %	-0.13	**-0.36°**
Partition coefficient	-0.16	0.06
Biomarkers (n=45)		
PICP, µg/L	0.13	0.08
PIIINP, µg/L	-0.06	0.24
MMP-1, µg/L	0.01	0.13
CITP, µg/L	0.08	0.12
CITP/MMP-1	0.01	-0.10
NT-proBNP, pg/ml	0.07	**0.42****
Hs-Troponin T, pg/ml	-0.08	0.13

** p<0.01; * p<0.05; ° p<0.1

PWV as an established surrogate of arterial stiffness was significantly related to LV geometry: the higher the PWV, the lower the LV end-systolic volume. Furthermore, there was a trend to higher PWV values when LV wall thickness was increased.

PWV was marginally related to myocardial strain: A trend to higher radial and lower circumferential strain values at higher PWV levels was observed. Extracellular volume fraction as a measure of cardiac fibrosis was marginally and inversely related to PWV. NT-proBNP, a biomarker of myocardial stretch, was directly correlated with PWV.

4.2.3. Left ventricular wall thickness and mass, CMR-derived measures and circulating biomarkers

The relationship between TTE-derived and CMR-derived measures of cardiac geometry is shown in table 4.10. A direct correlation between measures of LV mass, LV volumes and LA dimension was observed, in contrast, the correlation coefficients between LV wall thickness parameters were not significant.

Table 4.10. Pearson's correlation coefficients among TTE-derived and CMR-derived parameters of cardiac geometry.

	TTE-derived geometry					
	Interventricular septum, mm	Posterior wall, mm	LV mass, g	LV end-diastolic volume, ml	LV end-systolic volume, ml	LA diameter, mm
CMR-derived geometry						
Interventricular septum, mm	0.18					
Posterior wall, mm		0.13				
LV mass, g			**0.70****			
LV end-diastolic volume, ml				**0.38***		
LV end-systolic volume, ml					**0.45****	
LA diameter, mm						**0.51****

** p<0.01; * p<0.05

Regarding CMR-derived measures of function and fibrosis, LV wall thickness and mass were not related to cardiac function except for a trend to a higher LA emptying volume with higher LV mass (table 4.11).

In contrast, LV wall thickness and LV mass were consistently correlated with measures of cardiac fibrosis: the greater the LV posterior wall thickness or LV mass, the higher the extracellular volume fraction and partition coefficient. In addition, LV wall thickness and mass were directly related to levels of circulating hs-Troponin T and, to a lower degree, to levels of circulating NT-proBNP.

Table 4.11. Pearson's correlation coefficients among LV wall thickness and mass, myocardial strain, LA function and biomarkers.

	IV septum, mm	Posterior wall, mm	LV mass, g
Cardiac function (n=33)			
Radial strain, %	-0.11	-0.21	-0.28
Circumferential strain, %	-0.14	0.03	0.07
Longitudinal strain, %	0.03	0.12	0.16
LA total emptying volume, ml	-0.12	-0.05	**0.31°**
LA total emptying fraction, %	0.13	-0.04	-0.16
Cardiac fibrosis (n=29)			
Extracellular volume fraction, %	**0.38°**	**0.40***	**0.39***
Partition coefficient	**0.35°**	**0.61****	**0.55****
Biomarkers (n=36)			
PICP, µg/L	0.01	0.05	0.03
PIIINP, µg/L	0.72	0.22	0.02
MMP-1, µg/L	0.11	0.24	0.12
CITP, µg/L	0.12	0.19	0.16
CITP/MMP-1	-0.15	0.17	-0.17
NT-proBNP, pg/ml	0.10	**0.32°**	**0.33°**
Hs-Troponin T, pg/ml	**0.51****	**0.53****	**0.73****

** p<0.01; * p<0.05; ° p<0.1

4.2.4. Left atrial dimension and left ventricular volumes, CMR-derived measures and circulating biomarkers

LA diameter and LA reservoir function were significantly related (table 4.12). In addition, LA geometry was consistently related to measures of cardiac fibrosis and hs-Troponin T. LV end-systolic volume is mainly determined by afterload and contractility. In the present study, LV end-systolic volume was significantly related to myocardial strain: the greater the LA reservoir function, the higher the LV end-systolic volume, and the greater the reduction of radial ("more negative" values) and circumferential ("more positive" values) strain.

LV end-diastolic volume is an established surrogate for preload. In the present study, LV end-diastolic volume and cardiac function were significantly correlated: higher values of LV end-diastolic volume were related to an increase in LA reservoir function and a

decrease in radial strain. In addition, LV end-diastolic volume showed a positive relationship with cardiac fibrosis and hs-Troponin T, biomarker of myocardial injury, whereas no association with circulating biomarkers of fibrosis was found.

Table 4.12. Pearson's correlation coefficients among LA diameter and LV volumes, myocardial strain, LA function and biomarkers.

	LA diameter, mm	**LVES volume, ml**	**LVED volume, ml**
Cardiac function (n=33)			
Radial strain, %	-0.04	**-0.69****	**-0.42***
Circumferential strain, %	0.12	**0.35***	0.21
Longitudinal strain, %	0.23	0.16	0.18
LA total emptying volume, ml	**0.42***	**0.35***	**0.63****
LA total emptying fraction, %	-0.03	-0.09	-0.12
Cardiac fibrosis (n=29)			
Extracellular volume fraction, %	**0.48****	0.27	**0.39***
Partition coefficient	**0.35°**	0.13	0.25
Biomarkers (n=36)			
PICP, µg/L	-0.08	-0.03	0.09
PIIINP, µg/L	0.01	-0.17	-0.09
MMP-1, µg/L	0.15	0.10	0.25
CITP, µg/L	0.26	0.03	0.17
CITP/MMP-1	-0.07	-0.08	-0.17
NT-proBNP, pg/ml	0.19	0.07	0.21
Hs-Troponin T, pg/ml	**0.48****	0.12	**0.39***

** p<0.01; * p<0.05; ° p<0.1

4.2.5. Myocardial strain, cardiac fibrosis and circulating biomarkers

Longitudinal strain was related to cardiac fibrosis: the higher the values of ECV, the higher the values of longitudinal strain. In other words: the higher the degree of fibrosis, the greater the reduction in longitudinal strain (i.e. "more positive" values of longitudinal strain) (table 4.13). In addition, longitudinal strain showed a significant correlation with both CITP and MMP-1: A decrease in longitudinal strain was associated with higher levels of CITP and lower levels of the collagen-degrading enzyme MMP-1.

Consequently, longitudinal strain was associated with CITP/MMP-1: the higher CITP/MMP-1, the greater the reduction in longitudinal strain.

Circumferential strain was not related to cardiac fibrosis assessed by CMR, however, there was a trend to higher levels of CITP/MMP-1 when circumferential strain was reduced.

Radial strain was not related to CMR-assessed fibrosis or circulating biomarkers.

Table 4.13. Pearson's correlation coefficients among LV function, fibrosis and biomarkers.

	Radial strain, %	**Circumferential strain, %**	**Longitudinal strain, %**
Cardiac fibrosis (n=29)			
Extracellular volume fraction, %	-0.24	0.18	**0.42***
Partition coefficient	-0.17	0.16	0.22
Biomarkers (n=33)			
PICP, µg/L	0.08	-0.10	0.13
PIIINP, µg/L	0.16	-0.19	-0.08
MMP-1, µg/L	0.23	-0.28	**-0.33°**
CITP, µg/L	-0.28	0.18	**0.42***
CITP/MMP-1	-0.29	**0.32°**	**0.43***
NT-proBNP, pg/ml	0.05	-0.08	0.09
Hs-Troponin T, pg/ml	-0.07	0.04	0.11

* $p<0.05$; ° $p<0.1$

4.2.6. Left atrial function parameters, cardiac fibrosis and circulating biomarkers

LA emptying volume and fraction, two established surrogates of LA reservoir function, were not significantly related to measures of cardiac fibrosis or circulating biomarkers (table 4.14).

Table 4.14. Pearson's correlation coefficients among LA function, fibrosis and biomarkers.

	LA emptying volume, ml	LA emptying fraction, %
Cardiac fibrosis (n=29)		
Extracellular volume fraction, %	0.09	-0.01
Partition coefficient	0.04	-0.06
Biomarkers (n=36)		
PICP, µg/L	0.09	0.05
PIIINP, µg/L	0.17	0.09
MMP-1, µg/L	0.09	-0.15
CITP, µg/L	0.17	-0.09
CITP/MMP-1	-0.05	0.12
NT-proBNP, pg/ml	-0.09	-0.12
Hs-Troponin T, pg/ml	0.19	-0.10

* p<0.05; ° p<0.1

4.2.7. Cardiac fibrosis and circulating biomarkers

CMR-derived markers of cardiac fibrosis were not significantly related to circulating biomarkers of fibrosis (table 4.15). A positive correlation of hs-Troponin T and CMR-assessed partition coefficient was found, however, the relationship between extracellular volume fraction and hs-Troponin T was not significant.

Table 4.15. Pearson's correlation coefficients among cardiac fibrosis and circulating biomarkers.

	Extracellular volume fraction, %	Partition coefficient
Biomarkers (n=29)		
PICP, µg/L	0.06	0.02
PIIINP, µg/L	-0.23	0.08
MMP-1, µg/L	-0.01	0.05
CITP, µg/L	0.13	-0.11
CITP/MMP-1	0.05	-0.08
NT-proBNP, pg/ml	0.05	0.32
Hs-Troponin T, pg/ml	0.26	**0.51****

** p<0.01; * p<0.05; ° p<0.1

4.2.8. Circulating biomarkers of myocardial fibrosis, stretch and injury

Regarding molecular biomarkers of fibrosis, significant positive correlations were observed between PICP and PIIINP (table 4.16). PIIINP was further marginally related to MMP-1, CITP/MMP-1 and hs-Troponin T.

NT-proBNP and hs-Troponin T, molecular biomarkers of myocardial stretch and injury, respectively, were directly related.

Table 4.16. Pearson's correlation coefficients among circulating biomarkers.

	PICP, µg/L	**PIIINP, µg/L**	**MMP1, µg/L**	**CITP, µg/L**	**CITP/ MMP1**	**NT-proBNP, pg/ml**	**Hs-Troponin T, pg/ml**
PICP, µg/L	**X**						
PIIINP, µg/L	**0.42****	**X**					
MMP-1, µg/L	0.22	**0.27°**	**X**				
CITP, µg/L	-0.10	-0.09	-0.09	**X**			
CITP/MMP-1	-0.23	**-0.27°**	**-0.96****	**0.35***	**X**		
NTproBNP, pg/ml	-0.01	-0.02	0.08	0.08	-0.05	**X**	
hsTroponin T, pg/ml	-0.05	**0.27°**	0.16	0.06	-0.13	**0.34***	**X**

** p<0.01; * p<0.05; ° p<0.1

4.3. Determinants of morphological and functional parameters of fibrosis

Multiple regression analysis was performed in order to assess the factors associated with peripheral and central hemodynamics, CMR-derived parameters of myocardial strain, LA function, cardiac fibrosis, and molecular biomarkers of myocardial fibrosis, stretch and injury. Multicollinearity was checked for calculating the VIF for each regression model (cutoff-value of VIF for significant multicollinearity > 5). None of the following regression models showed VIF values higher than 2.39.

4.3.1. Relationship between vascular hemodynamics and components of cardiac geometry, myocardial strain, left atrial function and circulating biomarkers of fibrosis

The relationship between peripheral vascular hemodynamics and cardiac geometry is shown in table 4.17 and figure 4.2. 24-hour systolic BP was independently associated with LV mass, but not LV wall thickness, when gender, age, body constitution and heart rate were controlled for.

Myocardial strain as a surrogate of LV functioning was not related to peripheral hemodynamics in fully adjusted models.

No significant association between peripheral hemodynamics and molecular biomarkers of fibrosis was observed.

Table 4.17. Hemodynamic parameters associated with LV mass.

	R^2=0.50	
Variable	β	*p*
Gender, female	-0.20	0.30
Age, years	0.04	0.75
Height, cm	0.12	0.55
Weight, kg	**0.46**	**0.009**
Heart rate, bpm	0.05	0.69
24-h systolic BP, mmHg	**0.31**	**0.029**

Figure 4.2. Regression line, scatter plot and correlation coefficient for the association between LV mass and mean 24-hour systolic BP.

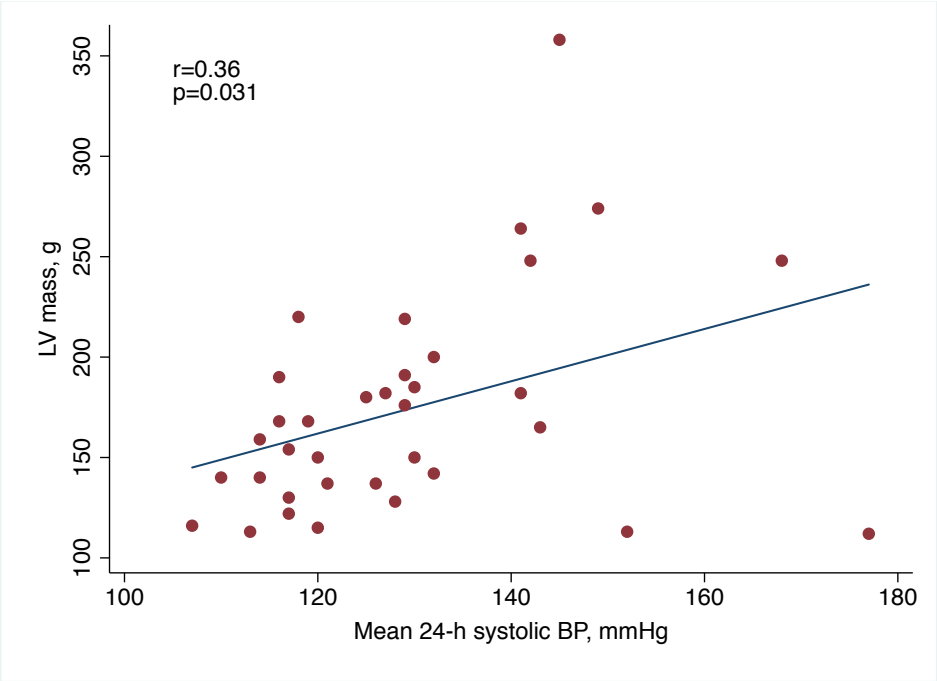

LA emptying fraction as a surrogate of LA reservoir function was inversely associated with 24-hour systolic BP and office BP (figure 4.3). Table 4.18 shows multiple regression models using LA function as the dependent variable.

Table 4.18. Hemodynamic parameters associated with LA reservoir function.

	R^2=0.29		R^2=0.26	
Variable	β	*p*	β	*p*
Gender, female	-0.03	0.90	-0.08	0.77
Age, years	0.06	0.73	-0.09	0.61
Height, cm	-0.10	0.73	-0.21	0.46
Weight, kg	0.05	0.83	-0.08	0.74
Heart rate, bpm	0.14	0.46	0.23	0.22
24-h systolic BP, mmHg	**-0.49**	**0.017**		
Office systolic BP, mmHg			**-0.47**	**0.022**

Figure 4.3. Regression line, scatter plot and correlation coefficient for the association between LA reservoir function and mean 24-hour systolic BP.

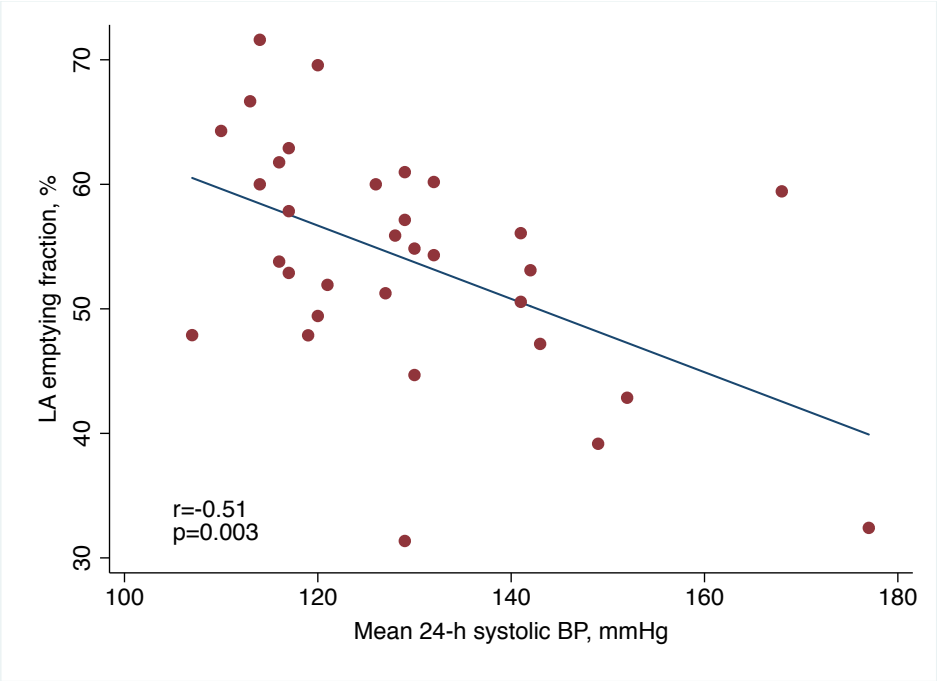

Regarding central hemodynamics, central systolic BP and PWV did not show significant independent association with parameters of cardiac geometry, myocardial strain, LA function or circulating biomarkers of fibrosis in fully adjusted models.

4.3.2. Relationship between cardiac fibrosis and components of cardiac geometry, myocardial strain and circulating biomarkers of fibrosis

4.3.2.1. Extracellular volume fraction

The main factors associated with cardiac fibrosis were investigated in regression models controlling for gender, age, body constitution, heart rate and 24-hour systolic BP (table 4.19). LA geometry was directly related to ECV, whereas no significant association with measures of LV geometry was found in fully adjusted models.

Among cardiac strain parameters, longitudinal strain, but not radial strain, was associated with ECV: an increase in ECV was significantly related to a decrease (i.e., “more positive” values) in longitudinal strain.

Circulating biomarkers of fibrosis did not show a significant association with ECV. Regression lines between ECV and independently associated factors are shown in figures 4.4 and 4.5.

Table 4.19. Factors associated with extracellular volume fraction.

	R^2=0.47		R^2=0.38	
Variable	β	*p*	β	*p*
Gender, female	-0.10	0.70	-0.31	0.29
Age, years	-0.39	0.06	-0.19	0.33
Height, cm	0.21	0.53	-0.30	0.37
Weight, kg	-0.26	0.41	0.30	0.29
Heart rate, bpm	-0.04	0.84	-0.09	0.66
24-h systolic BP, mmHg	-0.25	0.19	-0.05	0.82
LA diameter, cm	**0.75**	**0.005**		
Longitudinal strain, %			**0.43**	**0.030**

Figure 4.4. Regression line, scatter plot and correlation coefficient for the association between ECV and LA diameter.

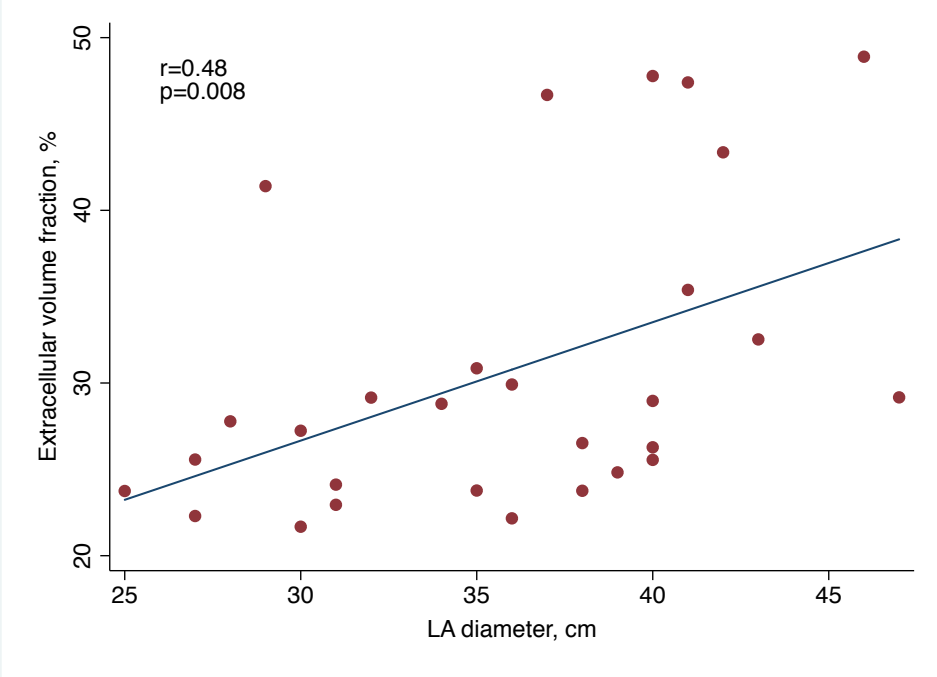

Figure 4.5. Regression line, scatter plot and correlation coefficient for the association between ECV and longitudinal strain.

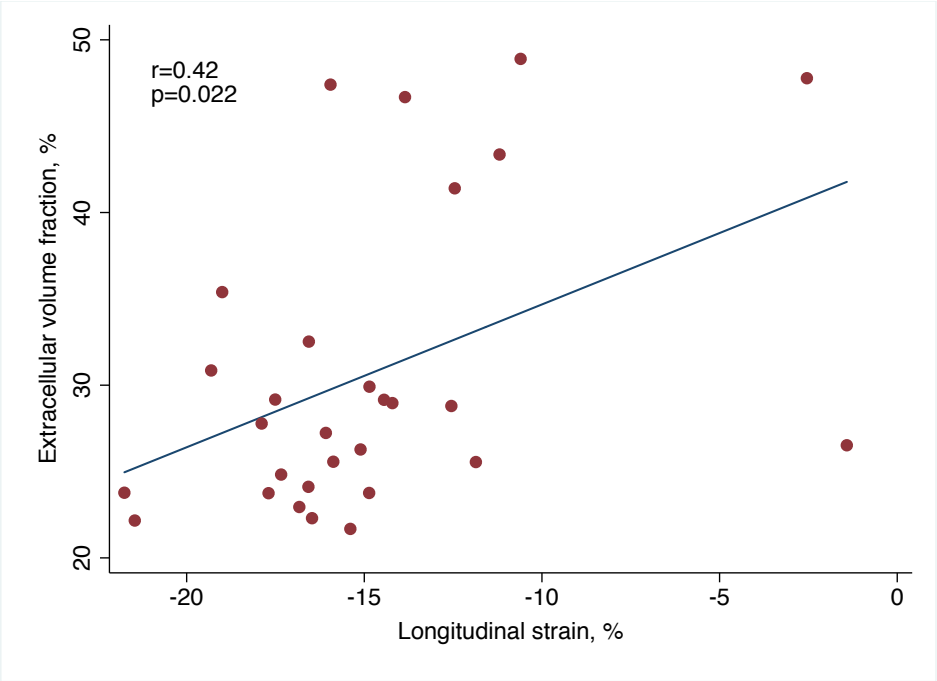

4.3.2.2. Partition coefficient

The only difference between partition coefficient and ECV is the hematocrit factor, therefore, both variables are closely related and generally translatable. LV posterior wall thickness was positively associated with the partition coefficient (table 4.20, figure 4.6). Parameters of cardiac geometry, myocardial strain and circulating biomarkers of fibrosis were not significantly related to partition coefficient in fully adjusted models.

Table 4.20. Factors associated with partition coefficient.

	R^2=0.49	
Variable	β	*p*
Gender, female	-0.19	0.54
Age, years	0.07	0.71
Height, cm	0.12	0.73
Weight, kg	0.01	0.98
Heart rate, bpm	-0.10	0.61
24-h systolic BP, mmHg	-0.04	0.83
LV posterior wall, cm	**0.53**	**0.046**

Figure 4.6. Regression line, scatter plot and correlation coefficient for the association between partition coefficient and LV posterior wall thickness.

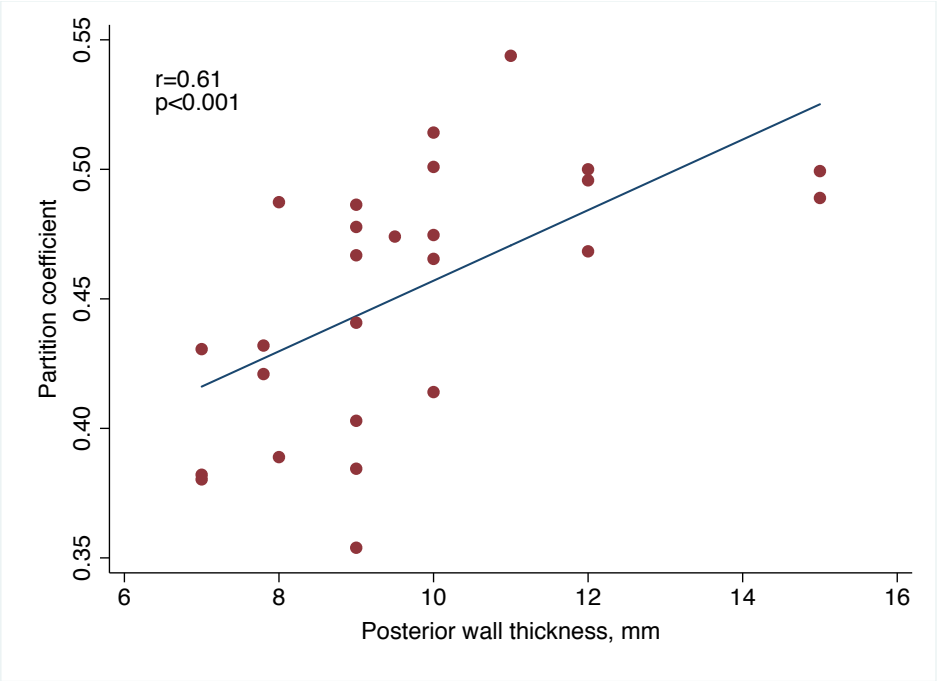

4.3.3. Relationship between myocardial strain and components of cardiac geometry and circulating biomarkers of fibrosis

CMR-derived strain measures are established surrogates of LV functioning. The main factors associated with longitudinal, circumferential and radial strain were investigated in regression models controlling for gender, age, body constitution, heart rate and 24-hour systolic BP.

4.3.3.1. Longitudinal strain

As shown in table 4.19 and figure 4.5, longitudinal strain and cardiac fibrosis expressed by ECV were significantly associated. In addition, longitudinal strain was significantly related to CITP and CITP/MMP-1: a decrease in longitudinal strain (i. e., “more positive” values) was associated with higher levels of CITP and CITP/MMP-1 (table 4.21, figures 4.7 and 4.8).

No significant association between longitudinal strain with parameters of cardiac geometry or LA function was observed in fully adjusted models.

Table 4.21. Factors associated with longitudinal strain.

	R^2=0.25		R^2=0.24	
Variable	β	*p*	β	*p*
Gender, female	0.13	0.67	-0.01	0.99
Age, years	0.05	0.79	0.05	0.80
Heigt, cm	0.21	0.53	0.07	0.85
Weight, kg	0.05	0.84	0.13	0.63
Heart rate, bpm	-0.1	0.64	-0.05	0.81
24-h systolic BP, mmHg	-0.22	0.30	-0.2	0.35
CITP, µg/L	**0.46**	**0.025**		
CITP/MMP-1			**0.46**	**0.030**

Figure 4.7. Regression line, scatter plot and correlation coefficient for the association between longitudinal strain and circulating CITP-levels.

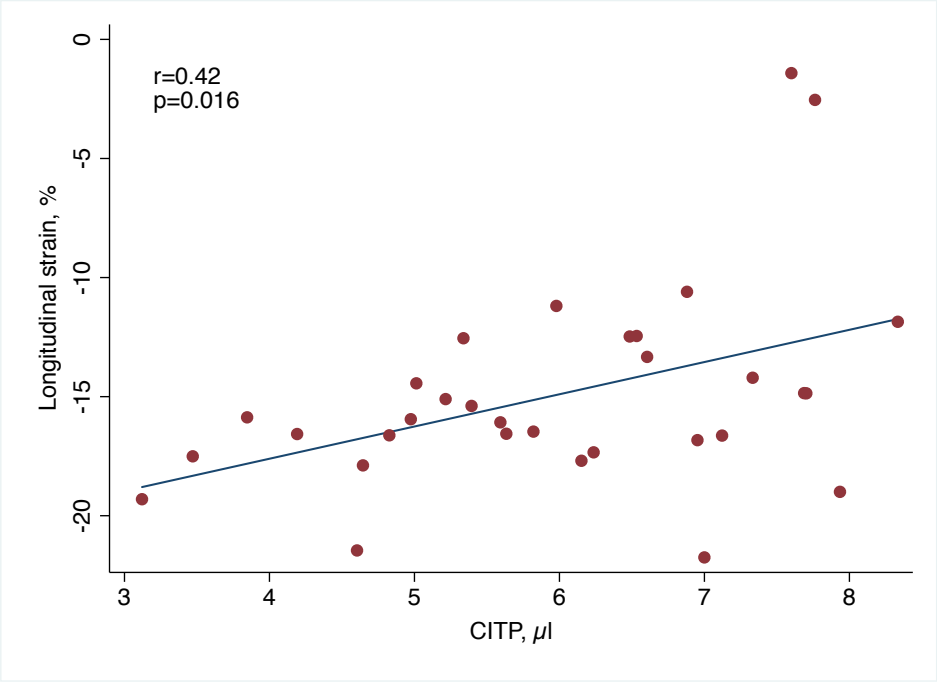

Figure 4.8. Regression line, scatter plot and correlation coefficient for the association between longitudinal strain and CITP/MMP-1.

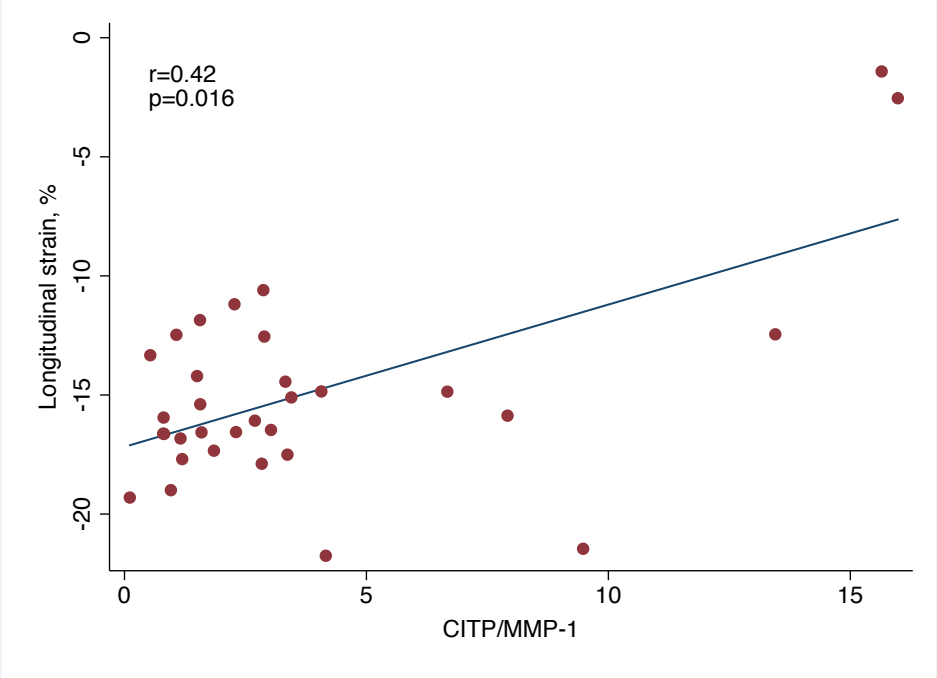

4.3.3.2. Circumferential strain

Circumferential strain and CITP/ MMP-1 were significantly associated: A decrease in circumferential strain (i.e., "more positive" values) was related to a higher ratio of CITP/MMP-1 (table 4.22, figure 4.9). The associations between circumferential strain and levels of CITP and MMP-1 were further evaluated in order to gain insight into the relationship of circumferential strain with CITP/MMP-1. Circulating levels of MMP-1, but not CITP, were related to circumferential strain in fully adjusted models (table 4.22, figure 4.10).

No significant association between circumferential strain with measures of cardiac geometry or function was identified in fully adjusted models.

Table 4.22. Factors associated with circumferential strain.

	R^2=0.32		R^2=0.37	
Variable	β	*p*	β	*p*
Gender, female	-0.1	0.71	-0.11	0.73
Age, years	0.22	0.24	0.20	0.27
Heigt, cm	-0.43	0.20	-0.49	0.15
Weight, kg	0.39	0.14	0.44	0.09
Heart rate, bpm	-0.35	0.08	-0.38	0.05
24-h systolic BP, mmHg	-0.36	0.08	-0.39	0.05
MMP-1, µg/L	**-0.38**	**0.047**		
CITP/MMP-1			**0.46**	**0.017**

Figure 4.9. Regression line, scatter plot and correlation coefficient for the association between circumferential strain and CITP/MMP-1.

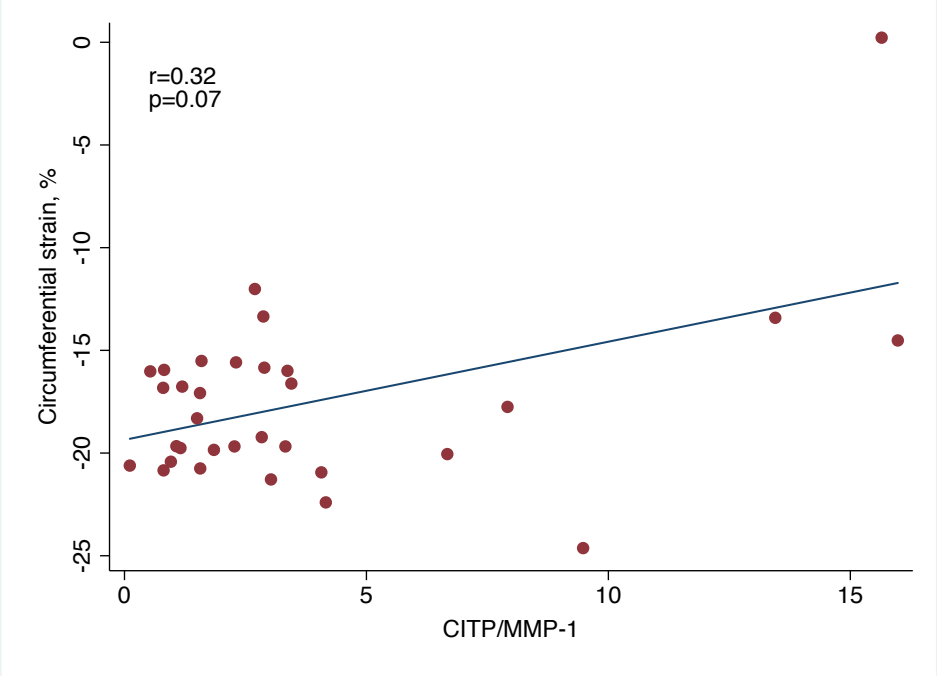

Figure 4.10. Regression line, scatter plot and correlation coefficient for the association between circumferential strain and MMP-1.

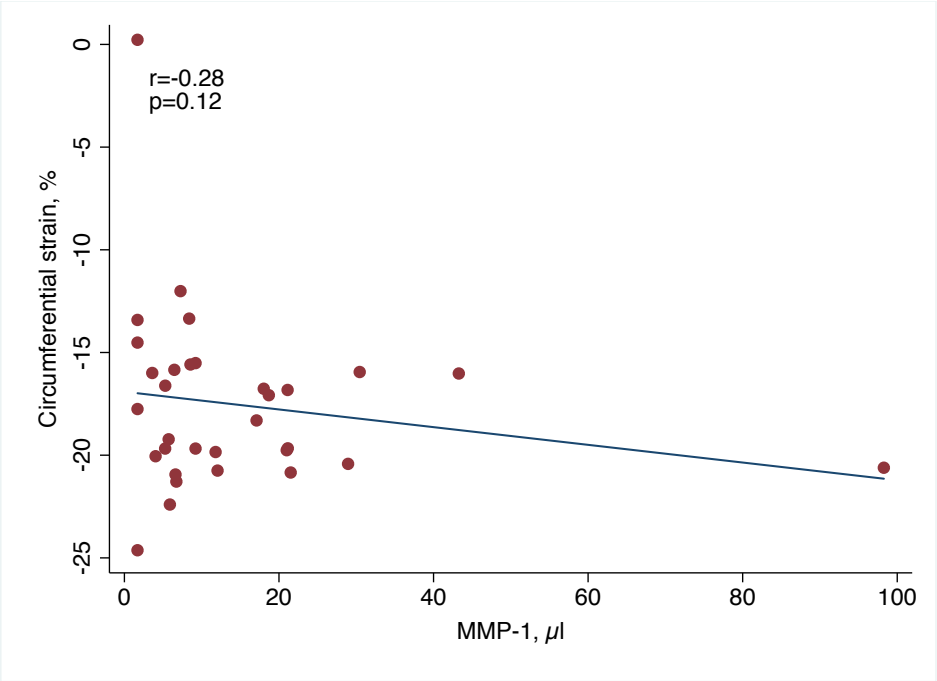

4.3.3.3. Radial strain

In fully adjusted models, LV end-systolic volume was inversely associated with radial strain: an increase in radial strain was associated with a decrease in LV end-systolic volume (table 4.23, figure 4.11). In other words, the higher the LV end-systolic volume, the lower the radial strain.

Table 4.23. Factors associated with radial strain.

	R^2=0.30	
Variable	β	*p*
Gender, female	-0.07	0.81
Age, years	-0.18	0.32
Height, cm	0.06	0.85
Weight, kg	-0.13	0.60
Heart rate, bpm	0.06	0.77
24-h systolic BP, mmHg	0.26	0.20
LV end-systolic volume, ml	**-0.44**	**0.048**

Figure 4.11. Regression line, scatter plot and correlation coefficient for the association between radial strain and LV end-systolic volume.

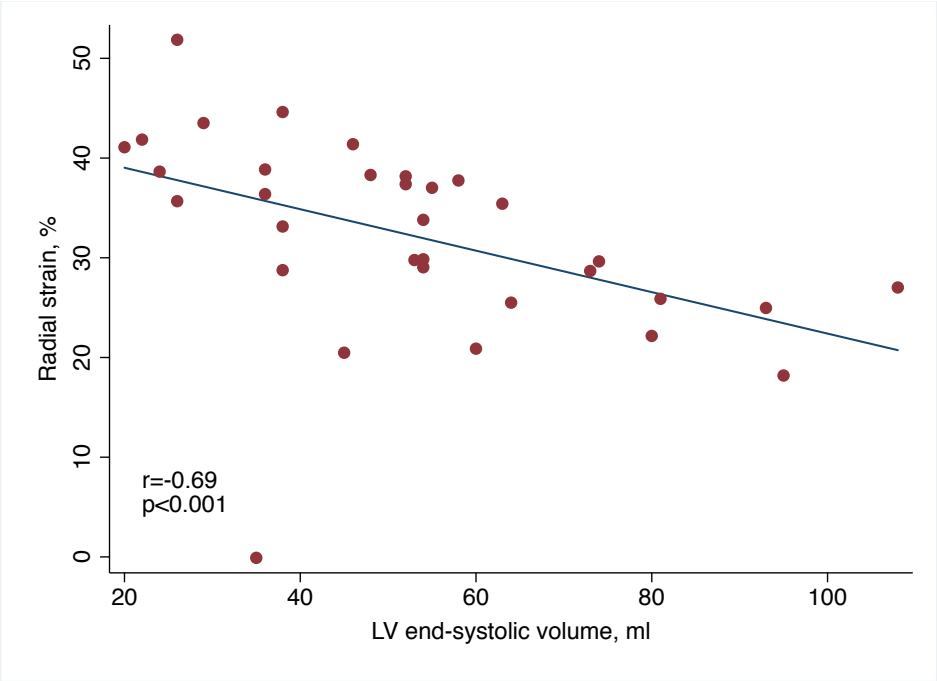

No significant association was found with cardiac geometry and function. Likewise, radial strain was not related to measures of cardiac fibrosis or molecular biomarkers of fibrosis in fully adjusted models.

5.3.4. Main factors associated with molecular biomarkers of myocardial stretch and injury

NT-proBNP and hs-Troponin T are established biomarkers of cardiac stretch and injury, respectively. The association between these biomarkers with central and peripheral hemodynamics, cardiac geometry, cardiac function and cardiac fibrosis was assessed controlling for gender, age, body constitution, heart rate and 24-hour systolic BP.

4.3.4.1. NT-proBNP

Circulating NT-proBNP was significantly associated with PWV (table 4.24). Peripheral central systolic BP, in contrast, was not related to NT-proBNP in fully adjusted models.

Cardiac geometry was independently related to NT-proBNP: Both greater posterior wall thickness and LV mass were associated with higher levels of NT-proBNP.

Myocardial strain and fibrosis did not show significant relationship with NT-proBNP in fully adjusted models. Regression lines between PWV and independently associated factors are shown in figures 4.12-14.

Table 4.24. Factors associated with NT-proBNP.

	R^2=0.30		R^2=0.26		R^2=0.29	
Variable	β	*p*	β	*p*	β	*p*
Gender, female	-0.12	0.55	0.49	0.14	0.29	0.29
Age, years	0.13	0.40	0.21	0.27	0.20	0.27
Height, cm	0.07	0.75	0.66	0.06	0.39	0.19
Weight, kg	-0.10	0.63	-0.29	0.27	-0.38	0.14
Heart rate, bpm	-0.29	0.07	-0.25	0.24	-0.18	0.32
24-h systolic BP, mmHg	-0.04	0.85	-0.18	-0.39	-0.21	0.32
Pulse wave velocity, m/s	**0.53**	**0.013**				
Posterior wall, mm			**0.50**	**0.051**		
LV mass, g					**0.58**	**0.038**

Figure 4.12. Regression line, scatter plot and correlation coefficient for the association between NT-proBNP and PWV.

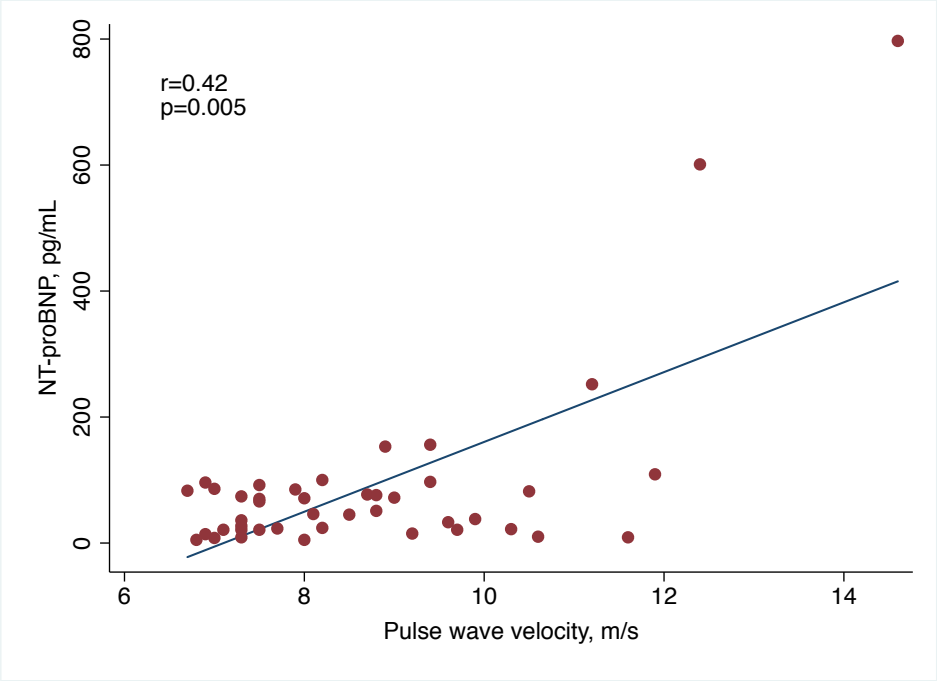

Figure 4.13. Regression line, scatter plot and correlation coefficient for the association between NT-proBNP and LV posterior wall thickness.

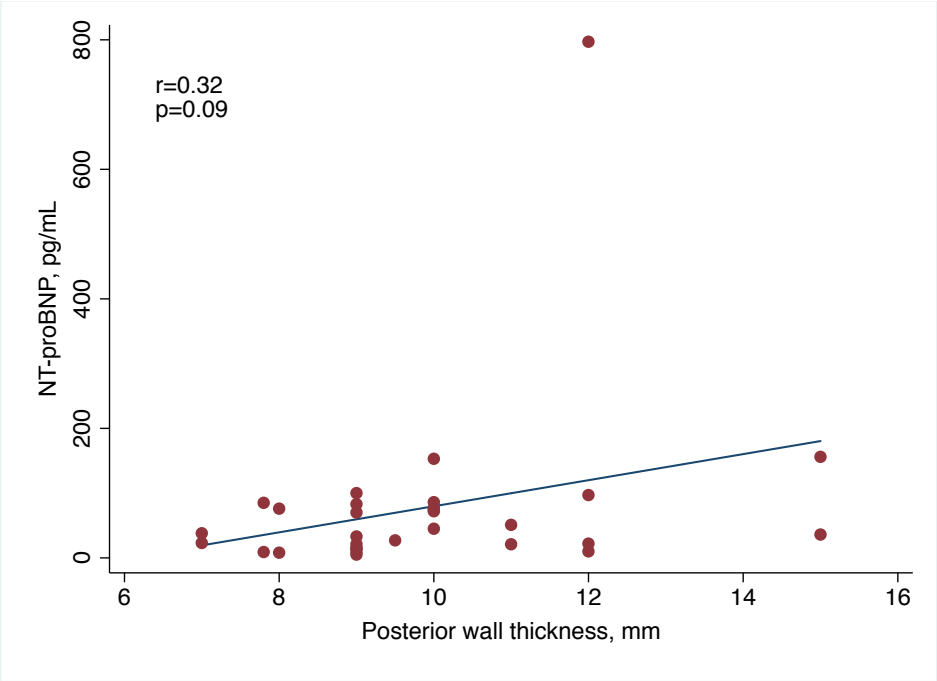

Figure 4.14. Regression line, scatter plot and correlation coefficient for the association between NT-proBNP and LV mass.

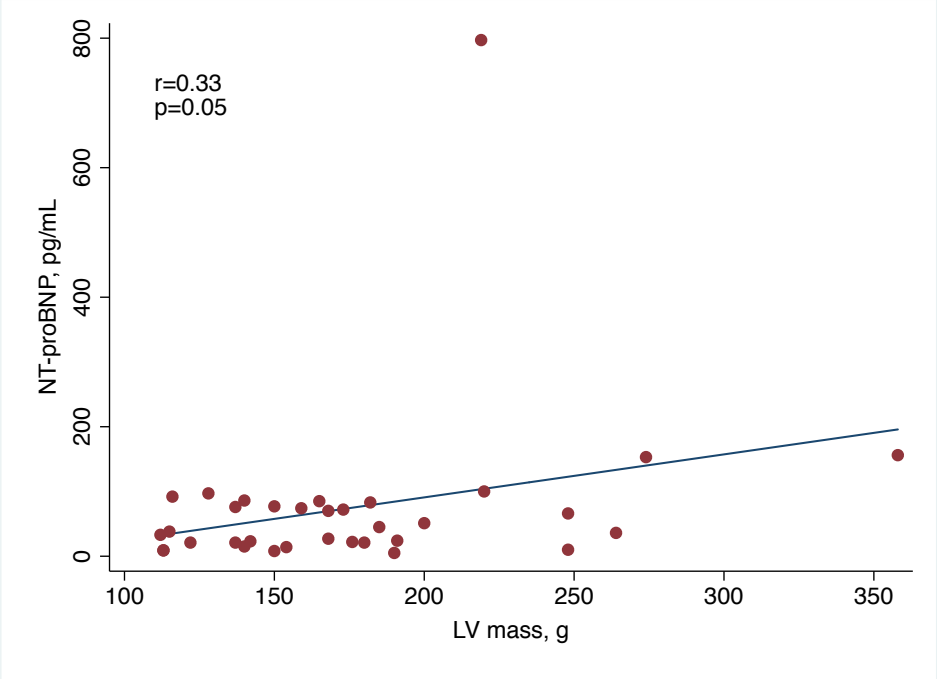

4.3.4.2. Hs-Troponin T

The factors independently associated with hs-Troponin T are shown in table 4.25 and figures 4.15 and 4.16. Cardiac geometry was closely related to circulating levels of hs-Troponin T: greater LA dimension and LV mass were associated with higher levels of hs-Troponin T.

Table 4.25. Factors associated with hs-Troponin T.

	Model A (R^2=0.45)		Model B (R^2=0.61)	
Variable	β	*p*	β	*p*
Gender, female	-0.10	0.70	-0.13	0.54
Age, years	-0.02	0.90	0.09	0.51
Height, cm	0.47	0.11	-0.05	0.81
Weight, kg	-0.16	0.50	-0.27	0.18
Heart rate, bpm	0.17	0.31	0.17	0.22
24-h systolic BP, mmHg	0.10	0.58	-0.05	0.74
LA diameter, mm	**0.47**	**0.025**		
LV mass, g			**0.92**	**<0.001**

Figure 4.15. Regression line, scatter plot and correlation coefficient for the association between hs-Troponin T and LA diameter.

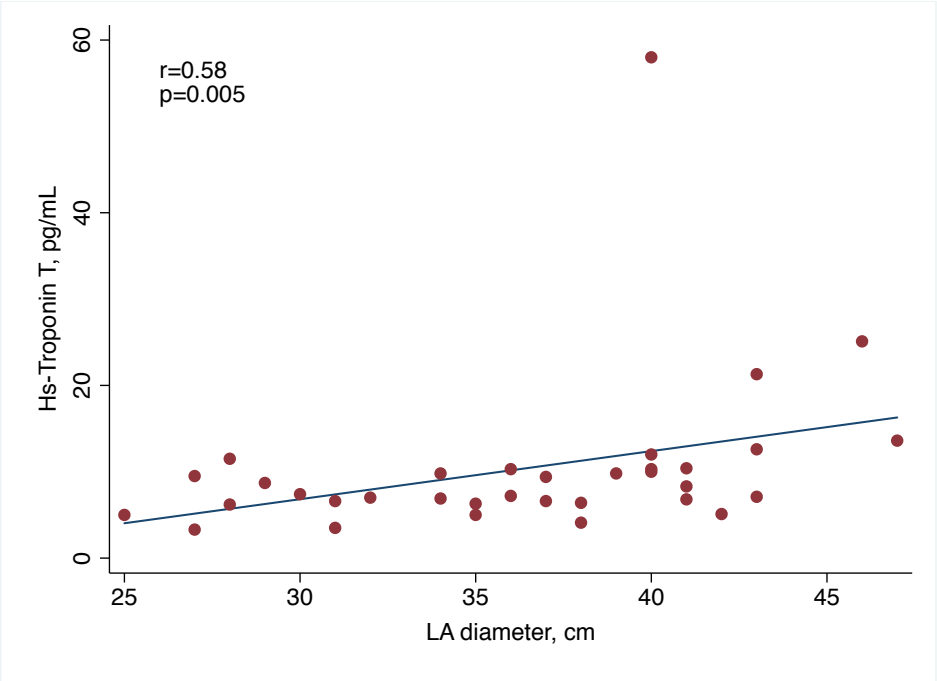

Figure 4.16. Regression line, scatter plot and correlation coefficient for the association between hs-Troponin T and LV mass.

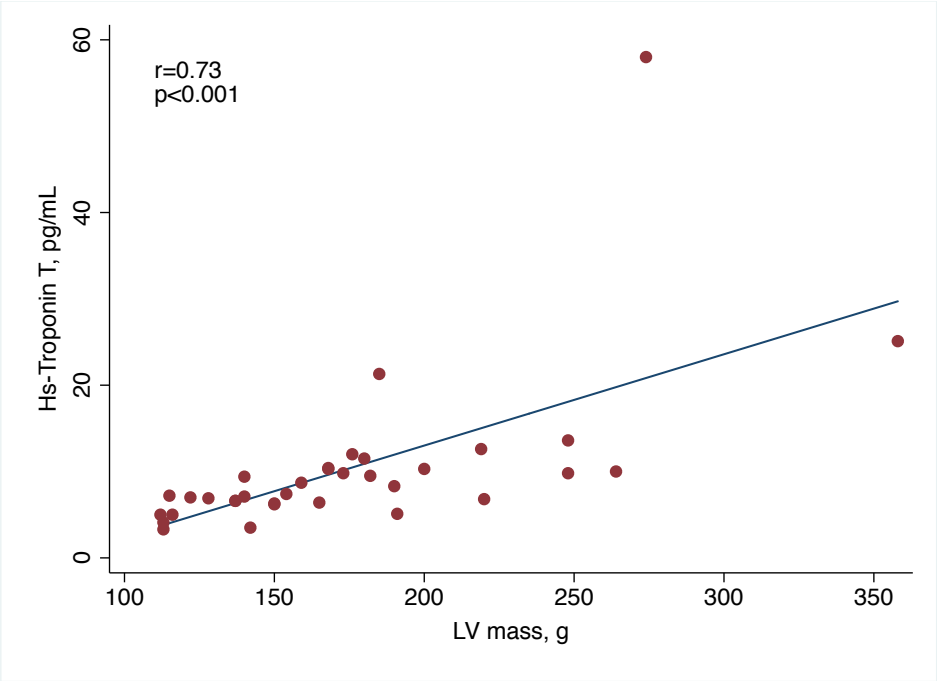

No significant relationship of hs-Troponin T with vascular hemodynamics, myocardial strain or fibrosis was found in fully adjusted models

4.4. Summary findings

The relationship between peripheral and central hemodynamics, CMR-derived cardiac geometry, strain, and fibrosis, and molecular biomarkers of myocardial fibrosis, stretch and injury is shown in figure 4.17. In hypertensives with HHD, LV walls contain a relevant amount of fibrotic tissue identified with CMR imaging. Myocardial fibrosis is associated with impaired cardiac deformation expressed as reduced longitudinal strain, which is related to molecular biomarkers of fibrosis. Moreover, changes in LV mass, LV wall thickness and LA dimension modify the levels of circulating biomarkers of myocardial stretch and injury.

Figure 4.17. Schematic representation of the relationship between vascular hemodynamics, CMR-derived cardiac geometry, strain and fibrosis, and molecular biomarkers of myocardial fibrosis, stretch and injury.

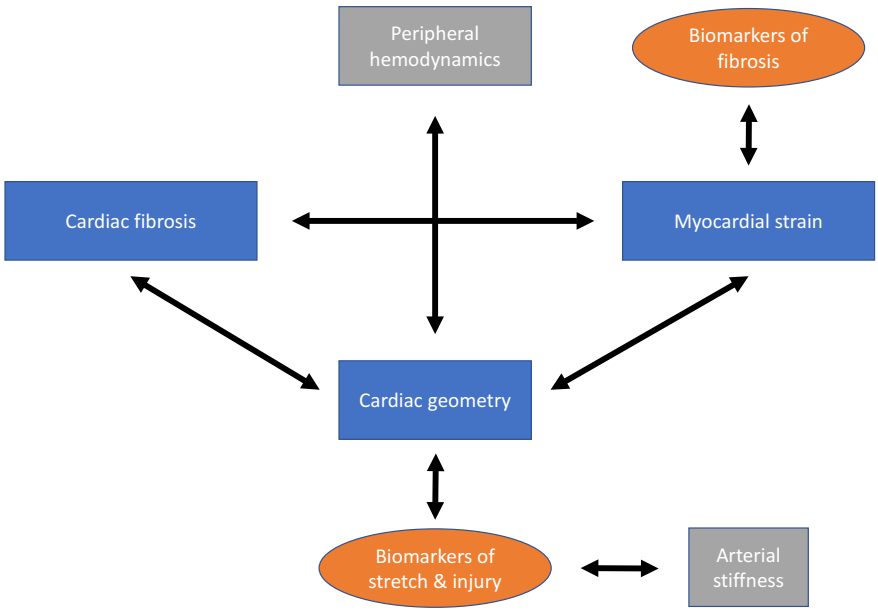

5. Discussion

5.1. Methods

5.1.1. Study population

The present study was conducted in Caucasian hypertensives aged from 40 to 60 years. Age is a well-established determinant of onset, progression and prognosis of HTN and related comorbidities (117,118). In addition, alterations in cardiac geometry and function, as well as the quantity and quality of myocardial fibrosis, are directly related to age (119–122). The exclusion of individuals older than 60 years in order to reduce the confounding effect of age is therefore a major strength of the present study.

The vast majority of study participants were male individuals (approximately 85%). Physiological circulatory differences between men and women include estrogen-mediated vascular relaxation, shorter length of the arterial tree, faster heart rate and different fat distribution in women (123). It has been proposed that, besides sex hormones, the impact of RAAS, sympathetic activation, oxidative stress and endothelin on BP levels might differ between genders (124). Thus, discrepancies between gender regarding peripheral and central hemodynamics, which are related to cardiac geometry and function, are expectable (125). As a consequence, the results of the present study can mainly be extrapolated to hypertensive males.

All individuals included in the present study had preserved renal function defined as estimated glomerular filtration rate (eGFR) > 60 ml/min/m^2. The adverse impact of kidney disease on vascular hemodynamics and cardiac function is well established (126). In addition, the reproducibility and standardization of serum or plasma assays used for the assessment of molecular biomarker is determined by renal function (127). It is therefore desirable to exclude individuals with renal dysfunction when the relationship between molecular biomarkers and cardiovascular mechanics is investigated.

Large epidemiological studies have shown that HTN is frequently associated with metabolic syndrome-related comorbidities, including diabetes, dyslipidemia and obesity (128–130). Moreover, the onset or progression of one of these conditions confers an increase in risk for the development or progression of the others (131–134). Accordingly, the prevalence of obesity, diabetes and dyslipidemia was high in the present study. Although impaired glucose and lipid metabolism as well as obesity are

related to adverse cardiac events, all participating individuals were free of overt cardiovascular disease at study enrolment.

All study participants were under active BP-lowering treatment, and 85% of patients received 2 or more drugs. Inhibitors of the renin-angiotensin system were used in all patients, followed by calcium channel blockers and diuretics. This is in accordance with the present treatment recommendations of the ESH, which favors inhibitors of the renin-angiotensin and calcium channel blockers as first-line treatments (101). However, BP control was poor in the present study. The prevalence of LVH is directly related to BP levels in treated hypertensives (135). Given the fact that all study patients met ECG-derived criteria of LVH, it is not surprising that almost two third of the study population had BP levels above target levels in both office and 24-hour BP measurements.

ECG-derived criteria of LVH might not provide sensitivity and specificity to determine the morphological pattern or extension of LVH, particularly in children and young adolescents, diabetics or obese subjects (136–138). Nevertheless, the Sokolow-Lyon Index and Cornell voltage criteria have shown prognostic value, and the assessment of ECG-derived LVH criteria is strongly recommended in all hypertensives, according to the ESH (101,139,140). Despite its limitations, ECG is still considered a valid screening tool for the detection of HHD in the hypertensive population (141).

5.1.2. Cardiac magnetic resonance imaging

The assessment of cardiac geometry and function is essential in the management of cardiac disease. Overt alterations in contractile or relaxation function can reliably be detected by TTE, which is the first-line cardiac imaging technique in clinical practice. However, the detection and quantification of subtle preclinical systolic or diastolic dysfunction is desirable in order to identify patients with elevated risk for adverse cardiovascular outcomes. CMR has become the gold standard for the non-invasive assessment of cardiac geometry and function, providing the highest accuracy and reproducibility among currently available imaging techniques (142,143). In the present study, LV mass measured by CMR and by echocardiography were highly correlated, similar to previously reported comparisons (144). In addition, LV volumes and LA

diameter by CMR and TTE were significantly related, suggesting a good agreement between the 2 techniques for the assessment of LV geometry.

Myocardial strain has been found to be an early marker of cardiac function and superior in terms of sensitivity compared to traditional cardiac function parameters measured by TTE (83,145). For the assessment of myocardial strain, CMR-FT and speckle tracking echocardiography (STE) are the most important imaging techniques. Both methods rely upon tissue tracking for the assessment of strain parameters, and numerous studies have shown a good agreement between both techniques (146–149). However, CMR-FT has several advantages compared to STE for the assessment of myocardial strain.

STE requires high quality images for post-processing and a specific frame rate during image acquisition (150). As a consequence, routinely acquired echocardiography studies are frequently not suitable for image post-processing, especially when the acoustic window during the echocardiography study is not optimal. The signal-to-noise ratio of TTE-derived images is lower than in CMR-derived images and some myocardial segments cannot be adequately imaged with STE. As a consequence, STE-measured values need to be averaged in order to assess global cardiac strain. In addition, STE is based on strain analysis during a single cardiac cycle, therefore, STE-derived strain cannot be assessed in patients with arrhythmias (151).

A standard CMR protocol covers all segments of both cardiac chambers in short axis and long axis views. The SSFP technique provides excellent contrast between myocardium and the blood pool at high spatial resolution, and images can be acquired in less than 8 seconds (152). However, CMR is not capable to distinguish features within the myocardium, probably due to the relatively large voxel dimensions and the homogeneous water content and tissue properties within the myocardium (84). Thus, CMR-FT is most effective around endocardial and epicardial borders. Moreover, the relatively low temporal resolution can affect tracking if the search window is big. Finally, there is a limitation inherent to the way the cine sequence is produced. Each frame of the cine loop is reconstructed with information obtained during several heartbeats. Thus, small beat to beat differences are smoothed out and this, in combination with suboptimal temporal resolution, may obscure rapid isovolumic phases leading to underestimation of myocardial displacement and therefore strain parameters.

CMR-FT has been validated in numerous clinical studies, and excellent reproducibility has been observed for global strain measures (153). In ischemic heart disease, all myocardial strain parameters have been found to be altered in infarcted territories. In addition, myocardial strain was associated with infarct size, infarct transmurality, myocardial area at risk, and recurrent myocardial infarction (154–158).

The role of CMR-FT-derived strain measures is less clear in non-ischemic cardiac disease. Global circumferential and longitudinal strain seem to be the most consistent strain parameters regarding measurement agreement and reproducibility (83,159,160). In contrast, radial strain measures have been found to suffer from high variability, questioning the use of radial strain in clinical practice (86,113). An important issue regarding measurement reproducibility is the growing availability of feature tracking software from several different vendors with independently developed software solutions (160–162). Consequently, reference values of strain parameters may depend on the imaging technique, magnetic field, administration of contrast and on the software applied for feature tracking. Intra-vendor and inter-vendor reproducibility of available strain parameters needs to be addressed in future clinical studies in order to standardize and optimize CMR-FT protocols.
Despite discrepancies regarding measurement of strain parameters, reference values for LV strain parameters have been published (114,163). CMR-FT has been applied for the quantification of LV systolic and diastolic function in healthy individuals (162,164,165) as well as in patients with non-ischemic cardiomyopathies, arrhythmias, and pulmonary hypertension (146,166–168). In contrast, the exact role of CMR-FT in the quantification of preclinical alterations of LV function in HHD has not been established yet.

Over the last decade, CMR-based tissue characterization and assessment of myocardial fibrosis have been performed in numerous studies using LGE (169). The test principle of LGE is based on changes in kinetic properties of gadolinium in pathologic areas of the extracellular space. In other words, LGE is a “difference test” that requires different signal intensities in order to differentiate between supposedly normal pathological myocardial areas. Consequently, LGE is a valid technique for the determination of focal

myocardial fibrosis and other focal cardiac diseases, but does not adequately estimate diffuse reactive fibrosis, the main morphological characteristic of HHD.

T1 mapping is currently the most promising technique for the quantification of diffuse myocardial fibrosis. Native T1 values have been found to be altered in numerous cardiac diseases (111). In addition, the quantity of myocardial fibrosis expressed as the partition coefficient and ECV can be assessed using native and post-contrast administration T1 values (169,170).

Among available T1 mapping techniques, MOLLI, shMOLLI, SASHA and SAPPHIRE have all been clinically evaluated and validated. In the present study, shMOLLI was used for the assessment of myocardial fibrosis. A comparison of available T1 mapping technique showed that shMOLLI and MOLLI had higher precision for T1 mapping compared to SASHA and SAPPHIRE, whereas reproducibility was similar among these techniques (171). In contrast, the accuracy of shMOLLI and MOLLI was lower compared to SASHA and SAPPHIRE, especially at higher T1 values. However, shMOLLI is considered an adequate technique for the precise assessment of myocardial T1 values, and therefore, the partition coefficient and ECV (111).

Importantly, ECV has been histologically validated with ECM expansion in myocardial biopsy samples. ShMOLLI-derived ECV directly correlated with human histological collagen volume fraction in patients with severe aortic stenosis (172). MOLLI-derived ECV was associated with histologically quantified ECV in LV biopsy samples of patients with heart failure and valvular heart disease (173,174). In addition, ECV has been found to have independent prognostic value for adverse clinical outcomes: ECV was a predictor of incident heart failure, atrial fibrillation and mortality in several studies (174–178).

5.1.3. Molecular biomarkers of fibrosis

Over the past years, numerous molecular biomarkers for the non-invasive quantification of myocardial fibrosis have been studied. Candidate molecules have shown association with clinical outcomes, surrogate endpoints and preclinical target organ damage (179). However, a given molecular biomarker actually reflects myocardial fibrosis when an association between the biomarker and histologically proven myocardial fibrosis is observed. Myocardial tissue biopsy is considered the gold standard for the diagnosis of

cardiac fibrosis. The collagen turnover-derived propeptides and telopeptides investigated in the present study have all been validated against collagen volume fraction (CVF), the percentage of total myocardial tissue occupied by collagen fibers. CVF can be assessed in myocardial biopsy samples with collagen-specific staining using automated image analysis systems (180,181).

PICP is released during the extracellular processing of procollagen type I into mature collagen type I by the enzyme procollagen type I carboxy-terminal proteinase and reflects the rate of synthesis of collagen type I (46). Serum levels of circulating PICP levels have shown to be directly related to CVF in hypertensive patients with LVH. Furthermore, PICP levels were associated with CVF in individuals with HHD and heart failure. Interestingly, serum PICP levels changed in parallel with CVF in response to treatment with losartan and torasemide in subjects with HHD (34,35). PICP also showed predictive value for clinical outcomes in hypertensive patients with heart failure (182). In patients with heart failure and reduced EF, PICP was directly and independently related to mortality (183,184). In view of available evidence, serum PICP can be considered as established molecular biomarker of myocardial fibrosis.

PIIINP is released during the conversion of procollagen type III into mature collagen type III by the enzyme procollagen type III aminoterminal proteinase and reflects the rate of synthesis of collagen type III (46). Serum levels of circulating PIIINP were directly related to CVF in patients with heart failure and dilated cardiomyopathy. Moreover, serum PIIINP changed in parallel with CVF in patients with severe heart failure with reduced EF treated with spironolactone (185). In these patients, PIIINP levels were additionally found to be predictors of mortality and hospitalization due to heart failure. Hypertensive patients with diastolic dysfunction showed higher PIIINP levels than hypertensives with preserved diastolic function (186). In patients with coronary heart disease and chronic heart failure, PIIINP levels were consistently related to mortality and adverse cardiac outcomes (52).

CITP is released by endopeptidase cleavage by MMPs during collagen type I degradation and is considered a biomarker of collagen breakdown. Available evidence on the relationship between CITP and CVF is inconsistent. CITP was directly related to CVF in heart failure patients with coronary heart disease or idiopathic dilated cardiomyopathy

(187). In contrast, lower levels of CITP were observed in individuals with dilated cardiomyopathy, heart failure and severe fibrosis compared to individuals with mild to moderate fibrosis (185). In the same cohort, patients with a reduction in myocardial fibrosis after treatment with spironolactone showed an increase in serum CITP levels. CITP was found to be an independent predictor of adverse cardiovascular events and mortality in elderly individuals, regardless of the presence of cardiac dysfunction (188). In patients with heart failure and reduced ejection fraction, CITP was an independent predictor for all-cause and cardiovascular mortality (184).

MMP-1 is a calcium-dependent endopeptidase and the main determinant of extracellular degradation of collagen. Activity of MMP-1 on collagen type I results in cleavage and release of CITP to the blood. MMP-1 was not related to CVF in patients with HHD, however, individuals with higher levels of MMP-1 showed reduced levels of perimysial and endomysial collagen in cardiac muscle connective tissue (189). Hypertensives with LVH exhibited lower levels of MMP-1 compared to hypertensives with normal LV mass (190). In addition, serum MMP-1 levels predicted target organ damage, cardiovascular events and mortality in hypertensive populations (191,192).

The ratio between CITP and MMP-1 has recently been proposed to reflect collagen cross-linking. Available evidence on the prognostic value of CITP/MMP-1 is limited. In hypertensive patients with heart failure, a low CITP/MMP-1 ratio was found to be predictor of adverse clinical outcomes and mortality (182).

5.1.4. Statistical analysis

In the present study, all continuous variables were tested for normality using the Shapiro-Wilk test. More than 40 tests are available to determine if a variable is normally distributed, including Shapiro-Wilk, Kolmogorov-Smirnov, Lilliefors and Anderson-Darling tests. Numerous studies recommend the Shapiro-Wilk test as first-line technique due to its superior power compared to other tests, particularly when the sample size is below 50 (193,194).

Differences regarding normally-distributed clinical and biochemical characteristics of the study population were checked for using 2 well-established methods in medical

research: *t* tests on the equality of means for continuous variables and Pearson's chi-squared for categorical variables (195).

The calculation of Pearson´s correlation coefficient is a common technique when the relationship between 2 continuous variables is assessed (195). For multivariate analysis, linear regression analysis was performed. Model 1 contained 3 independent variables, whereas model 2 contained up to 7 independent variables. Over the past decades, the maximum number of independent variables that should be entered into regression models has been a matter of debate. A common "rule of thumb" is that regression analysis requires at least 10 cases per independent variable in order to avoid overfitting. This might be true for logistic regression models and Cox proportional hazards models, however, recent evidence shows that the minimum number of subjects per independent variable in linear regression models is 2 (196). In the present study, the number of subjects per independent variable was at least 4 in all models, therefore, the estimated regression coefficients and R^2 statistics are adequately assessed.

5.2. Results

The present study conducted in middle-aged, cardiovascular disease-free hypertensive individuals with LVH found a direct relationship between CMR-derived cardiac fibrosis, cardiac geometry and myocardial strain as a measure of cardiac functioning: The greater the extension of fibrosis, the greater the cardiac dimension and the lower the myocardial strain. Molecular biomarkers of fibrosis were associated with myocardial strain but not with the extension of CMR-derived cardiac fibrosis. Cardiac geometry was further related to peripheral hemodynamics and molecular biomarkers of myocardial stretch and injury.

Available evidence on the relationship between CMR-derived cardiac fibrosis and myocardial strain in the hypertensive population is scarce. In the present study, a higher ECV was associated with a reduction in global longitudinal strain. In accordance with this finding, Edwards *et al* showed that ECV assessed with shMOLLI and longitudinal strain were inversely related in a study including hypertensives, patients with chronic kidney

disease stage 2-4 and healthy controls (197). Furthermore, MOLLI-derived ECV was negatively associated with circumferential strain in hypertensives with or without LVH (198,199). Rommel *et al* invasively traced pressure-volume loops, the gold standard for the assessment of LV mechanical diastolic properties, in patients with poor BP control and observed a high correlation between ECV and LV stiffness (200). On the other hand, a lack of significant association of ECV with strain was reported in a study including well-controlled hypertensives with a low prevalence of LVH (<35%) (201).

The inverse relationship between myocardial fibrosis and strain can largely be explained by alterations in cardiac wall properties and consecutive adaption of pathophysiological mechanisms in the heart. Increased collagen deposition in the ECM leads to an increase in LV wall thickness and stiffness, as a consequence, the end-diastolic muscle fiber length is reduced. According to Frank-Starling´s law, a reduction in muscle fiber length at the end of diastole leads to a reduced contraction of the cardiac muscle, and therefore, to a reduction in longitudinal strain.

In fact, myocardial fibrosis showed a direct association with cardiac dimension and wall thickness in the present study. ECV was associated with left atrial diameter, a surrogate for end-diastolic LV filling pressure, and the partition coefficient was associated with LV posterior wall thickness in fully adjusted regression models. In addition, ECV was directly related to LV end-diastolic volume and posterior wall thickness in univariate analysis, and there was a trend to a greater interventricular wall thickness at higher levels of ECV in correlation models. These findings reflect the morphological alterations of cardiac cellular components observed in HHD: besides cardiomyocyte hypertrophy, the disproportionate growth of the heart due to systemic HTN is characterized by an excess of collagen in the myocardial tissue.

Surprisingly, ECV was not related to LV mass in fully adjusted regression models in the present study. Nevertheless, a direct correlation of LV mass with both ECV and partition coefficient was observed. Treibel *et al* found a significant association of ECV with LV mass index and the presence of LVH in univariate regression analysis including 46 hypertensive patients and 50 healthy controls, but did not report the results of multivariate analysis (201). However, given the relatively small number of study participants with available T1 mapping and the fact that all participants met ECG and

TTE-derived criteria of LVH, the study is likely underpowered to detect significant associations of LV mass with myocardial fibrosis when covariates are controlled for.

Elevated systemic pressure is the main risk factor for an increase in LV mass, and subsequently, diffuse myocardial fibrosis. A direct relationship between CMR-assessed myocardial fibrosis and HTN-induced pressure overload was observed in both animal models and hypertensive patients (199,201). In addition, ECV has been found to be useful for the determination of the extension of LVH in hypertensives (198).
Peripheral BP measures were significantly associated with LV mass, but not with ECV or the partition coefficient in the present study. In addition, no significant associations between central hemodynamics, cardiac geometry and myocardial fibrosis were observed. BP levels failed to predict ECV in hypertensives with LVH in a previous study (202) However, the absence of a significant association in the present study is likely due to the impact of BP treatment in the investigated cohort. All individuals were under active antihypertensive treatment, and the vast majority received 2 or more BP lowering drugs. Moreover, all patients received RAAS inhibitors, a drug class with effects on cardiac microstructure and vessel function independent of the BP lowering effect (203,204). On the other hand, a non-linear relationship between myocardial fibrosis and systemic BP has been proposed. Upregulation of pro-fibrotic genetic pathways and excessive sympathetic activity in the heart independent of BP levels have been observed (205,206). It is possible, that BP levels do not increase in parallel with LV mass in order to avoid excessive increase in afterload, which would have a negative impact on the already stressed LV mechanics. Further studies are needed to gain insight into the complex relationship between vascular hemodynamics and myocardial fibrosis.

CMR-derived myocardial strain has been extensively investigated in ischemic heart disease, idiopathic dilated cardiomyopathy, hypertrophic cardiomyopathy, valve stenosis, chemotherapy-induced cardiotoxicity, and for the evaluation of treatment response (82,86). In contrast, the role of CMR-FT in the quantification of preclinical alterations of cardiac function in HHD has not been firmly established yet.
In the present study, myocardial strain parameters showed no significant association with LV wall thickness or mass. In contrast, longitudinal strain was independently

associated with TTE-measured LV mass in a study including 320 newly-diagnosed hypertensives and 160 controls (207). The participants of the present study were characterized by an advanced state of HDD with a LVH prevalence of 100%, therefore, the study may be underpowered to find a significant association of LV mass with strain. However, strain parameters were related to LV volumes, which depend on cardiac structure and functioning. Radial strain was inversely related to LV end-systolic volume in fully adjusted regression models, and correlated negatively with LV end-diastolic volume. Furthermore, circumferential strain correlated inversely with LV end-systolic volume. It is well known that LV chamber filling and myocardial shortening or lengthening are closely interrelated (208,209). A reduction in radial strain confers a decrease in radial thickening during the cardiac cycle, leading to a reduced inward displacement of the endocardium and consequently an increase in LV cavity volume. Circumferential strain reflects the myocardial shortening along the circular perimeter and is a major determinant of stroke volume and ejection fraction (210). Consequently, a reduction in circumferential strain will lead to a reduction in systolic function and an increase in LV end-systolic volume.

Interestingly, strain parameters were not significantly related to peripheral or central hemodynamics in the present study. Myocardial contraction and relaxation depend on the prevailing hemodynamic loads in the left ventricle, therefore, a significant relationship between strain parameters and BP levels was expected. Numerous studies found lower strain parameters in hypertensives or heart failure patients compared to healthy controls (211,212). In addition, BP control was reported to be related to strain parameters in the hypertensive population (213). However, Ye *et al* used STE for the assessment of longitudinal strain in a population-based cohort including more than 500 individuals and did not find a significant association of strain with systolic BP levels (214). In another population-based study of similar sample size, STE-derived longitudinal strain was associated with ambulatory BP, but not with office BP in fully adjusted models (215). The exact interaction between vascular hemodynamics and strain as an indicator of early subclinic cardiac dysfunction is not fully understood. In the present study, the relatively low number of study participants together with the high prevalence of BP-lowering treatment might contribute to the absence of a significant relationship

between strain and vascular hemodynamics. However, 24-hour systolic BP was inversely associated with LA reservoir function, a surrogate for LV functioning, and therefore, myocardial strain.

Myocardial strain parameters were associated with molecular biomarkers of fibrosis. Higher levels of circulating CITP, a marker of collagen type I degradation, were associated with a decrease in longitudinal strain. Plaksej *et al* observed higher CITP levels and lower longitudinal strain in the upper LV mass index tertile of 81 hypertensives and 20 healthy controls (216). In treated hypertensives, CITP levels predicted independently diastolic function and heart failure (217). Importantly, CITP was associated with impaired systolic function and adverse clinical outcomes in prospective studies (187,216). Elevated CITP levels further predicted cardiovascular and all-cause mortality in a study including patients with heart failure and impaired LV systolic function (184). In view of available evidence and in accordance with the present findings, high CITP levels can be considered as a predictor of impaired cardiac function in the hypertensive population.

Circumferential strain, a major determinant of systolic function, was directly associated with circulating levels of MMP-1: the lower the circumferential strain, the lower the levels of MMP-1. In accordance with the present finding, low levels of MMP-1 were associated with systolic dysfunction defined as EF ≤ 35 % and mortality in 260 heart failure patients (218). Low levels of MMP-1 further determined functional status and prognosis in chronic heart failure patients (219). In contrast, higher levels of MMP-1 were related to target organ damage and predicted adverse clinical events in hypertensives (191,192). In another study conducted in treated hypertensives, MMP-1 levels failed to predict diastolic dysfunction or heart failure (217).

The CITP/MMP-1 index has recently been proposed to reflect CCL, and hypertensive heart failure patients with a low CITP/MMP-1 ratio were found to have a higher risk for heart failure hospitalization (59). In the same cohort, the combination of low CITP/MMP-1 and high PICP levels predicted cardiovascular death (182). In the present study, a high CITP/MMP-1 ratio was associated with a reduction in longitudinal and circumferential

strain. Importantly, the observed associations were not independent of the individual biomarkers. In other words, longitudinal strain was associated with CITP and CITP/MMP-1 in fully adjusted regression models and marginally related to MMP-1 in univariate analysis. Circumferential strain was associated with MMP-1 and CITP/MMP-1 in fully adjusted models, but not with CITP levels. Importantly, CITP/MMP-1 correlated highly with MMP-1 (Pearson´s *r* = -0.96), therefore, it is not surprising to see an elevation in CITP/MMP-1 when MMP-1 decreases, even at a low-level decrease.

Although CITP, MMP-1 and CITP/MMP-1 were related to strain measures, no significant association of PICP or PIIINP with measures of cardiac geometry or myocardial fibrosis were observed. It is important to stress several aspects regarding molecular biomarkers of fibrosis and the presence or lack of significant associations with CMR-derived measures of geometry, function and fibrosis in the present study.

First, BP lowering treatment affects plasma levels of molecular biomarkers of fibrosis, particularly inhibitors of the RAAS system and diuretics. In hypertensives, an increase in CITP levels and a decrease in PICP levels was observed following treatment with losartan, an angiotensin II antagonist, and after treatment with Ramipril, an angiotensin-converting enzyme inhibitor, in combination with hydrochlorothiazide or canrenone (a thiazide-type diuretic and an antagonist of aldosterone, respectively) (35,220). Treatment with losartan also lowered PICP levels in hypertensives with HHD (221). Díez *et al* observed a significant decrease in PICP and PIIINP levels after treatment with lisinopril, an angiotensin-converting enzyme inhibitor (222). Izawa *et al* found a significant decrease in CITP, PICP and PIIINP levels after treatment with spironolactone, an antagonist of aldosterone, in patients with idiopathic dilated cardiomyopathy (185). CITP was also reduced after treatment with bisoprolol, a cardioselective beta blocker (223). Treatment with torasemide, a loop diuretic, led to a significant decrease of PICP levels in patients with chronic heart failure (34). Collectively, first-line BP lowering drugs affect circulating levels of molecular biomarkers of fibrosis, therefore, observed findings have to be interpreted with caution when a study population with a high prevalence of antihypertensive treatment is investigated.

Second, disease severity might have an impact on molecular biomarkers of fibrosis. It is possible that potential associations might have been observed if hypertensives with LVH

would have been compared to hypertensives without LVH or to healthy controls. In fact, molecular biomarkers of fibrosis were related to LVH, myocardial fibrosis and diastolic dysfunction in hypertensives when subjects at different stages of HHD were compared (186,224–227).

Third, molecular biomarkers of fibrosis may be released from non-cardiac sources of collagen turnover, therefore, they are not specific for the myocardium. For example, molecular biomarkers of fibrosis have been used in the assessment of liver fibrosis and idiopathic pulmonary fibrosis (228,229). As a consequence, circulating levels of biomarkers might be influenced by fibrotic diseases other than HHD.

NT-proBNP and hs-Troponin T, two well-established biomarkers of myocardial stretch and injury, respectively, were consistently associated with measures of cardiac geometry and LV mass. Numerous studies have confirmed a direct relationship between NT-proBNP or BNP with LV structure and LV mass in hypertensives (230–234). Furthermore, levels of NT-proBNP were predictors of cardiovascular events and death in hypertensive patients with LVH (235). In HHD, the increased LV wall stress and elevated filling pressures lead to ventricular production of natriuretic peptides, which promote vasodilatation, natriuresis, and consequently diuresis *per se* (236). The diuretic effect of natriuretic peptides offsets the adverse effects of volume overload in cardiac chambers by improving myocardial relaxation. In addition, natriuretic peptides counteract vascoconstriction and sodium retention mediated by RAAS (237).

NT-proBNP was further associated with PWV, the gold standard for the assessment of arterial stiffness. This finding was reported before (238) and is not surprising, because a high level of arterial stiffness confers an increase in afterload and subsequently greater LV chamber stress.

Hs-Troponin T was consistently related to LV structure, mass and prevalence of LVH in numerous studies conducted in the general population and hypertensive patients (116,239,239–243). In a population-based study including more than 3500 individuals, hs-Troponin T was consistently associated with CMR-derived measures of LV structure and all-cause mortality (241). Subclinical myocardial injury due to hemodynamic stress

leads to the release of a relatively small amount of cardiac troponins into systemic circulation, which can be measured using high sensitive assays (239).

In addition, in the present study, there was a trend to higher levels of PIIINP when hs-Troponin T was increased. A significant association of hs-Troponin T with PIIINP and CITP was observed in a prospective study including heart failure patients, suggesting that cardiac microinjury adversely affects biomarkers of collagen metabolism (116). The biological processes involved in tissue repair require an adequate amount and quality of collagen (244,245), therefore, it is not surprising that hsTroponin T and molecular biomarkers of fibrosis were found to be interrelated.

In summary, CMR-derived strain analysis, T1 mapping and molecular biomarkers of fibrosis are interrelated and might be useful tools for the identification and characterization of preclinical cardiac dysfunction and diffuse myocardial fibrosis in hypertensives with LVH. The present study gives insight into the complex pathophysiological mechanisms implicated in the development and progression of HHD, and explores emerging technologies nowadays available for the evaluation of LVH in the hypertensive population.

CMR imaging has become the gold standard for the assessment of cardiac geometry, systolic and diastolic function, however, the role of strain analysis and T1 mapping has not been firmly established yet. The observed associations in the present study do not allow recommending the routinely use of these techniques in clinical practice. Harmonization of measurement methods for the assessment of CMR-derived strain and ECV would be desirable for an adequate comparison of performance of these parameters among different study populations.

Molecular biomarkers of fibrosis were related to strain but performed poorly as predictors of LV wall thickness, LV mass or CMR-derived cardiac fibrosis in the present study. Therefore, the determination of these biomarkers should remain restricted to investigational purpose and is not suitable for clinical decision making under present conditions. It is important to point out that a relatively small number of study participants with a complete dataset was available for statistical analysis. Moreover, the cross-sectional design is not appropriate to determine cause and effect of observed

associations, and temporal relationships between the exposure and outcome cannot be ascertained. In future studies, the performance of strain imaging, T1 mapping and molecular biomarkers of fibrosis for the prediction of target organ damage and cardiovascular events needs to be investigated in large longitudinal studies in order to clarify the potential role of these techniques in the assessment of HHD.

6. Conclusions

- Peripheral hemodynamics, but not central hemodynamics, were independently associated with LV mass and LA reservoir function.

- CMR-assessed fibrosis showed significant associations with cardiac geometry and myocardial strain: A greater extension of cardiac fibrosis was related to an increase in cardiac dimensions and a decrease in longitudinal strain. Cardiac fibrosis was a relevant component of changes in LV posterior wall thickness and LA diameter.

- Myocardial strain and LV volumes were directly related. Radial strain was independently and inversely associated with LV end-systolic volume, an established surrogate for afterload and contractility.

- Myocardial strain was associated with molecular biomarkers of fibrosis: A decrease in longitudinal or circumferential strain was related to higher levels of CITP and lower levels of MMP-1, respectively.

- NT-proBNP and hs-Troponin T, established biomarkers of myocardial stretch and injury, were directly related to LV mass. NT-proBNP and hs-Troponin T were further associated with LV posterior wall thickness and LA diameter, respectively.

- In hypertensives with HHD, LV walls contain a relevant amount of fibrotic tissue identified with CMR imaging. Myocardial fibrosis is associated with impaired cardiac deformation expressed as reduced longitudinal strain, which is related to molecular biomarkers of fibrosis. Moreover, changes in LV mass, LV wall thickness and LA dimension modify the levels of circulating biomarkers of myocardial stretch and injury.

7. References

1. World Health Organization. A global brief on hypertension: silent killer, global public health crisis. [Internet]. [cited 2017 May 30]. Available from: http://ish-world.com/downloads/pdf/global_brief_hypertension.pdf

2. Lim SS, Vos T, Flaxman AD, Danaei G, Shibuya K, Adair-Rohani H, et al. A comparative risk assessment of burden of disease and injury attributable to 67 risk factors and risk factor clusters in 21 regions, 1990-2010: a systematic analysis for the Global Burden of Disease Study 2010. Lancet Lond Engl. 2012 Dec 15;380(9859):2224–60.

3. Mayet J, Hughes A. Cardiac and vascular pathophysiology in hypertension. Heart Br Card Soc. 2003 Sep;89(9):1104–9.

4. Lorell BH, Carabello BA. Left ventricular hypertrophy: pathogenesis, detection, and prognosis. Circulation. 2000 Jul 25;102(4):470–9.

5. Lazzeroni D, Rimoldi O, Camici PG. From Left Ventricular Hypertrophy to Dysfunction and Failure. Circ J Off J Jpn Circ Soc. 2016;80(3):555–64.

6. McMaster WG, Kirabo A, Madhur MS, Harrison DG. Inflammation, immunity, and hypertensive end-organ damage. Circ Res. 2015 Mar 13;116(6):1022–33.

7. Devereux RB, Casale PN, Hammond IW, Savage DD, Alderman MH, Campo E, et al. Echocardiographic detection of pressure-overload left ventricular hypertrophy: effect of criteria and patient population. J Clin Hypertens. 1987 Mar;3(1):66–78.

8. Wan S-H, Vogel MW, Chen HH. Pre-clinical diastolic dysfunction. J Am Coll Cardiol. 2014 Feb 11;63(5):407–16.

9. Niemeijer MN, Leening MJG, van den Berg ME, Hofman A, Franco OH, Deckers JW, et al. Subclinical Abnormalities in Echocardiographic Parameters and Risk of Sudden Cardiac Death in a General Population: The Rotterdam Study. J Card Fail. 2016 Jan;22(1):17–23.

10. Cramariuc D, Gerdts E. Epidemiology of left ventricular hypertrophy in hypertension: implications for the clinic. Expert Rev Cardiovasc Ther. 2016 Aug;14(8):915–26.

11. Anand IS, Florea VG, Fisher L. Surrogate end points in heart failure. J Am Coll Cardiol. 2002 May 1;39(9):1414–21.

12. Klapholz M. β-Blocker Use for the Stages of Heart Failure. Mayo Clin Proc. 2009 Aug;84(8):718–29.

13. Devereux RB, Wachtell K, Gerdts E, Boman K, Nieminen MS, Papademetriou V, et al. Prognostic significance of left ventricular mass change during treatment of hypertension. JAMA. 2004 Nov 17;292(19):2350–6.

14. Redfield MM, Jacobsen SJ, Burnett JC, Mahoney DW, Bailey KR, Rodeheffer RJ. Burden of systolic and diastolic ventricular dysfunction in the community:

appreciating the scope of the heart failure epidemic. JAMA. 2003 Jan 8;289(2):194–202.

15. Berk BC, Fujiwara K, Lehoux S. ECM remodeling in hypertensive heart disease. J Clin Invest. 2007 Mar 1;117(3):568–75.

16. Dávila DF, Donis JH, Odreman R, Gonzalez M, Landaeta A. Patterns of left ventricular hypertrophy in essential hypertension: should echocardiography guide the pharmacological treatment? Int J Cardiol. 2008 Feb 29;124(2):134–8.

17. Sugden PH, Clerk A. Cellular mechanisms of cardiac hypertrophy. J Mol Med Berl Ger. 1998 Oct;76(11):725–46.

18. Fortuño MA, Ravassa S, Fortuño A, Zalba G, Díez J. Cardiomyocyte apoptotic cell death in arterial hypertension: mechanisms and potential management. Hypertens Dallas Tex 1979. 2001 Dec 1;38(6):1406–12.

19. Anversa P, Olivetti G, Leri A, Liu Y, Kajstura J. Myocyte cell death and ventricular remodeling. Curr Opin Nephrol Hypertens. 1997 Mar;6(2):169–76.

20. Moreno MU, Eiros R, Gavira JJ, Gallego C, González A, Ravassa S, et al. The Hypertensive Myocardium: From Microscopic Lesions to Clinical Complications and Outcomes. Med Clin North Am. 2017 Jan;101(1):43–52.

21. Chandrashekhar Y. Role of apoptosis in ventricular remodeling. Curr Heart Fail Rep. 2005 Mar;2(1):18–22.

22. Drazner MH. The Progression of Hypertensive Heart Disease. Circulation. 2011 Jan 25;123(3):327–34.

23. Brilla CG, Zhou G, Rupp H, Maisch B, Weber KT. Role of angiotensin II and prostaglandin E2 in regulating cardiac fibroblast collagen turnover. Am J Cardiol. 1995 Nov 2;76(13):8D–13D.

24. Norton GR, Tsotetsi J, Trifunovic B, Hartford C, Candy GP, Woodiwiss AJ. Myocardial Stiffness Is Attributed to Alterations in Cross-Linked Collagen Rather Than Total Collagen or Phenotypes in Spontaneously Hypertensive Rats. Circulation. 1997 Sep 16;96(6):1991–8.

25. Kenchaiah S, Pfeffer MA. Cardiac remodeling in systemic hypertension. Med Clin North Am. 2004 Jan;88(1):115–30.

26. Feihl F, Liaudet L, Levy BI, Waeber B. Hypertension and microvascular remodelling. Cardiovasc Res. 2008 May 1;78(2):274–85.

27. Paulus WJ, Tschöpe C. A Novel Paradigm for Heart Failure With Preserved Ejection Fraction. J Am Coll Cardiol. 2013 Jul;62(4):263–71.

28. Funck RC, Wilke A, Rupp H, Brilla CG. Regulation and role of myocardial collagen matrix remodeling in hypertensive heart disease. Adv Exp Med Biol. 1997;432:35–44.

29. Brilla CG, Reams GP, Maisch B, Weber KT. Renin-angiotensin system and myocardial fibrosis in hypertension: regulation of the myocardial collagen matrix. Eur Heart J. 1993 Nov;14 Suppl J:57–61.

30. Brooks A, Schinde V, Bateman AC, Gallagher PJ. Interstitial fibrosis in the dilated non-ischaemic myocardium. Heart Br Card Soc. 2003 Oct;89(10):1255–6.

31. Weidemann F, Herrmann S, Störk S, Niemann M, Frantz S, Lange V, et al. Impact of myocardial fibrosis in patients with symptomatic severe aortic stenosis. Circulation. 2009 Aug 18;120(7):577–84.

32. Marijianowski MM, Teeling P, Mann J, Becker AE. Dilated cardiomyopathy is associated with an increase in the type I/type III collagen ratio: a quantitative assessment. J Am Coll Cardiol. 1995 May;25(6):1263–72.

33. Marijianowski MM, Teeling P, Becker AE. Remodeling after myocardial infarction in humans is not associated with interstitial fibrosis of noninfarcted myocardium. J Am Coll Cardiol. 1997 Jul;30(1):76–82.

34. López B, Querejeta R, González A, Sánchez E, Larman M, Díez J. Effects of loop diuretics on myocardial fibrosis and collagen type I turnover in chronic heart failure. J Am Coll Cardiol. 2004 Jun 2;43(11):2028–35.

35. Díez J, Querejeta R, López B, González A, Larman M, Martínez Ubago JL. Losartan-dependent regression of myocardial fibrosis is associated with reduction of left ventricular chamber stiffness in hypertensive patients. Circulation. 2002 May 28;105(21):2512–7.

36. Weber KT, Brilla CG. Pathological hypertrophy and cardiac interstitium. Fibrosis and renin-angiotensin-aldosterone system. Circulation. 1991;83(6):1849–1865.

37. Sutton MG, Sharpe N. Left ventricular remodeling after myocardial infarction: pathophysiology and therapy. Circulation. 2000 Jun 27;101(25):2981–8.

38. Bohl S, Wassmuth R, Abdel-Aty H, Rudolph A, Messroghli D, Dietz R, et al. Delayed enhancement cardiac magnetic resonance imaging reveals typical patterns of myocardial injury in patients with various forms of non-ischemic heart disease. Int J Cardiovasc Imaging. 2008 Aug;24(6):597–607.

39. Mahrholdt H, Wagner A, Judd RM, Sechtem U, Kim RJ. Delayed enhancement cardiovascular magnetic resonance assessment of non-ischaemic cardiomyopathies. Eur Heart J. 2005 Aug;26(15):1461–74.

40. Piek A, de Boer RA, Silljé HHW. The fibrosis-cell death axis in heart failure. Heart Fail Rev. 2016 Mar;21(2):199–211.

41. Zarate YA, Hopkin RJ. Fabry's disease. Lancet Lond Engl. 2008 Oct 18;372(9647):1427–35.

42. Shah KB, Inoue Y, Mehra MR. Amyloidosis and the heart: a comprehensive review. Arch Intern Med. 2006 Sep 25;166(17):1805–13.

43. Pichler G, Haller MC, Kainz A, Wolf M, Redon J, Oberbauer R. Prognostic value of bone- and vascular-derived molecular biomarkers in hemodialysis and renal transplant patients: a systematic review and meta-analysis. Nephrol Dial Transplant. 2016 Dec 26;

44. Medugorac I, Jacob R. Characterisation of left ventricular collagen in the rat. Cardiovasc Res. 1983 Jan;17(1):15–21.

45. Weber KT, Janicki JS, Shroff SG, Pick R, Chen RM, Bashey RI. Collagen remodeling of the pressure-overloaded, hypertrophied nonhuman primate myocardium. Circ Res. 1988 Apr;62(4):757–65.

46. Miyahara M, Njieha FK, Prockop DJ. Formation of collagen fibrils in vitro by cleavage of procollagen with procollagen proteinases. J Biol Chem. 1982 Jul 25;257(14):8442–8.

47. Fan D, Takawale A, Lee J, Kassiri Z. Cardiac fibroblasts, fibrosis and extracellular matrix remodeling in heart disease. Fibrogenesis Tissue Repair. 2012;5(1):15.

48. Timpl R, Glanville RW. The aminopropeptide of collagen. Clin Orthop. 1981 Aug;(158):224–42.

49. Baicu CF, Zhang Y, Van Laer AO, Renaud L, Zile MR, Bradshaw AD. Effects of the absence of procollagen C-endopeptidase enhancer-2 on myocardial collagen accumulation in chronic pressure overload. Am J Physiol Heart Circ Physiol. 2012 Jul 15;303(2):H234-240.

50. López B, González A, Ravassa S, Beaumont J, Moreno MU, San José G, et al. Circulating Biomarkers of Myocardial Fibrosis. J Am Coll Cardiol. 2015 Jun;65(22):2449–56.

51. Prockop DJ, Kivirikko KI. Collagens: molecular biology, diseases, and potentials for therapy. Annu Rev Biochem. 1995;64:403–34.

52. J Lijnen P, Maharani T, Finahari N, S Prihadi J. Serum collagen markers and heart failure. Cardiovasc Haematol Disord-Drug Targets Former Curr Drug Targets-Cardiovasc Hematol Disord. 2012;12(1):51–55.

53. Malemud CJ. Matrix metalloproteinases (MMPs) in health and disease: an overview. Front Biosci J Virtual Libr. 2006 May 1;11:1696–701.

54. Sternlicht MD, Werb Z. How matrix metalloproteinases regulate cell behavior. Annu Rev Cell Dev Biol. 2001;17:463–516.

55. Badenhorst D, Maseko M, Tsotetsi OJ, Naidoo A, Brooksbank R, Norton GR, et al. Cross-linking influences the impact of quantitative changes in myocardial collagen on cardiac stiffness and remodelling in hypertension in rats. Cardiovasc Res. 2003 Mar;57(3):632–41.

56. Mukherjee D, Sen S. Collagen phenotypes during development and regression of myocardial hypertrophy in spontaneously hypertensive rats. Circ Res. 1990 Dec;67(6):1474–80.

57. Shoulders MD, Raines RT. Collagen structure and stability. Annu Rev Biochem. 2009;78:929–58.

58. Visse R, Nagase H. Matrix Metalloproteinases and Tissue Inhibitors of Metalloproteinases: Structure, Function, and Biochemistry. Circ Res. 2003 May 2;92(8):827–39.

59. López B, Ravassa S, González A, Zubillaga E, Bonavila C, Bergés M, et al. Myocardial Collagen Cross-Linking Is Associated With Heart Failure Hospitalization in Patients With Hypertensive Heart Failure. J Am Coll Cardiol. 2016 Jan;67(3):251–60.

60. Panagopoulou V, Deftereos S, Kossyvakis C, Raisakis K, Giannopoulos G, Bouras G, et al. NTproBNP: an important biomarker in cardiac diseases. Curr Top Med Chem. 2013;13(2):82–94.

61. Hall C. Essential biochemistry and physiology of (NT-pro)BNP. Eur J Heart Fail. 2004 Mar 15;6(3):257–60.

62. Weber M, Mitrovic V, Hamm C. B-type natriuretic peptide and N-terminal pro-B-type natriuretic peptide – Diagnostic role in stable coronary artery disease. Exp Clin Cardiol. 2006;11(2):99–101.

63. Takeda S, Yamashita A, Maeda K, Maéda Y. Structure of the core domain of human cardiac troponin in the Ca(2+)-saturated form. Nature. 2003 Jul 3;424(6944):35–41.

64. Sato Y, Yamamoto E, Sawa T, Toda K, Hara T, Iwasaki T, et al. High-sensitivity cardiac troponin T in essential hypertension. J Cardiol. 2011 Nov;58(3):226–31.

65. Fridén V, Starnberg K, Muslimovic A, Ricksten S-E, Bjurman C, Forsgard N, et al. Clearance of cardiac troponin T with and without kidney function. Clin Biochem. 2017 Jun;50(9):468–74.

66. Shave R, George K, Gaze D. The influence of exercise upon cardiac biomarkers: a practical guide for clinicians and scientists. Curr Med Chem. 2007;14(13):1427–36.

67. Sandhu R, Aronow WS, Rajdev A, Sukhija R, Amin H, D'aquila K, et al. Relation of cardiac troponin I levels with in-hospital mortality in patients with ischemic stroke, intracerebral hemorrhage, and subarachnoid hemorrhage. Am J Cardiol. 2008 Sep 1;102(5):632–4.

68. Hamm CW, Giannitsis E, Katus HA. Cardiac troponin elevations in patients without acute coronary syndrome. Circulation. 2002 Dec 3;106(23):2871–2.

69. Olivetti G, Giordano G, Corradi D, Melissari M, Lagrasta C, Gambert SR, et al. Gender differences and aging: effects on the human heart. J Am Coll Cardiol. 1995 Oct;26(4):1068–79.

70. Latini R, Masson S, Anand IS, Missov E, Carlson M, Vago T, et al. Prognostic value of very low plasma concentrations of troponin T in patients with stable chronic heart failure. Circulation. 2007 Sep 11;116(11):1242–9.

71. Masson S, Anand I, Favero C, Barlera S, Vago T, Bertocchi F, et al. Serial measurement of cardiac troponin T using a highly sensitive assay in patients with chronic heart failure: data from 2 large randomized clinical trials. Circulation. 2012 Jan 17;125(2):280–8.

72. Ganau A, Devereux RB, Roman MJ, de Simone G, Pickering TG, Saba PS, et al. Patterns of left ventricular hypertrophy and geometric remodeling in essential hypertension. J Am Coll Cardiol. 1992 Jun;19(7):1550–8.

73. Pewsner D, Jüni P, Egger M, Battaglia M, Sundström J, Bachmann LM. Accuracy of electrocardiography in diagnosis of left ventricular hypertrophy in arterial hypertension: systematic review. BMJ. 2007 Oct 6;335(7622):711.

74. Kannel WB, Gordon T, Offutt D. Left ventricular hypertrophy by electrocardiogram. Prevalence, incidence, and mortality in the Framingham study. Ann Intern Med. 1969 Jul;71(1):89–105.

75. Bacharova L, Chen H, Estes EH, Mateasik A, Bluemke DA, Lima JAC, et al. Determinants of discrepancies in detection and comparison of the prognostic significance of left ventricular hypertrophy by electrocardiogram and cardiac magnetic resonance imaging. Am J Cardiol. 2015 Feb 15;115(4):515–22.

76. Devereux RB, Dahlöf B, Gerdts E, Boman K, Nieminen MS, Papademetriou V, et al. Regression of hypertensive left ventricular hypertrophy by losartan compared with atenolol: the Losartan Intervention for Endpoint Reduction in Hypertension (LIFE) trial. Circulation. 2004 Sep 14;110(11):1456–62.

77. Salcedo EE, Gockowski K, Tarazi RC. Left ventricular mass and wall thickness in hypertension. Comparison of M mode and two dimensional echocardiography in two experimental models. Am J Cardiol. 1979 Oct 22;44(5):936–40.

78. Devereux RB, Alonso DR, Lutas EM, Gottlieb GJ, Campo E, Sachs I, et al. Echocardiographic assessment of left ventricular hypertrophy: comparison to necropsy findings. Am J Cardiol. 1986 Feb 15;57(6):450–8.

79. Kühl HP, Schreckenberg M, Rulands D, Katoh M, Schäfer W, Schummers G, et al. High-resolution transthoracic real-time three-dimensional echocardiography: quantitation of cardiac volumes and function using semi-automatic border

detection and comparison with cardiac magnetic resonance imaging. J Am Coll Cardiol. 2004 Jun 2;43(11):2083–90.

80. Narayanan A, Aurigemma GP, Chinali M, Hill JC, Meyer TE, Tighe DA. Cardiac mechanics in mild hypertensive heart disease: a speckle-strain imaging study. Circ Cardiovasc Imaging. 2009 Sep;2(5):382–90.

81. Jiji RS, Kramer CM. Cardiovascular magnetic resonance: applications in daily practice. Cardiol Rev. 2011 Oct;19(5):246–54.

82. Scatteia A, Baritussio A, Bucciarelli-Ducci C. Strain imaging using cardiac magnetic resonance. Heart Fail Rev. 2017 Jul;22(4):465–76.

83. Hor KN, Gottliebson WM, Carson C, Wash E, Cnota J, Fleck R, et al. Comparison of magnetic resonance feature tracking for strain calculation with harmonic phase imaging analysis. JACC Cardiovasc Imaging. 2010 Feb;3(2):144–51.

84. Pedrizzetti G, Claus P, Kilner PJ, Nagel E. Principles of cardiovascular magnetic resonance feature tracking and echocardiographic speckle tracking for informed clinical use. J Cardiovasc Magn Reson [Internet]. 2016 Dec [cited 2017 Sep 30];18(1). Available from: http://jcmr-online.biomedcentral.com/articles/10.1186/s12968-016-0269-7

85. Liang T, Yung L, Yu W. On feature motion decorrelation in ultrasound speckle tracking. IEEE Trans Med Imaging. 2013 Feb;32(2):435–48.

86. Schuster A, Hor KN, Kowallick JT, Beerbaum P, Kutty S. Cardiovascular Magnetic Resonance Myocardial Feature Tracking: Concepts and Clinical Applications. Circ Cardiovasc Imaging. 2016 Apr;9(4):e004077.

87. Jerosch-Herold M, Kwong RY. Cardiac T1 Imaging: Top Magn Reson Imaging. 2014 Feb;23(1):3–11.

88. Taylor AJ, Salerno M, Dharmakumar R, Jerosch-Herold M. T1 Mapping. JACC Cardiovasc Imaging. 2016 Jan;9(1):67–81.

89. Messroghli DR, Walters K, Plein S, Sparrow P, Friedrich MG, Ridgway JP, et al. Myocardial T1 mapping: application to patients with acute and chronic myocardial infarction. Magn Reson Med. 2007 Jul;58(1):34–40.

90. Piechnik SK, Ferreira VM, Dall'Armellina E, Cochlin LE, Greiser A, Neubauer S, et al. Shortened Modified Look-Locker Inversion recovery (ShMOLLI) for clinical myocardial T1-mapping at 1.5 and 3 T within a 9 heartbeat breathhold. J Cardiovasc Magn Reson Off J Soc Cardiovasc Magn Reson. 2010 Nov 19;12:69.

91. Chow K, Flewitt JA, Green JD, Pagano JJ, Friedrich MG, Thompson RB. Saturation recovery single-shot acquisition (SASHA) for myocardial T(1) mapping. Magn Reson Med. 2014 Jun;71(6):2082–95.

92. Bull S, White SK, Piechnik SK, Flett AS, Ferreira VM, Loudon M, et al. Human non-contrast T1 values and correlation with histology in diffuse fibrosis. Heart Br Card Soc. 2013 Jul;99(13):932–7.

93. Ferreira VM, Piechnik SK, Dall'Armellina E, Karamitsos TD, Francis JM, Choudhury RP, et al. Non-contrast T1-mapping detects acute myocardial edema with high diagnostic accuracy: a comparison to T2-weighted cardiovascular magnetic resonance. J Cardiovasc Magn Reson Off J Soc Cardiovasc Magn Reson. 2012 Jun 21;14:42.

94. Karamitsos TD, Piechnik SK, Banypersad SM, Fontana M, Ntusi NB, Ferreira VM, et al. Noncontrast T1 mapping for the diagnosis of cardiac amyloidosis. JACC Cardiovasc Imaging. 2013 Apr;6(4):488–97.

95. Sado D, White SK, Piechnik SK, Banypersad SM, Treibel TA, Fontana M, et al. Native T1 lowering in iron overload and Anderson Fabry disease; a novel and early marker of disease. J Cardiovasc Magn Reson. 2013 Jan 1;15(S1):O71.

96. Ellims AH, Shaw JA, Stub D, Iles LM, Hare JL, Slavin GS, et al. Diffuse myocardial fibrosis evaluated by post-contrast t1 mapping correlates with left ventricular stiffness. J Am Coll Cardiol. 2014 Mar 25;63(11):1112–8.

97. Pichler G, Martinez F, Vicente A, Solaz E, Calaforra O, Redon J. Pulse pressure amplification and its determinants. Blood Press. 2016 Feb;25(1):1–7.

98. Pichler G, Martinez F, Vicente A, Solaz E, Calaforra O, Redon J. Carotid-femoral pulse wave velocity assessment by two different methods: implications for risk assessment. J Hypertens. 2015 Sep;33(9):1868–75.

99. Pichler G, Martinez F, Vicente A, Solaz E, Calaforra O, Lurbe E, et al. Influence of obesity in central blood pressure. J Hypertens. 2015 Feb;33(2):308–13.

100. Coutinho T, Turner ST, Kullo IJ. Cardiovascular risk assessment in the vascular laboratory. In: Strandness´s Duplex scanning in vascular disorders. Fifth edition. Lippincott Williams & Wilkins; 2014.

101. Mancia G, Fagard R, Narkiewicz K, Redón J, Zanchetti A, Böhm M, et al. 2013 ESH/ESC Guidelines for the management of arterial hypertension: the Task Force for the management of arterial hypertension of the European Society of Hypertension (ESH) and of the European Society of Cardiology (ESC). J Hypertens. 2013 Jul;31(7):1281–357.

102. Pauca AL, O'Rourke MF, Kon ND. Prospective evaluation of a method for estimating ascending aortic pressure from the radial artery pressure waveform. Hypertension. 2001 Oct;38(4):932–7.

103. Kossmann CE, Brody DA, Burch GE, Hecht HH, Johnston FD, Kay C, et al. Recommendations for Standardization of Leads and of Specifications for

Instruments in Electrocardiography and Vectorcardiography. Circulation. 1967 Mar 1;35(3):583–602.

104. Sokolow M, Lyon TP. The ventricular complex in left ventricular hypertrophy as obtained by unipolar precordial and limb leads. Am Heart J. 1949 Feb;37(2):161–86.

105. Casale PN, Devereux RB, Alonso DR, Campo E, Kligfield P. Improved sex-specific criteria of left ventricular hypertrophy for clinical and computer interpretation of electrocardiograms: validation with autopsy findings. Circulation. 1987 Mar 1;75(3):565–72.

106. Schiller NB, Shah PM, Crawford M, DeMaria A, Devereux R, Feigenbaum H, et al. Recommendations for quantitation of the left ventricle by two-dimensional echocardiography. American Society of Echocardiography Committee on Standards, Subcommittee on Quantitation of Two-Dimensional Echocardiograms. J Am Soc Echocardiogr Off Publ Am Soc Echocardiogr. 1989 Oct;2(5):358–67.

107. de Simone G, Devereux RB, Ganau A, Hahn RT, Saba PS, Mureddu GF, et al. Estimation of left ventricular chamber and stroke volume by limited M-mode echocardiography and validation by two-dimensional and Doppler echocardiography. Am J Cardiol. 1996 Oct 1;78(7):801–7.

108. Lang RM, Badano LP, Mor-Avi V, Afilalo J, Armstrong A, Ernande L, et al. Recommendations for cardiac chamber quantification by echocardiography in adults: an update from the American Society of Echocardiography and the European Association of Cardiovascular Imaging. Eur Heart J Cardiovasc Imaging. 2015 Mar;16(3):233–70.

109. Ginat DT, Fong MW, Tuttle DJ, Hobbs SK, Vyas RC. Cardiac imaging: Part 1, MR pulse sequences, imaging planes, and basic anatomy. AJR Am J Roentgenol. 2011 Oct;197(4):808–15.

110. Blume GG, Mcleod CJ, Barnes ME, Seward JB, Pellikka PA, Bastiansen PM, et al. Left atrial function: physiology, assessment, and clinical implications. Eur J Echocardiogr J Work Group Echocardiogr Eur Soc Cardiol. 2011 Jun;12(6):421–30.

111. Moon JC, Messroghli DR, Kellman P, Piechnik SK, Robson MD, Ugander M, et al. Myocardial T1 mapping and extracellular volume quantification: a Society for Cardiovascular Magnetic Resonance (SCMR) and CMR Working Group of the European Society of Cardiology consensus statement. J Cardiovasc Magn Reson Off J Soc Cardiovasc Magn Reson. 2013 Oct 14;15:92.

112. Montgomery DC, Peck EA, Vining GG. Introduction to Linear Regression Analysis, 5th Edition. Wiley, New York; 2012.

113. Claus P, Omar AMS, Pedrizzetti G, Sengupta PP, Nagel E. Tissue Tracking Technology for Assessing Cardiac Mechanics: Principles, Normal Values, and Clinical Applications. JACC Cardiovasc Imaging. 2015 Dec;8(12):1444–60.

114. Taylor RJ, Moody WE, Umar F, Edwards NC, Taylor TJ, Stegemann B, et al. Myocardial strain measurement with feature-tracking cardiovascular magnetic resonance: normal values. Eur Heart J - Cardiovasc Imaging. 2015 Aug 1;16(8):871–81.

115. Dabir D, Child N, Kalra A, Rogers T, Gebker R, Jabbour A, et al. Reference values for healthy human myocardium using a T1 mapping methodology: results from the International T1 Multicenter cardiovascular magnetic resonance study. J Cardiovasc Magn Reson. 2014 Oct 21;16:69.

116. Ravassa S, Kuznetsova T, Varo N, Thijs L, Delles C, Dominiczak A, et al. Biomarkers of cardiomyocyte injury and stress identify left atrial and left ventricular remodelling and dysfunction: A population-based study. Int J Cardiol. 2015 Apr;185:177–85.

117. Strait JB, Lakatta EG. Aging-associated cardiovascular changes and their relationship to heart failure. Heart Fail Clin. 2012 Jan;8(1):143–64.

118. Lionakis N, Mendrinos D, Sanidas E, Favatas G, Georgopoulou M. Hypertension in the elderly. World J Cardiol. 2012 May 26;4(5):135–47.

119. Horn MA, Trafford AW. Aging and the cardiac collagen matrix: Novel mediators of fibrotic remodelling. J Mol Cell Cardiol. 2016 Apr;93:175–85.

120. Biernacka A, Frangogiannis NG. Aging and Cardiac Fibrosis. Aging Dis. 2011 Apr;2(2):158–73.

121. Kass DA. Age-related changes in venticular-arterial coupling: pathophysiologic implications. Heart Fail Rev. 2002 Jan;7(1):51–62.

122. Liu C-Y, Lai S, Kawel-Boehm N, Chahal H, Ambale-Venkatesh B, Lima JAC, et al. Healthy aging of the left ventricle in relationship to cardiovascular risk factors: The Multi-Ethnic Study of Atherosclerosis (MESA). PloS One. 2017;12(6):e0179947.

123. Smulyan H, Asmar RG, Rudnicki A, London GM, Safar ME. Comparative effects of aging in men and women on the properties of the arterial tree. J Am Coll Cardiol. 2001 Apr;37(5):1374–80.

124. Gudmundsdottir H, Høieggen A, Stenehjem A, Waldum B, Os I. Hypertension in women: latest findings and clinical implications. Ther Adv Chronic Dis. 2012 May;3(3):137–46.

125. Santos M, Shah AM. Alterations in cardiac structure and function in hypertension. Curr Hypertens Rep. 2014 May;16(5):428.

126. London GM. Cardiovascular disease in chronic renal failure: pathophysiologic aspects. Semin Dial. 2003 Apr;16(2):85–94.

127. D'Marco L, Bellasi A, Raggi P. Cardiovascular biomarkers in chronic kidney disease: state of current research and clinical applicability. Dis Markers. 2015;2015:586569.

128. Fryar CD, Hirsch R, Eberhardt MS, Yoon SS, Wright JD. Hypertension, high serum total cholesterol, and diabetes: racial and ethnic prevalence differences in U.S. adults, 1999-2006. NCHS Data Brief. 2010 Apr;(36):1–8.

129. Shrestha PL, Shrestha PA, Vivo RP. Epidemiology of comorbidities in patients with hypertension. Curr Opin Cardiol. 2016 Jul;31(4):376–80.

130. Johnson ML, Pietz K, Battleman DS, Beyth RJ. Prevalence of comorbid hypertension and dyslipidemia and associated cardiovascular disease. Am J Manag Care. 2004 Dec;10(12):926–32.

131. Kidy FF, Dhalwani N, Harrington DM, Gray LJ, Bodicoat DH, Webb D, et al. Associations Between Anthropometric Measurements and Cardiometabolic Risk Factors in White European and South Asian Adults in the United Kingdom. Mayo Clin Proc. 2017 Jun;92(6):925–33.

132. Salonen JT, Lakka TA, Lakka HM, Valkonen VP, Everson SA, Kaplan GA. Hyperinsulinemia is associated with the incidence of hypertension and dyslipidemia in middle-aged men. Diabetes. 1998 Feb;47(2):270–5.

133. Sur G, Sur M, Kudor-Szabadi L, Sur L, Sporis D, Sur D. Arterial hypertension - prevalence of risk factors and morbide associations that increase cardiovascular risk. Maedica. 2010 Jan;5(1):34–40.

134. Nguyen NT, Magno CP, Lane KT, Hinojosa MW, Lane JS. Association of hypertension, diabetes, dyslipidemia, and metabolic syndrome with obesity: findings from the National Health and Nutrition Examination Survey, 1999 to 2004. J Am Coll Surg. 2008 Dec;207(6):928–34.

135. Cuspidi C, Lonati L, Sampieri L, Macca G, Michev I, Salerno M, et al. Impact of blood pressure control on prevalence of left ventricular hypertrophy in treated hypertensive patients. Cardiology. 2000;93(3):149–54.

136. Rider OJ, Ntusi N, Bull SC, Nethononda R, Ferreira V, Holloway CJ, et al. Improvements in ECG accuracy for diagnosis of left ventricular hypertrophy in obesity. Heart Br Card Soc. 2016 Oct 1;102(19):1566–72.

137. Somaratne JB, Whalley GA, Poppe KK, ter Bals MM, Wadams G, Pearl A, et al. Screening for left ventricular hypertrophy in patients with type 2 diabetes mellitus in the community. Cardiovasc Diabetol. 2011 Apr 14;10:29.

138. Bratincsák A, Williams M, Kimata C, Perry JC. The Electrocardiogram Is a Poor Diagnostic Tool to Detect Left Ventricular Hypertrophy in Children: A Comparison with Echocardiographic Assessment of Left Ventricular Mass. Congenit Heart Dis. 2015 Aug;10(4):E164-171.

139. Okin PM, Devereux RB, Jern S, Kjeldsen SE, Julius S, Nieminen MS, et al. Regression of electrocardiographic left ventricular hypertrophy during antihypertensive

treatment and the prediction of major cardiovascular events. JAMA. 2004 Nov 17;292(19):2343–9.

140. Levy D, Salomon M, D'Agostino RB, Belanger AJ, Kannel WB. Prognostic implications of baseline electrocardiographic features and their serial changes in subjects with left ventricular hypertrophy. Circulation. 1994 Oct;90(4):1786–93.

141. Mulè' G, Nardi E, Guarneri M, Cottone S. Electrocardiography for Assessment of Hypertensive Heart Disease: A New Role for an Old Tool. J Clin Hypertens Greenwich Conn. 2016 Sep;18(9):843–5.

142. Chuang ML, Hibberd MG, Salton CJ, Beaudin RA, Riley MF, Parker RA, et al. Importance of imaging method over imaging modality in noninvasive determination of left ventricular volumes and ejection fraction: assessment by two- and three-dimensional echocardiography and magnetic resonance imaging. J Am Coll Cardiol. 2000 Feb;35(2):477–84.

143. Pennell DJ. Cardiovascular magnetic resonance: twenty-first century solutions in cardiology. Clin Med Lond Engl. 2003 Jun;3(3):273–8.

144. Armstrong AC, Gjesdal O, Almeida A, Nacif M, Wu C, Bluemke DA, et al. Left ventricular mass and hypertrophy by echocardiography and cardiac magnetic resonance: the multi-ethnic study of atherosclerosis. Echocardiogr Mt Kisco N. 2014;31(1):12–20.

145. Kerwin WS, Prince JL. Cardiac material markers from tagged MR images. Med Image Anal. 1998 Dec;2(4):339–53.

146. Onishi T, Saha SK, Ludwig DR, Onishi T, Marek JJ, Cavalcante JL, et al. Feature tracking measurement of dyssynchrony from cardiovascular magnetic resonance cine acquisitions: comparison with echocardiographic speckle tracking. J Cardiovasc Magn Reson Off J Soc Cardiovasc Magn Reson. 2013 Oct 17;15:95.

147. Amaki M, Savino J, Ain DL, Sanz J, Pedrizzetti G, Kulkarni H, et al. Diagnostic Concordance of Echocardiography and Cardiac Magnetic Resonance–Based Tissue Tracking for Differentiating Constrictive Pericarditis From Restrictive CardiomyopathyCLINICAL PERSPECTIVE. Circ Cardiovasc Imaging. 2014 Sep 1;7(5):819–27.

148. Obokata M, Nagata Y, Wu VC-C, Kado Y, Kurabayashi M, Otsuji Y, et al. Direct comparison of cardiac magnetic resonance feature tracking and 2D/3D echocardiography speckle tracking for evaluation of global left ventricular strain. Eur Heart J - Cardiovasc Imaging. 2016 May 1;17(5):525–32.

149. Onishi T, Saha SK, Delgado-Montero A, Ludwig DR, Onishi T, Schelbert EB, et al. Global Longitudinal Strain and Global Circumferential Strain by Speckle-Tracking Echocardiography and Feature-Tracking Cardiac Magnetic Resonance Imaging: Comparison with Left Ventricular Ejection Fraction. J Am Soc Echocardiogr. 2015 May 1;28(5):587–96.

150. Marwick TH, Leano RL, Brown J, Sun J-P, Hoffmann R, Lysyansky P, et al. Myocardial Strain Measurement With 2-Dimensional Speckle-Tracking Echocardiography: Definition of Normal Range. JACC Cardiovasc Imaging. 2009 Jan 1;2(1):80–4.

151. Mondillo S, Galderisi M, Mele D, Cameli M, Lomoriello VS, Zacà V, et al. Speckle-tracking echocardiography: a new technique for assessing myocardial function. J Ultrasound Med Off J Am Inst Ultrasound Med. 2011 Jan;30(1):71–83.

152. Thiele H, Paetsch I, Schnackenburg B, Bornstedt A, Grebe O, Wellnhofer E, et al. Improved accuracy of quantitative assessment of left ventricular volume and ejection fraction by geometric models with steady-state free precession. J Cardiovasc Magn Reson Off J Soc Cardiovasc Magn Reson. 2002;4(3):327–39.

153. Morais P, Marchi A, Bogaert JA, Dresselaers T, Heyde B, D'hooge J, et al. Cardiovascular magnetic resonance myocardial feature tracking using a non-rigid, elastic image registration algorithm: assessment of variability in a real-life clinical setting. J Cardiovasc Magn Reson Off J Soc Cardiovasc Magn Reson. 2017 Feb 17;19(1):24.

154. Gao H, Allan A, McComb C, Luo X, Berry C. Left ventricular strain and its pattern estimated from cine CMR and validation with DENSE. Phys Med Biol. 2014;59(13):3637.

155. Shetye AM, Nazir SA, Razvi NA, Price N, Khan JN, Lai FY, et al. Comparison of global myocardial strain assessed by cardiovascular magnetic resonance tagging and feature tracking to infarct size at predicting remodelling following STEMI. BMC Cardiovasc Disord. 2017 Jan 5;17:7.

156. McComb C, Carrick D, McClure JD, Woodward R, Radjenovic A, Foster JE, et al. Assessment of the relationships between myocardial contractility and infarct tissue revealed by serial magnetic resonance imaging in patients with acute myocardial infarction. Int J Cardiovasc Imaging. 2015 Aug 1;31(6):1201–9.

157. Buss SJ, Krautz B, Hofmann N, Sander Y, Rust L, Giusca S, et al. Prediction of functional recovery by cardiac magnetic resonance feature tracking imaging in first time ST-elevation myocardial infarction. Comparison to infarct size and transmurality by late gadolinium enhancement. Int J Cardiol. 2015 Mar 15;183:162–70.

158. Khan JN, Singh A, Nazir SA, Kanagala P, Gershlick AH, McCann GP. Comparison of cardiovascular magnetic resonance feature tracking and tagging for the assessment of left ventricular systolic strain in acute myocardial infarction. Eur J Radiol. 2015 May 1;84(5):840–8.

159. Morton G, Schuster A, Jogiya R, Kutty S, Beerbaum P, Nagel E. Inter-study reproducibility of cardiovascular magnetic resonance myocardial feature tracking. J Cardiovasc Magn Reson Off J Soc Cardiovasc Magn Reson. 2012 Jun 21;14:43.

160. Schuster A, Stahnke V-C, Unterberg-Buchwald C, Kowallick JT, Lamata P, Steinmetz M, et al. Cardiovascular magnetic resonance feature-tracking assessment of myocardial mechanics: Intervendor agreement and considerations regarding reproducibility. Clin Radiol. 2015 Sep;70(9):989–98.

161. Habibi M, Chahal H, Opdahl A, Gjesdal O, Helle-Valle TM, Heckbert SR, et al. Association of CMR-measured LA function with heart failure development: results from the MESA study. JACC Cardiovasc Imaging. 2014 Jun;7(6):570–9.

162. Maret E, Todt T, Brudin L, Nylander E, Swahn E, Ohlsson JL, et al. Functional measurements based on feature tracking of cine magnetic resonance images identify left ventricular segments with myocardial scar. Cardiovasc Ultrasound. 2009 Nov 16;7:53.

163. Andre F, Steen H, Matheis P, Westkott M, Breuninger K, Sander Y, et al. Age- and gender-related normal left ventricular deformation assessed by cardiovascular magnetic resonance feature tracking. J Cardiovasc Magn Reson Off J Soc Cardiovasc Magn Reson. 2015 Mar 10;17:25.

164. Kowallick JT, Lamata P, Hussain ST, Kutty S, Steinmetz M, Sohns JM, et al. Quantification of left ventricular torsion and diastolic recoil using cardiovascular magnetic resonance myocardial feature tracking. PloS One. 2014;9(10):e109164.

165. Schuster A, Kutty S, Padiyath A, Parish V, Gribben P, Danford DA, et al. Cardiovascular magnetic resonance myocardial feature tracking detects quantitative wall motion during dobutamine stress. J Cardiovasc Magn Reson Off J Soc Cardiovasc Magn Reson. 2011 Oct 12;13:58.

166. Heermann P, Hedderich DM, Paul M, Schülke C, Kroeger JR, Baeßler B, et al. Biventricular myocardial strain analysis in patients with arrhythmogenic right ventricular cardiomyopathy (ARVC) using cardiovascular magnetic resonance feature tracking. J Cardiovasc Magn Reson Off J Soc Cardiovasc Magn Reson. 2014 Oct 7;16:75.

167. Taylor RJ, Umar F, Moody WE, Meyyappan C, Stegemann B, Townend JN, et al. Feature-tracking cardiovascular magnetic resonance as a novel technique for the assessment of mechanical dyssynchrony. Int J Cardiol. 2014 Jul 15;175(1):120–5.

168. Ohyama Y, Ambale-Venkatesh B, Chamera E, Shehata ML, Corona-Villalobos CP, Zimmerman SL, et al. Comparison of strain measurement from multimodality tissue tracking with strain-encoding MRI and harmonic phase MRI in pulmonary hypertension. Int J Cardiol. 2015 Mar 1;182:342–8.

169. Mewton N, Liu CY, Croisille P, Bluemke D, Lima JAC. Assessment of Myocardial Fibrosis With Cardiovascular Magnetic Resonance. J Am Coll Cardiol. 2011 Feb;57(8):891–903.

170. Iles L, Pfluger H, Phrommintikul A, Cherayath J, Aksit P, Gupta SN, et al. Evaluation of diffuse myocardial fibrosis in heart failure with cardiac magnetic resonance contrast-enhanced T1 mapping. J Am Coll Cardiol. 2008 Nov 4;52(19):1574–80.

171. Roujol S, Weingärtner S, Foppa M, Chow K, Kawaji K, Ngo LH, et al. Accuracy, Precision, and Reproducibility of Four T1 Mapping Sequences: A Head-to-Head Comparison of MOLLI, ShMOLLI, SASHA, and SAPPHIRE. Radiology. 2014 Sep;272(3):683–9.

172. Fontana M, White SK, Banypersad SM, Sado DM, Maestrini V, Flett AS, et al. Comparison of T1 mapping techniques for ECV quantification. Histological validation and reproducibility of ShMOLLI versus multibreath-hold T1 quantification equilibrium contrast CMR. J Cardiovasc Magn Reson Off J Soc Cardiovasc Magn Reson. 2012 Dec 28;14:88.

173. Kammerlander AA, Marzluf BA, Zotter-Tufaro C, Aschauer S, Duca F, Bachmann A, et al. T1 Mapping by CMR Imaging. JACC Cardiovasc Imaging. 2016 Jan;9(1):14–23.

174. Duca F, Kammerlander AA, Zotter-Tufaro C, Aschauer S, Schwaiger ML, Marzluf BA, et al. Interstitial Fibrosis, Functional Status, and Outcomes in Heart Failure With Preserved Ejection Fraction: Insights From a Prospective Cardiac Magnetic Resonance Imaging Study. Circ Cardiovasc Imaging. 2016 Dec;9(12).

175. Wong TC, Piehler K, Meier CG, Testa SM, Klock AM, Aneizi AA, et al. Association between extracellular matrix expansion quantified by cardiovascular magnetic resonance and short-term mortality. Circulation. 2012 Sep 4;126(10):1206–16.

176. Banypersad SM, Fontana M, Maestrini V, Sado DM, Captur G, Petrie A, et al. T1 mapping and survival in systemic light-chain amyloidosis. Eur Heart J. 2015 Jan 21;36(4):244–51.

177. Wong TC, Piehler KM, Kang IA, Kadakkal A, Kellman P, Schwartzman DS, et al. Myocardial extracellular volume fraction quantified by cardiovascular magnetic resonance is increased in diabetes and associated with mortality and incident heart failure admission. Eur Heart J. 2014 Mar;35(10):657–64.

178. Neilan TG, Mongeon F-P, Shah RV, Coelho-Filho O, Abbasi SA, Dodson JA, et al. Myocardial extracellular volume expansion and the risk of recurrent atrial fibrillation after pulmonary vein isolation. JACC Cardiovasc Imaging. 2014 Jan;7(1):1–11.

179. Motiwala SR, Gaggin HK. Biomarkers to Predict Reverse Remodeling and Myocardial Recovery in Heart Failure. Curr Heart Fail Rep. 2016 Oct;13(5):207–18.

180. Hoyt RH, Ericksen E, Collins SM, Skorton DJ. Computer-assisted quantitation of myocardial fibrosis in histologic sections. Arch Pathol Lab Med. 1984 Apr;108(4):280–3.

181. Chimenti C, Frustaci A. Contribution and risks of left ventricular endomyocardial biopsy in patients with cardiomyopathies: a retrospective study over a 28-year period. Circulation. 2013 Oct 1;128(14):1531–41.

182. Ravassa S, López B, Querejeta R, Echegaray K, San José G, Moreno MU, et al. Phenotyping of myocardial fibrosis in hypertensive patients with heart failure. Influence on clinical outcome. J Hypertens. 2017 Apr;35(4):853–61.

183. Zannad F, Alla F, Dousset B, Perez A, Pitt B. Limitation of excessive extracellular matrix turnover may contribute to survival benefit of spironolactone therapy in patients with congestive heart failure: insights from the randomized aldactone evaluation study (RALES). Rales Investigators. Circulation. 2000 Nov 28;102(22):2700–6.

184. Löfsjögård J, Kahan T, Díez J, López B, González A, Ravassa S, et al. Usefulness of Collagen Carboxy-Terminal Propeptide and Telopeptide to Predict Disturbances of Long-Term Mortality in Patients ≥60 Years With Heart Failure and Reduced Ejection Fraction. Am J Cardiol. 2017 Jun;119(12):2042–8.

185. Izawa H, Murohara T, Nagata K, Isobe S, Asano H, Amano T, et al. Mineralocorticoid receptor antagonism ameliorates left ventricular diastolic dysfunction and myocardial fibrosis in mildly symptomatic patients with idiopathic dilated cardiomyopathy: a pilot study. Circulation. 2005 Nov 8;112(19):2940–5.

186. Martos R, Baugh J, Ledwidge M, O'Loughlin C, Conlon C, Patle A, et al. Diastolic heart failure: evidence of increased myocardial collagen turnover linked to diastolic dysfunction. Circulation. 2007 Feb 20;115(7):888–95.

187. Klappacher G, Franzen P, Haab D, Mehrabi M, Binder M, Plesch K, et al. Measuring extracellular matrix turnover in the serum of patients with idiopathic or ischemic dilated cardiomyopathy and impact on diagnosis and prognosis. Am J Cardiol. 1995 May 1;75(14):913–8.

188. Barasch E, Gottdiener JS, Aurigemma G, Kitzman DW, Han J, Kop WJ, et al. The Relationship Between Serum Markers of Collagen Turnover and Cardiovascular Outcome in the Elderly: The Cardiovascular Health Study. Circ Heart Fail. 2011 Nov 1;4(6):733–9.

189. López B, González A, Querejeta R, Larman M, Díez J. Alterations in the Pattern of Collagen Deposition May Contribute to the Deterioration of Systolic Function in Hypertensive Patients With Heart Failure. J Am Coll Cardiol. 2006 Jul 4;48(1):89–96.

190. Laviades C, Varo N, Fernández J, Mayor G, Gil MJ, Monreal I, et al. Abnormalities of the extracellular degradation of collagen type I in essential hypertension. Circulation. 1998;98(6):535–540.

191. Agrinier N, Thilly N, Boivin J-M, Dousset B, Alla F, Zannad F. Prognostic value of serum PIIINP, MMP1 and TIMP1 levels in hypertensive patients: a community-based prospective cohort study. Fundam Clin Pharmacol. 2013 Oct;27(5):572–80.

192. Morillas P, Quiles J, de Andrade H, Castillo J, Tarazón E, Roselló E, et al. Circulating biomarkers of collagen metabolism in arterial hypertension: relevance of target organ damage. J Hypertens. 2013 Aug;31(8):1611–7.

193. Mohd Razali N, Yap B. Power Comparisons of Shapiro-Wilk, Kolmogorov-Smirnov, Lilliefors and Anderson-Darling Tests. J Stat Model Anal. 2011 Jan 1;2.

194. Ghasemi A, Zahediasl S. Normality tests for statistical analysis: a guide for non-statisticians. Int J Endocrinol Metab. 2012;10(2):486–9.

195. Jekel JF. Epidemiology, biostatistics, and preventive medicine. Philadelphia, PA: Saunders Elsevier; 2007.

196. Austin PC, Steyerberg EW. The number of subjects per variable required in linear regression analyses. J Clin Epidemiol. 2015 Jun;68(6):627–36.

197. Edwards NC, Moody WE, Yuan M, Hayer MK, Ferro CJ, Townend JN, et al. Diffuse interstitial fibrosis and myocardial dysfunction in early chronic kidney disease. Am J Cardiol. 2015 May 1;115(9):1311–7.

198. Kuruvilla S, Janardhanan R, Antkowiak P, Keeley EC, Adenaw N, Brooks J, et al. Increased Extracellular Volume and Altered Mechanics Are Associated With LVH in Hypertensive Heart Disease, Not Hypertension Alone. JACC Cardiovasc Imaging. 2015 Feb;8(2):172–80.

199. Wu L-M, An D-AL, Yao Q-Y, Ou Y-RZ, Lu Q, Jiang M, et al. Hypertrophic cardiomyopathy and left ventricular hypertrophy in hypertensive heart disease with mildly reduced or preserved ejection fraction: insight from altered mechanics and native T1 mapping. Clin Radiol. 2017 Oct;72(10):835–43.

200. Rommel K-P, von Roeder M, Latuscynski K, Oberueck C, Blazek S, Fengler K, et al. Extracellular Volume Fraction for Characterization of Patients With Heart Failure and Preserved Ejection Fraction. J Am Coll Cardiol. 2016 Apr 19;67(15):1815–25.

201. Treibel TA, Zemrak F, Sado DM, Banypersad SM, White SK, Maestrini V, et al. Extracellular volume quantification in isolated hypertension - changes at the detectable limits? J Cardiovasc Magn Reson Off J Soc Cardiovasc Magn Reson. 2015 Aug 12;17:74.

202. Rodrigues JCL, Amadu AM, Dastidar AG, Szantho GV, Lyen SM, Godsave C, et al. Comprehensive characterisation of hypertensive heart disease left ventricular phenotypes. Heart Br Card Soc. 2016 Oct 15;102(20):1671–9.

203. Redon J, Pichler G, Missed Dose Study Group. Comparative study of the efficacy of olmesartan/amlodipine vs. perindopril/amlodipine in peripheral blood pressure after missed dose in type 2 diabetes. J Hypertens. 2016 Feb;34(2):359–67.

204. Redon J, Pichler G, Missed Dose Study Group. Comparative Study of the Efficacy of Olmesartan/Amlodipine vs. Perindopril/Amlodipine in Peripheral and Central Blood Pressure Parameters After Missed Dose in Type 2 Diabetes. Am J Hypertens. 2016 Sep;29(9):1055–62.

205. Adams JW, Sakata Y, Davis MG, Sah VP, Wang Y, Liggett SB, et al. Enhanced Galphaq signaling: a common pathway mediates cardiac hypertrophy and apoptotic heart failure. Proc Natl Acad Sci U S A. 1998 Aug 18;95(17):10140–5.

206. Seravalle G, Lonati L, Buzzi S, Cairo M, Quarti Trevano F, Dell'Oro R, et al. Sympathetic nerve traffic and baroreflex function in optimal, normal, and high-normal blood pressure states. J Hypertens. 2015 Jul;33(7):1411–7.

207. Ikonomidis I, Tzortzis S, Triantafyllidi H, Parissis J, Papadopoulos C, Venetsanou K, et al. Association of impaired left ventricular twisting-untwisting with vascular dysfunction, neurohumoral activation and impaired exercise capacity in hypertensive heart disease. Eur J Heart Fail. 2015 Dec;17(12):1240–51.

208. Opdahl A, Remme EW, Helle-Valle T, Lyseggen E, Vartdal T, Pettersen E, et al. Determinants of left ventricular early-diastolic lengthening velocity: independent contributions from left ventricular relaxation, restoring forces, and lengthening load. Circulation. 2009 May 19;119(19):2578–86.

209. Zile MR, Gaasch WH. Mechanical loads and the isovolumic and filling indices of left ventricular relaxation. Prog Cardiovasc Dis. 1990 Apr;32(5):333–46.

210. Maciver DH. The relative impact of circumferential and longitudinal shortening on left ventricular ejection fraction and stroke volume. Exp Clin Cardiol. 2012;17(1):5–11.

211. MacIver DH, Adeniran I, Zhang H. Left ventricular ejection fraction is determined by both global myocardial strain and wall thickness. Int J Cardiol Heart Vasc. 2015 Jun 1;7:113–8.

212. Morris DA, Ma X-X, Belyavskiy E, Aravind Kumar R, Kropf M, Kraft R, et al. Left ventricular longitudinal systolic function analysed by 2D speckle-tracking echocardiography in heart failure with preserved ejection fraction: a meta-analysis. Open Heart. 2017;4(2):e000630.

213. Chen X-J, Sun X-L, Zhang Q, Gao X-L, Liang Y-J, Jiang J, et al. Uncontrolled blood pressure as an independent risk factor of early impaired left ventricular systolic function in treated hypertension. Echocardiogr Mt Kisco N. 2016 Oct;33(10):1488–94.

214. Ye Z, Coutinho T, Pellikka PA, Villarraga HR, Borlaug BA, Kullo IJ. Associations of Alterations in Pulsatile Arterial Load With Left Ventricular Longitudinal Strain. Am J Hypertens. 2015 Nov;28(11):1325–31.

215. Sera F, Jin Z, Russo C, Lee ES, Schwartz JE, Rundek T, et al. Relationship of Office and Ambulatory Blood Pressure With Left Ventricular Global Longitudinal Strain. Am J Hypertens. 2015 Dec 7;

216. Plaksej R, Kosmala W, Frantz S, Herrmann S, Niemann M, Störk S, et al. Relation of circulating markers of fibrosis and progression of left and right ventricular dysfunction in hypertensive patients with heart failure. J Hypertens. 2009 Dec;27(12):2483–91.

217. Martos R, Baugh J, Ledwidge M, O'Loughlin C, Murphy NF, Conlon C, et al. Diagnosis of heart failure with preserved ejection fraction: improved accuracy with the use of markers of collagen turnover. Eur J Heart Fail. 2009 Feb;11(2):191–7.

218. Lopez-Andrès N, Rossignol P, Iraqi W, Fay R, Nuée J, Ghio S, et al. Association of galectin-3 and fibrosis markers with long-term cardiovascular outcomes in patients with heart failure, left ventricular dysfunction, and dyssynchrony: insights from the CARE-HF (Cardiac Resynchronization in Heart Failure) trial. Eur J Heart Fail. 2012 Jan;14(1):74–81.

219. Jordán A, Roldán V, García M, Monmeneu J, de Burgos FG, Lip GYH, et al. Matrix metalloproteinase-1 and its inhibitor, TIMP-1, in systolic heart failure: relation to functional data and prognosis. J Intern Med. 2007 Sep;262(3):385–92.

220. Bosone D, Costa A, Ghiotto N, Ramusino MC, Zoppi A, D'Angelo A, et al. Effect of ramipril/hydrochlorothiazide and ramipril/canrenone combination on atrial fibrillation recurrence in hypertensive type 2 diabetic patients with and without cardiac autonomic neuropathy. Arch Med Sci. 2017;3:550–7.

221. López B, Querejeta R, Varo N, González A, Larman M, Martínez Ubago JL, et al. Usefulness of serum carboxy-terminal propeptide of procollagen type I in assessment of the cardioreparative ability of antihypertensive treatment in hypertensive patients. Circulation. 2001 Jul 17;104(3):286–91.

222. Díez J, Laviades C, Mayor G, Gil MJ, Monreal I. Increased serum concentrations of procollagen peptides in essential hypertension. Relation to cardiac alterations. Circulation. 1995 Mar 1;91(5):1450–6.

223. Fukui M, Goda A, Komamura K, Nakabo A, Masaki M, Yoshida C, et al. Changes in collagen metabolism account for ventricular functional recovery following beta-blocker therapy in patients with chronic heart failure. Heart Vessels. 2016 Feb;31(2):173–82.

224. Demir M, Acartürk E, Inal T, Attila G, Dönmez Y, Avkaroğullari M, et al. Procollagen type I carboxy-terminal peptide shows left ventricular hypertrophy and diastolic

dysfunction in hypertensive patients. Cardiovasc Pathol Off J Soc Cardiovasc Pathol. 2007 Apr;16(2):69–74.

225. Querejeta R, Varo N, Lopez B, Larman M, Artinano E, Etayo JC, et al. Serum Carboxy-Terminal Propeptide of Procollagen Type I Is a Marker of Myocardial Fibrosis in Hypertensive Heart Disease. Circulation. 2000 Apr 11;101(14):1729–35.

226. Querejeta R, López B, González A, Sánchez E, Larman M, Martínez Ubago JL, et al. Increased collagen type I synthesis in patients with heart failure of hypertensive origin: relation to myocardial fibrosis. Circulation. 2004 Sep 7;110(10):1263–8.

227. Alla F, Kearney-Schwartz A, Radauceanu A, Das Dores S, Dousset B, Zannad F. Early changes in serum markers of cardiac extra-cellular matrix turnover in patients with uncomplicated hypertension and type II diabetes. Eur J Heart Fail. 2006 Mar;8(2):147–53.

228. Ley B, Brown KK, Collard HR. Molecular biomarkers in idiopathic pulmonary fibrosis. Am J Physiol Lung Cell Mol Physiol. 2014 Nov 1;307(9):L681-691.

229. Liu T, Wang X, Karsdal MA, Leeming DJ, Genovese F. Molecular serum markers of liver fibrosis. Biomark Insights. 2012;7:105–17.

230. Nishikimi T, Yoshihara F, Morimoto A, Ishikawa K, Ishimitsu T, Saito Y, et al. Relationship between left ventricular geometry and natriuretic peptide levels in essential hypertension. Hypertens Dallas Tex 1979. 1996 Jul;28(1):22–30.

231. Muscholl MW, Schunkert H, Muders F, Elsner D, Kuch B, Hense HW, et al. Neurohormonal activity and left ventricular geometry in patients with essential arterial hypertension. Am Heart J. 1998 Jan;135(1):58–66.

232. Irzmański R, Banach M, Piechota M, Kowalski J, Barylski M, Cierniewski C, et al. Atrial and brain natriuretic peptide and endothelin-1 concentration in patients with idiopathic arterial hypertension: the dependence on the selected morphological parameters. Clin Exp Hypertens N Y N 1993. 2007 Apr;29(3):149–64.

233. Irzmanski R, Barylski M, Banach M, Piechota M, Kowalski J, Cierniewski C, et al. The concentration of atrial and brain natriuretic peptide in patients with idiopathic hypertension. Med Sci Monit Int Med J Exp Clin Res. 2007 Oct;13(10):CR449-456.

234. Irzmański R, Pawlicki L, Charłusz M, Kowalski J. Concentration of natriuretic peptides in patients suffering from idiopathic arterial hypertension and left ventricular diastolic dysfunction confirmed by echocardiography. Clin Exp Hypertens N Y N 1993. 2012;34(7):530–40.

235. Olsen MH, Wachtell K, Tuxen C, Fossum E, Bang LE, Hall C, et al. N-terminal pro-brain natriuretic peptide predicts cardiovascular events in patients with hypertension and left ventricular hypertrophy: a LIFE study. J Hypertens. 2004 Aug;22(8):1597–604.

236. Nakao K, Ogawa Y, Suga S, Imura H. Molecular biology and biochemistry of the natriuretic peptide system. II: Natriuretic peptide receptors. J Hypertens. 1992 Oct;10(10):1111–4.

237. Nakagawa O, Ogawa Y, Itoh H, Suga S, Komatsu Y, Kishimoto I, et al. Rapid transcriptional activation and early mRNA turnover of brain natriuretic peptide in cardiocyte hypertrophy. Evidence for brain natriuretic peptide as an "emergency" cardiac hormone against ventricular overload. J Clin Invest. 1995 Sep;96(3):1280–7.

238. Chatzis D, Tsioufis C, Tsiachris D, Taxiarchou E, Lalos S, Kyriakides Z, et al. Brain natriuretic peptide as an integrator of cardiovascular stiffening in hypertension. Int J Cardiol. 2010 Jun 11;141(3):291–6.

239. Neeland IJ, Drazner MH, Berry JD, Ayers CR, deFilippi C, Seliger SL, et al. Biomarkers of chronic cardiac injury and hemodynamic stress identify a malignant phenotype of left ventricular hypertrophy in the general population. J Am Coll Cardiol. 2013 Jan 15;61(2):187–95.

240. Masson S, Latini R, Mureddu GF, Agabiti N, Miceli M, Cesaroni G, et al. High-sensitivity cardiac troponin T for detection of subtle abnormalities of cardiac phenotype in a general population of elderly individuals. J Intern Med. 2013 Mar;273(3):306–17.

241. de Lemos JA, Drazner MH, Omland T, Ayers CR, Khera A, Rohatgi A, et al. Association of troponin T detected with a highly sensitive assay and cardiac structure and mortality risk in the general population. JAMA. 2010 Dec 8;304(22):2503–12.

242. Khouri MG, Peshock RM, Ayers CR, de Lemos JA, Drazner MH. A 4-tiered classification of left ventricular hypertrophy based on left ventricular geometry: the Dallas heart study. Circ Cardiovasc Imaging. 2010 Mar;3(2):164–71.

243. Nadir MA, Rekhraj S, Wei L, Lim TK, Davidson J, MacDonald TM, et al. Improving the primary prevention of cardiovascular events by using biomarkers to identify individuals with silent heart disease. J Am Coll Cardiol. 2012 Sep 11;60(11):960–8.

244. González A, López B, Querejeta R, Zubillaga E, Echeverría T, Díez J. Filling pressures and collagen metabolism in hypertensive patients with heart failure and normal ejection fraction. Hypertens Dallas Tex 1979. 2010 Jun;55(6):1418–24.

245. Lindsay MM, Maxwell P, Dunn FG. TIMP-1: a marker of left ventricular diastolic dysfunction and fibrosis in hypertension. Hypertens Dallas Tex 1979. 2002 Aug;40(2):136–41.